OPTICS EXPERIMENT AP E4018 Applied Physics Laboratory

In this laboratory you will investigate laser beam propagation, interference and diffraction, and optical spectroscopy. Textbooks with background information for this lab are *Optics* by Klein, *Optics* by Hecht, *Laser Electronics* by Verdeyen, *Fundamentals of Photonics* by Saleh and Teich, and *Quantum Electronics* and *Optical Electronics* by Yariv. **Week 1** covers light detection by photodiodes and the propagation of lasers. **Week 2** covers optical spectroscopy measurements and the use of a photomultiplier. **Week 3** covers the properties of diffraction gratings and how to build a grating spectrometer.

Week 1

The goals in the first week are to acquaint yourself with optical hardware, to make measurements of laser power and the beam profiles, and to investigate the propagation of a laser in free space and after a positive lens.

The He-Ne laser source you will use has a wavelength of 6328 Å and is rated to have a power of 0.5 milliwatts. See the attached week 1 notes for some information about this laser. It is linearly polarized and has a stated beam divergence of 1.7 mrad. Though as lasers go this one is fairly innocuous (Class II), you should always remember the following:

Always keep the laser beam and all of its reflections on the table. Use beam blocks to prevent it from leaving the table.

Always keep the height of the laser below eye level, and closer to waist level. Never bend down to level of the laser.

Never look directly into the laser or any of its reflections. Make sure that everybody else (including your lab partner) is also protected.

Note that all of the optical components are attached to posts that are mountable on the optical rail. These mounts are meant to be loosened from the rail, slid to the proper position, and then tightened again. After loosening the posts, the height and rotation angle of the mounted element can be adjusted. The post should then be tightened. It is good

practice to keep all beams along the axis of the rail (when possible) and parallel to the table top.

Examine the different sets of optical components. Note that the laser mount has an additional angular degree of freedom to allow you make the output beam horizontal. There is a beam block in front of the laser for temporary blocking. **When you want to insert an optical element in the path of the laser, it is good practice to first block the laser, insert the element, unblock the laser, and then make minor readjustments.** (That is, don't just stick the element in the beam path. Sometimes you can get stray reflections that way.)

Another assembly has a linear translation stage with a micrometer drive attached to it. On top of this stage are an adjustable slit and a photodiode assembly. Initially, when you measure laser power you will want to remove the slit, and direct the laser into the center of the photodiode (by adjusting the photodiode and/or the laser position). When you re-insert the slit, first, momentarily block the laser and then center the slit.

The two other rail mounts have a lens and a diffraction grating mounted on them. **Make sure that your fingerprints never appear on these or any other optical components.** The diffraction grating is held in place by the two horizontal brass screws, which are to be left alone. The grating is mounted on a mirror mount with two angular degrees of freedom, adjustable by the two screws in the back. Make sure that you never change the vertical adjustment so much that it directs the reflected beam too high.

1) Laser Power Measurement

Properly mount the laser on the optical bench so that the beam is parallel to the bench. Make sure that the beam is blocked at the end of the table. Measure the laser power with the photodiode. (The slit must be totally open or, preferably, removed.) To make this measurement you need to examine how the photodiode is being used and read relevant parts of the photodiode description (which is attached) including the calibration data. Do this for the ~1.1 KΩ load resistor and for the ~500 Ω resistor. Is there a relationship between voltage and resistance? Why? From now on use the resistor that gives you the largest signals. Now estimate the light intensity impinging on the top of the laboratory

table from the fluorescent lights above. Place the diode on the table facing up (without the slit in front) and measure the light intensity. How does this compare with your estimate?

2) Laser Polarization, Profile Measurement and Single Slit Diffraction

You should review the theory about laser profiles and propagation, which is in the appendix (and in the texts listed above).

(a) Place the laser at one extreme on the rail so that it propagates along the rail at constant height, and keep it there for the rest of today. There should be nothing else on the rail. Place a white screen where the laser hits the wall. Inspect the polaroid polarizer. You will see two tick marks at the edges that define the absorption axis. When the (linearly polarized) electric field of the laser is along the axis, there is nearly total absorption. By placing the polarizer right after the laser and looking at the screen, show that the laser is horizontally polarized.

(b) Examine the slit. One full turn (= 50 gradations) opens the slit by 1 mm (20 μm/gradation). The "zero" position needs to be determined by closing the slit and slowing opening it. Call the zero the point when you start feeling resistance. Alternately, you can look throught the slit and determine the zero visually. You may use as your reference the pointer at the side of the slit assembly or the home-made pointer on top. (As you will see, the one on top may be more convenient.)

Now place the slit right after the laser, with the slit centered and totally open. Make sure that you are able to determine the width of the slit from the dial. Observe the single-slit diffraction pattern on the white screen as you close the slit. Take enough measurements of the width of the central lobe vs. slit width (for the fixed slit/screen separation, which you also need to measure) to prove the far field (Fraunhofer) diffraction result.

(c) Now re-install the photodiode after the slit, as described earlier. Place the slit/translation stage assembly as close to the laser as possible. The slit assembly should be centered, with the slit open. Close the slit so that the transmitted power is ~ 10 - 20% of that with the slit open. (Make sure that the slit is still centered when it is partially closed.) Determine the slit width. (It may be difficult to do this accurately because it will be barely open and the zero is somewhat uncertain.) Measure the transmitted power for different lateral positions of the slit by scanning across the entire beam from zero transmitted power

on one side to the other. The step size in this scan should be about the slit width. (It the beam symmetrical?) Do you have to account for a background due to room lights? (Notice that the scale on the stationary part of the micrometer (in the translation stage) is in mm. Two turns (= 100 gradations) correspond to 1 mm of travel (10 μm/gradation).)

Repeat the scan with the slit open to 0.5 mm and the same step size as in the first scan.

Determine the beam radius for both choices of slit width. Does the beam look gaussian? Is the measured beam radius w different for the different slit widths? Quantitatively, account for these different observations.

<u>If time is running short, do part (4) before you attempt (3).</u>

3) Divergence of the Laser

Repeat the laser profiling in step 3, which was done with the slit a distance $z' \sim 0$ from the output mirror of the laser, for $z' \sim 25$, 50, and 75 cm. Use the same small slit width and scan step size that you used in your first scan in (2c). Determine $w(z')$ and compare it to Eq. 2 (Appendix) and with the divergence angle given by the manufacturer.

4) Focusing Lasers

Repeat step 3 for the laser focused by a lens with $f = 10$ cm. Place the lens right after the laser. Measure $w(z)$ for a distance $z = 1, 4, 8, 12, 20, 40$, and 70 cm past the lens, and compare these results with Eq. 5 (Appendix). For $z < \sim 20$ cm you should use the slit width from parts 2c and 3, while for larger z you may have to open to slit a little further to get a large enough signal. Where is the focus? How does it compare with the expected value? (Try not to put the slit right at the focus because you can burn pits into the slit.) What is the peak laser intensity near the output of the laser? What is the peak intensity at the focus?

Week 3

In this week you will perform optical spectroscopy on a discharge by using a small grating spectrometer (monochrometer), your own personal photon detectors (your eyes), and a photomultiplier. Since the details of the operation of gratings and spectrometers will be covered in week 3, you should read ahead.

5) Using a Grating Spectrometer

(a) The spectrometer has a grating with 675 grooves/mm and the distance between its slit and focusing mirror is ~ 18 cm. (As you will see later, it has very limited spectral dispersion and resolution, but will be fine for the purposes here.) It has adjustable entrance and exit slits. The wavelength is tuned with the dial on top. Keep the dial within the range of numbers, which is in units of micrometers (microns) (1 μm = 10,000 Å = 1000 nm).

Direct a flashlight into the entrance slit (the one without the lens). Place a white screen after the exit slit, and now tune the spectrometer. (With this flashlight incident you can also look into exit slit, but **never** do this when using lasers.) How do the wavelengths at the exit slit compare with the dial setting. Does it make sense? (It does if you have read on into week 3 and learned that diffraction grating can have several orders, so that at a wavelength setting of $\lambda_{spectrometer} = m\,\lambda_{that\ you\ see}$, you can see the mth order (m = integer) of light.) Explain what you see in terms of the diffraction order. (Can orders overlap?) What happens if you repeat this with different slit widths?

(b) Now send the He-Ne laser through the spectrometer so that the output is incident onto a white screen. (Do **not** look into the slit now.) Keep the slits as small as possible for best spectral resolution. At what setting do you see the laser? If $\lambda_{spectrometer} = m\,\lambda_{that\ you\ see} + \delta_{error}$, determine m and δ_{error} (which you will use later).

(c) Now examine the Ne discharge lamp. Direct the light from the lamp into the spectrometer, and scan it while looking at the white screen after the exit slit. Make sure that the room is dark, and try to keep the slits as small as possible. (Always keep the entrance and exit slits the same width, and scan the spectrometer from the same direction, say from shorter to longer λ. Because there may be weak lines, initially keep the slits open. Then scan again with smaller slits.) At what λ_{actual} are there spectral lines?

(d) After learning how to use the photomultiplier you will repeat these measurements with the photomultiplier. It has a sensitivity far beyond that of the photodiode you used in week 1.

Care must be used in using the photomultiplier (PMT) because high voltages are used in its operation (see handout). **Do not rearrange the PMT wiring.** You are using an RCA C31000A, which has a maximum operating voltage of – 3000 V. The maximum voltage that you will use is – 1500 V. Since the PMT is a sensitive detector of light and a high gain amplifier, extraneous sources of light must always be prevented from reaching it. The light levels incident on to the PMT must always be kept low so that the output current is never above the threshold for damaging it (< 0.01 mA). The PMT output current is sent through a 160 kΩ resistor to ground and you will be measuring the voltage drop across that resistor. (What is the maximum voltage you should ever measure to prevent damage to the PMT?) The PMT voltage should still be off.

You will be directing the light from the exit slit of the spectrometer to the PMT with a fiber optic bundle. This particular bundle is fairly stiff because of the type of cable it is housed in. Examine how the flashlight propagates through the fiber optic bundle. Then send the light from the spectrometer to the PMT. [Note: Since we have relatively high light levels in this experiment, we are not imaging the light into the spectrometer (with a lens as we will in week 3), nor are we trying to collect and detect all of the light after the exit slit (by using a second lens) as one would normally do).]

With the slits fairly wide open, tune the spectrometer to the setting of the strongest peaks you saw with the Ne lamp. Measure the signal vs. PMT voltage. Are they linearly related?

(e) Now take a scan of the Ne discharge with the slits quite narrow, say 1 mm. Set the voltage at ~ – 1300 V. Scan the dial slowly towards increasing λ. Take a careful spectrum by starting at 0.700 μm on the dial and ending at 1.600 μm, taking data in increments of 0.005 μm, i.e., at and halfway between the gradations. Compared to part (c), do you see additional lines? Are they sharp? Do they have structure? (You may be able to see more structure if you were to close the slits further. However, you would be limited by the ultimate spectral dispersion and resolution of this instrument.) Does the spectrum compare well with that expected from Ne? Does the color of the discharge make sense on the basis of your measured spectrum? (In this part and in part (f) remember that

you may see lines either in first- or second-order.) Does the Ne line that lases in the He-Ne laser dominate the emission spectrum of this Ne lamp? Should it?

(f) Repeat part (e) for the two supplied, and unidentified, discharge lamps. Does the color of each discharge agree with its spectrum? Identify the gas in each lamp on the basis of the emission spectra you measured. Hint: You need to consider only atomic (not molecular or ionic) transitions.

Week 2

In the third week you will examine the properties of a diffraction grating and will use it to build a spectrometer.

6) Properties of a Diffraction Grating

Diffraction gratings are commonly used as dispersive elements in spectrometers, as we will soon see. The diffraction orders of a grating arise from multiple beam interference, while the relative intensity of each order depends on how the grooves are blazed.

With the laser mounted at one end of the optical table, mount the diffraction grating assembly at the other end. Initially mount it so that the laser hits it normally, and near the center. This diffraction grating has 1200 grooves/mm etched into the aluminum thin film, which is atop the glass substrate. (We know these grooves are vertical now because the grating has been mounted with the arrow on top.) **Don't touch the grating surface because it cannot be cleaned. (As all people working with optics know: your fingerprints can be identified easily.)** Put the cover on it when you are finished. Refer to the week 3 notes for more information about gratings.

In these measurements you will need to measure angles of incidence and reflection. This can be accomplished by using a protractor or in the following, more clever way. Make sure that the grating surface is above a hole in the optical breadboard. Now you can measure angle using this board and simple trigonometry. The angle of incidence can be determined with reference to $m = 0$ (reflection) mode (be careful about a factor of two) and use this information for the other orders.

(a) Place the grating nearly (but not exactly) normal to the laser beam. How many beams do you see bouncing off this grating? "Reflection" from a grating can be ascribed to different orders m (all integers, positive and negative). With an angle of incidence of θ_i, the angles of reflection of θ_r for the different orders are given by:

$$m\lambda = d(\sin\theta_i - \sin\theta_r)$$

where d is the spacing of the grooves. (See the attached notes.) For this grating, and with the angle of incidence nearly zero, how many orders are possible? Does this agree with your observation? Note that $m = 0$ corresponds to ordinary reflection, as from a mirror.

(b) Now rotate the grating mount post rod and notice how the the different orders track with each other. For a range of angles of incidence, for instance $\theta_i \sim -40^o, -20^o, 0^o, 20^o$, and 40°, measure θ_r and check the grating equation.

(c) For what angle of incidence will the first order (m = 1) be retroreflected back to the laser? Retroreflection of any order (other than m = 0) is called the Littrow configuration. Use the measured angles and the grating parameters to determine the laser wavelength? How precise is this wavelength measurement? Do you expect this value of θ_i to be the same for other wavelengths, as is it for 6328 Å? A grating can be used to provide (retroreflection) feedback in a laser at different wavelengths by properly rotating the grating. This is often used in carbon dioxide lasers to select which spectral wavelength is going to lase (because optical cavity losses are minimized for this chosen wavelength).

(d) Measure the laser power before the grating. Rotate the grating so that no beam is ~ 5 - 10° away from retroreflection to the laser, with the grating arrow pointing (somewhat) towards the laser, as opposed to away. Now measure the power of each reflected beam, while trying to minimize the amount of room lighting incident on the photodiode. Why should you take this precaution? Is the power into each order the same? (The grating equation is a consequence of multi-slit wave interference. The grooves in the grating are ruled in precise shapes to form a diffraction pattern to give the desired distribution of reflected power into the different orders. This procedure leads to a blaze angle (of incidence) and a blaze wavelength for which diffraction is most efficient.) Does their sum add up to the incident power? Does your result violate the conservation of energy? Why or why not?

7) Building a Grating Spectrometer

The goal here is to build a simple spectrometer using a diffraction grating. For a given diffraction order, measurement of the angles of incidence and reflection will determine the wavelength. The wavelength resolution that can be obtained in a spectrometer improves as the light covers more grooves, just as the peaks in a multiple slit interference experiment narrow as the number of slits increases. Therefore in a spectrometer it is important to send onto the grating a parallel beam (why?) that covers most of the grating, and high resolution spectrometers must have large gratings.

See the figures on the next page for a layout of a typical Czerny-Turner spectrometer (like the one you used in week 2) and for the version that you will build here.

(Do you see any relative disadvantages in our approach?) Build the spectometer using the two optical rails to mount the optics on either side, with the grating mounted on the breadboard in between. Leave room for the laser to be mounted before the first lens, and put the optics in sequential order (with the light path as reference). The laser should be roughly in the center of the lenses and the grating. Note that the input lens (f.l. ~ 1") and the second lens (f.l. ~ 4 ") are both positioned a focal length away from the (right) slit, just as in a telescope. (Why?) Place the first slit at the focus in the telescope, and place the mirror a few inches away. Make sure that the grating is positioned exactly halfway in between the two rails, laterally lining up roughly near the slit, and that it is operating in first order. The positions of the mirror, lens and slit on the second rail should be at the same locations as on the first rail. Align the spectrometer by using the He-Ne laser. Make use of the mirror mount screws to tune the grating. (Note that the screw has 60 threads per inch, it pivots 1 inch away from the screw, and that there is a black dot on the screw for reference.) Over what range of grating angle do you see the red light at the output? Explain this in terms of the spectrometer resolution and dispersion. (see calculations in week 3 notes) Is the entire grating filled with light?

Now use the white light projector source as an input. The spectrometer can now be used as a monochromator. Compare the m = 0, 1 and 2 orders leaving the grating. Vary the grating angle to see the range of wavelengths after the output slit, using the 6328 Å wavelength of the He-Ne laser as a reference. Is this wavelength/angle variation expected? Why? (see notes) Now calculate the spectral resolution of your spectrometer. (see notes) What was the resolution of the spectrometer that you used in week 2?

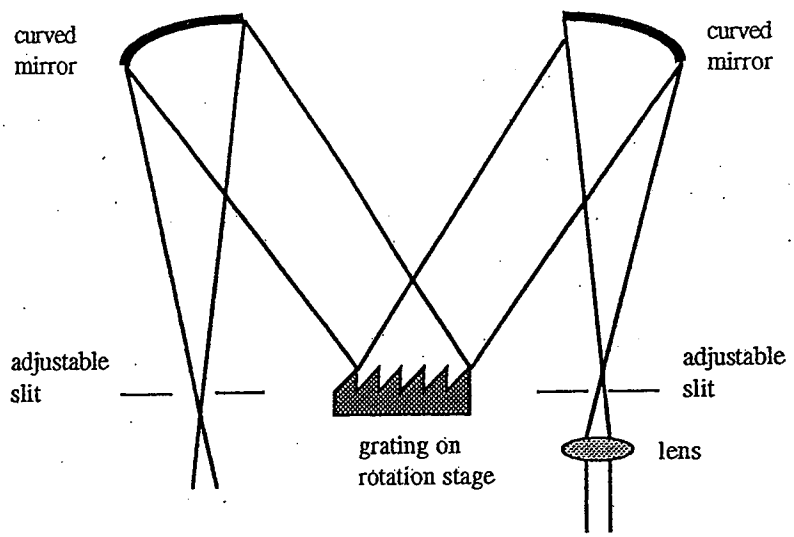

Czerny-Turner spectrometer

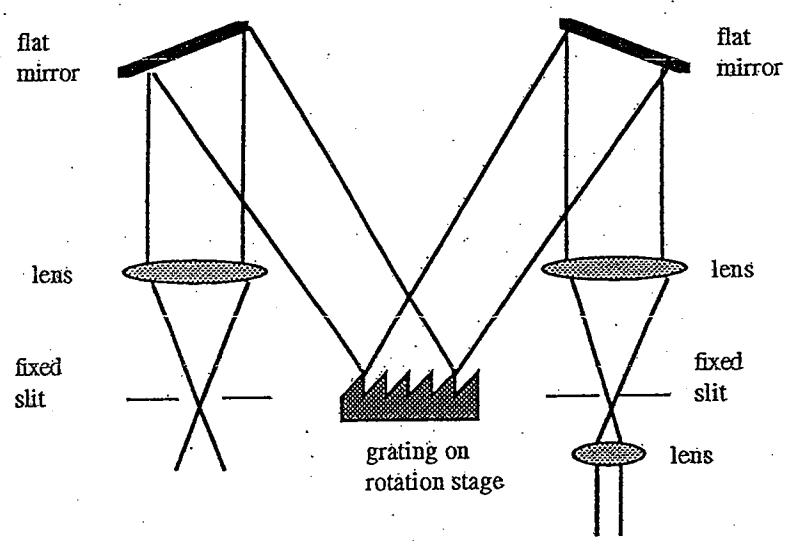

our spectrometer

Appendix:

Some theory for part 2 (also see the texts listed at the beginning):

The magnitude of the electric field of a laser travelling in the z direction varies as:

$$E(r,z) = E_0 \exp[-r^2/w(z)^2] \tag{1}$$

where w is the beam radius or spot size and varies as:

$$w(z) = w_0 \sqrt{1 + (z/z_0)^2} \tag{2}$$

where $z_0 = \pi w_0^2/\lambda$. This assumes that the laser is in a TEM_{00} mode, which is commonly the case for many cw (continuous wave) lasers, including this He-Ne laser. In Eq. 2, λ is the laser wavelength and $w = w_0$ at $z = 0$, the beam waist, where the spot size is a minimum and where the radius of curvature of the wavefront is infinite. If one of the laser mirrors is flat, as it probably is here, z is the distance from that mirror. (This is why the distance from the output mirror is called z' in part 3.) z_0 is known as the Rayleigh range, and defines how far the laser must propagate beyond $z = 0$ for the peak intensity to decrease by two. For $z << z_0$, i.e. in the near field, the spot size increases very slowly (quadratically) with z. For $z >> z_0$, i.e. in the far field, w increases linearly with z, as $w = (w_0/z_0)\, z = (\lambda/\pi w_0)\, z$. Then full divergence angle in the far field would then be about $2\lambda/\pi w_0$.

From Poynting's vector, the laser intensity is:

$$I(r,z) = I_0 \exp[-2r^2/w(z)^2] \tag{3}$$

where $I_0 = cE_0^2/8\pi$. If the laser has power P, then conservation of energy gives $I_0 = 2P/\pi w(z)^2$ by integrating $I(r,z)$ over r and θ (or x and y) at any z. Also, $E_0^2 = 16P/cw^2$.

To measure w, one could place an opaque screen with a pinhole (with radius $r_0 << w$) in the beam path and measure the transmitted power (by directing the transmitted beam into a laser power meter) as the hole is translated across the laser beam profile. The transmitted power would be $\pi r_0^2 I(r,z)$. Since Eq. 3 is radially symmetric, one can do the same thing by scanning a slit of width $a << w$ across the beam. Assuming the slit is in the y direction, the transmitted power would be:

$$P_t(x,z) = \int_{x+a/2}^{x-a/2} \int_{\infty}^{-\infty} I_0 \exp[-2(x^2+y^2)/w^2]\, dy\, dx$$

$$= \sqrt{\frac{\pi}{2}}\, a\, w\, I_0 \exp[-2x^2/w^2] \qquad (4)$$

Equations 1-3 are valid for a beam propagating in free space. If the laser is focused by a lens then the spot size becomes:

$$w^2(z) = w_i^2 \left[\left(1 - \frac{z}{f}\right)^2 + \left(\frac{z}{z_i}\right)^2\right] \qquad (5)$$

where w_i is the spot size at the lens, $z_i = \pi w_i^2/\lambda$, and z is the distance past the lens. This expression is valid when the Rayleigh range of the beam hitting the lens $z_i >>$ the lens focal length f.

Week 1 Notes

Lasers A. Siegman / University Science (1986)

He-Ne Lasers

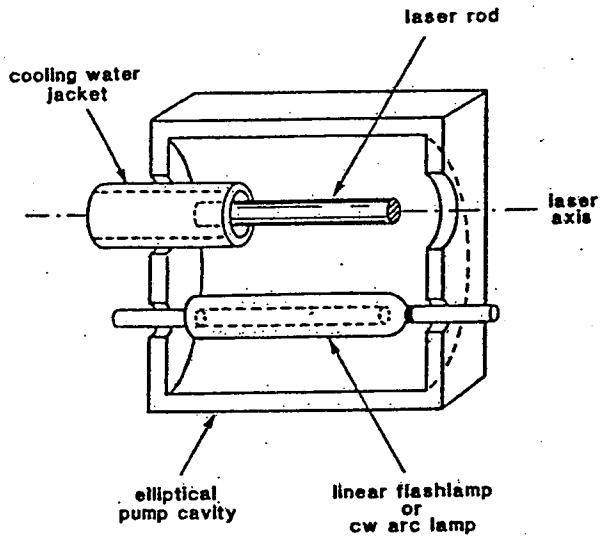

FIGURE 1.52
Elliptical pump cavity used in many optically pumped solid-state lasers.

lasers. The round-trip gains in ruby and other solid-state lasers are often much higher than in gas lasers—up to round-trip power gains of 10X and higher—so that mirrors with much lower reflectivity or higher transmission output can be employed.

Pulsed solid-state lasers are used for a variety of smaller-scale laser cutting, drilling, and marking applications; as military rangefinders and target designators; and in an enormous variety of scientific and technological experiments. By taking advantage of improved lamp efficiencies and laser materials, as well as the fact that most other materials are four-level lasers, we can also operate several solid-state lasers continuously at cw power outputs in the 1–100 W range with efficiencies of ~ 1% or slightly higher, using electrical inputs of 100 W to 10 kW into xenon or krypton-filled arc lamps. (Both laser rod and lamps must, of course, be carefully water-cooled.) Even ruby can, with some difficulty, be made to oscillate on a cw basis. We will discuss the very useful Nd^{3+} laser system in detail in later chapters.

The Helium-Neon Laser

Another of the most common and familiar types of laser is the helium-neon gas laser developed at the Bell Telephone Laboratories in 1960 and 1961. The laser tube in a He-Ne laser consists of a few Torr of helium combined with approximately one-tenth that pressure of neon inside a quartz plasma discharge tube, which is usually provided with an aluminum cold cathode and an anode, as in Figure 1.53. This discharge tube may be 10 to 50 cm long and a few mm in diameter in a typical small laser. To avoid broadening of the laser transition by isotope shifts (and for other more complex reasons), a mixture of single-isotope He^3 and Ne^{20} is usually employed; and it is found empirically that the optimum pressure-diameter product pd in such a laser is a few Torr-mm and that the optimum gain per unit length varies inversely with tube diameter d.

This tube is then excited with a dc discharge voltage typically of order 1,000 to 1,500 vdc, producing a dc current typically of order ~10 mA from a special

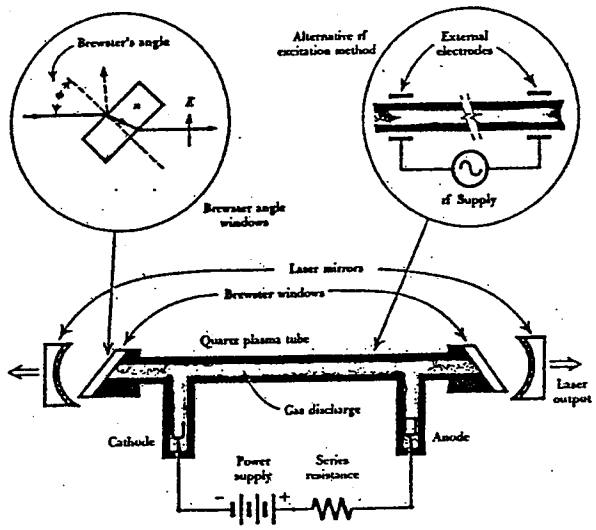

FIGURE 1.53
Elementary design for a helium-neon laser.

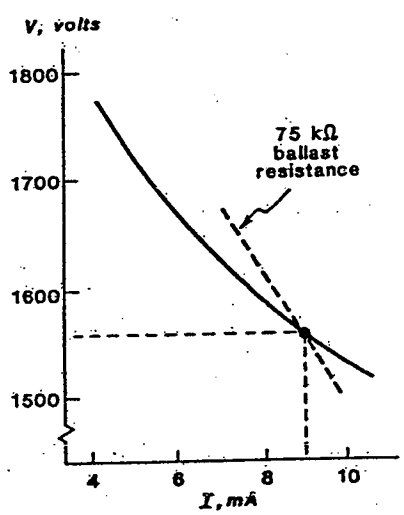

FIGURE 1.54
The glow discharge in a He-Ne laser tube has a negative-resistance I-V curve.

high-purity aluminum cold cathode. (Radio-frequency excitation through external electrodes was also employed in many early lasers, but has been found to be generally less convenient.) Because a dc glow discharge in this pressure range has a negative-resistance I-V curve (Figure 1.54), a ballast resistance in series with the dc voltage supply is necessary to stabilize the discharge; and an initial higher-voltage spike must be supplied to ionize the gas and break down the gas discharge each time the tube is turned on.

The discharge tubes in many gas lasers (especially with longer lasers, or lasers for research purposes) may be provided with Brewster-angle end windows which transmit light of the proper linear polarization with essentially zero reflection loss at either face. (Because of the very low gain in the He-Ne system, reflection losses of several percent at each of the air-dielectric interfaces would be totally intolerable.) In many small inexpensive internal-mirror He-Ne lasers, however,

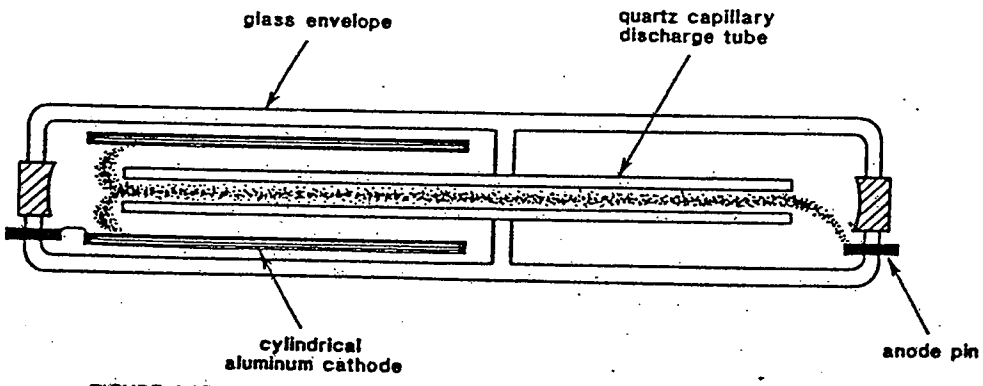

FIGURE 1.55
An internal-mirror He-Ne laser design.

the end mirrors are sealed directly onto the discharge tube, as part of the laser structure (Figure 1.55). Extreme cleanliness and purity of the laser gas fill is vital in the inherently low-gain He-Ne system; the tube envelope must be very carefully outgassed during fabrication, and a special aluminum cathode employed, at least in long-lived sealed-off lasers. The end mirrors themselves are carefully polished flat or curved mirrors with multilayer evaporated dielectric coatings, having as many as 21 carefully designed and evaporated layers to give power reflectivities in excess of 99.5% in some cases.

The pumping mechanism in the He-Ne laser is slightly more complex than those we have discussed so far. The helium gas, as the majority component, dominates the discharge properties of the He-Ne laser tube. Helium atoms have in fact two very long-lived or metastable energy levels, generally referred to as the 2^1S ("2-singlet-S") and 2^3S ("2-triplet-S") metastable levels, located ~20 eV above the helium ground level. Free electrons that are accelerated by the axial voltage in the laser tube and that collide with ground-state neutral helium atoms in the laser tube then can excite helium atoms up into these metastable levels, where they remain for long times.

There is then a fortuitous—and very fortunate—near coincidence in energy between each of these helium metastable levels and certain sublevels within the so-called $2s$ and $3s$ groups of excited levels of the neutral neon atoms, as shown in Figure 1.56. (The atomic energy levels in neon, as in other gases, are commonly labeled by means of several different forms of spectroscopic notation of various degrees of obscurity.)

When an excited He atom in one of the metastable levels collides with a ground-state Ne atom, the excited He atom may drop down and give up its energy, while the Ne atom simultaneously takes up almost exactly the same amount of energy and is thus excited upward to its near-coincident energy level. This important type of collision and energy-exchange process between the He and Ne atoms is commonly referred to as a "collision of the second kind." Any small energy defect in the process is taken up by small changes in the kinetic energy of motion of one or the other atom.

This process thus amounts to a selective pumping process, carried out via the helium atoms, which efficiently pumps neon atoms into certain specified excited energy levels. As Figure 1.56 shows, laser action is then potentially possible from these levels into various lower energy levels in the so-called $2p$ and $3p$ groups.

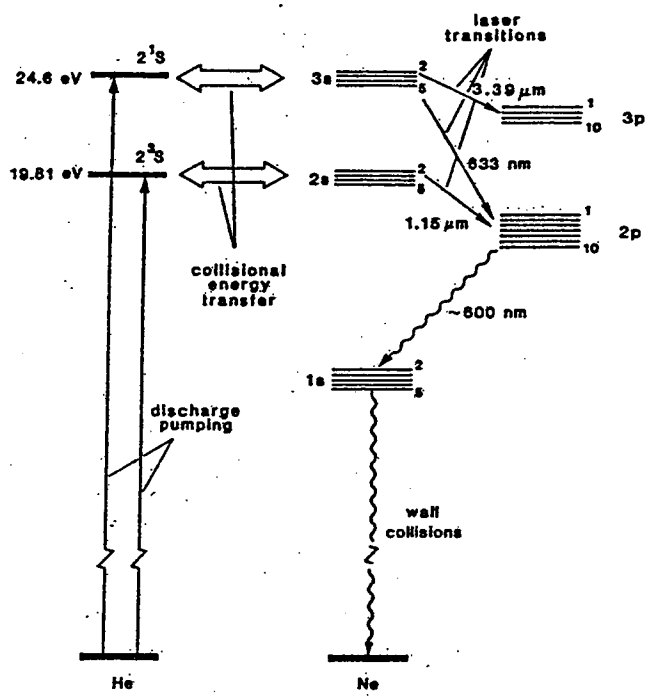

FIGURE 1.56
Energy levels in the He-Ne laser.

The first successful laser action in any gas laser was in fact accomplished by A. Javan and co-workers at Bell Labs in late 1960 on the $2s_2 \rightarrow 2p_4$ transition of helium-neon at 1.1523 microns in the near infrared. Shortly thereafter A. D. White and J. D. Rigden discovered that the same system would lase on the familiar and very useful $3s_2 \rightarrow 2p_4$ visible red transition at 633 nm (or 6328Å), as well as on a much stronger and quite high-gain set of $3s \rightarrow 3p$ transitions near 3.39 microns. (A half-dozen or so different nearby transitions within each of these groups can actually be made to lase, with the strongest transition in each group being determined in part by the relative pumping efficiencies into each sublevel and in part by the relative transition strengths of the different transitions.)

Characteristics of Gas Lasers

The laser gain in the He-Ne 633 nm system is quite low, with perhaps $2\alpha_m \approx 0.02$ to $0.1\ \text{cm}^{-1}$ (often expressed as "2% to 10% gain per meter"); and the typical power output from a small He-Ne laser may be 0.5 to 2.0 mW. With a dc power input of ~10 W, this corresponds to an efficiency of ~0.01%. Several manufacturers supply inexpensive self-contained laser tubes of this type for about $100 retail and considerably less in volume production. Such lasers are very useful as alignment tools in surveying, for industrial and scientific alignment purposes, supermarket scanners, video disk players, laser printers, and the like. (The dominance of the He-Ne laser in such applications may soon be ended by even cheaper and simpler semiconductor injection lasers.) Larger He-Ne lasers

with lengths of 1 to 2 meters that can yield up to 100 mW output at comparable efficiencies are also available.

There are also scores of other gas lasers that are excited by using electrical glow discharges, higher-current arc discharges, hollow-cathode discharges, and transverse arc discharges. One notable family of such lasers are the rare-gas ion lasers, including argon, krypton, and xenon ion lasers, in which much larger electron discharge currents passing through, for example, a He-Ar mixture can directly excite very high-lying argon levels to produce laser action in both singly ionized Ar^+ and doubly ionized Ar^{++} ions. Such ion lasers are generally larger than the He-Ne lasers, and even less efficient, but when heavily driven can produce from hundreds of milliwatts to watts of cw oscillation at various wavelengths in the near infrared, visible, and near ultraviolet. Longer-wavelength molecular lasers, such as the CO_2 laser, and shorter-wavelength excimer lasers are other examples of important gas laser systems.

REFERENCES

For a recent summary of practical laser systems and many of their applications, see, for example W. W. Duley, *Laser Processing and Analysis of Materials* (Plenum Press, 1983).

1.9 OTHER PROPERTIES OF REAL LASERS

Practical lasers in fact come in a great variety of forms and types, using many different kinds of atoms, molecules, and ions, in the form of gases, liquids, crystals, glasses, plastics, and semiconductors. These systems oscillate at a great many different wavelengths, using many different pumping mechanisms. Nearly all real lasers have, however, certain useful properties in common.

Temporal and Spatial Coherence

As we have discussed in some detail in earlier sections, nearly all lasers can be:

(a) *Very monochromatic.* Real laser oscillators can in certain near-ideal situations oscillate in a single, essentially discrete oscillation frequency, exactly like a coherent single-frequency electronic oscillator in more-familiar frequency ranges. This oscillation will, as with any other real oscillator, still have some very small residual frequency or phase modulation and drift, because of mechanical vibrations and thermal expansion of the laser structure and other noise effects, as well as small amplitude fluctuations due to power supply ripple and the like. Such a high-quality laser can still be, however, one of the most spectrally pure oscillators available in any frequency range.

More typically, a real laser device will oscillate in some number of discrete frequencies, ranging from perhaps 5 or 10 simultaneous discrete axial modes in narrower-line lasers up to a few thousand discrete and closely spaced frequencies in less well-behaved lasers with wider atomic linewidths.

UV Series

Photodiodes

Features

- Planar Diffused Structure
- Oxide Passivated
- Wide Spectral Range
- Flat Noise Spectrum to DC
- Linearity Over Wide Dynamic Range
- Peak Responsivity: 0.62 A/W at 900 Nanometers
- UV Responsivity: 0.14 A/W at 254 Nanometers
- Low Noise

Operating Data and Specifications at 23°C: Typical Performance at 0 V Bias

Characteristic	UV-040BG UV-040BQ	UV-100BG UV-100BQ	UV-215BG UV-215BQ	UV-250BG UV-250BQ	UV-360BG UV-360BQ	UV-444BQ	Units
Active Area	0.31	5.1	23.4	21.1	36.0	100	Sq. mm
Spectral Range[1]	250-1150						nm
	185-1150						
Responsivity	0.62	0.62	0.62	0.62	0.62	0.62	A/W at 900
Responsivity	0.14	0.14	0.14	0.14	0.14	0.14	A/W at 254
Responsivity[2]	0.08	0.08	0.08	0.08	0.08	0.08	A/W at 200
Capacitance	25	150	700	630	1100	2800	Picofarads
Shunt Resistance	>500	>100	>50	>75	>20	>10	Megohms
Noise Current	6	15	20	18	28	40	10^{-15} Amps/Hz$^{1/2}$
NEP (900,10,1)	1.0	2.5	3.0	2.8	4.3	6.2	10^{-14} W/Hz$^{1/2}$
NEP (200,10,1)	7.5	18	25	23	35	50	10^{-14} W/Hz$^{1/2}$
Response Linearity	<1%						Over 7 decades
Surface Uniformity	1%						With 0.13 mm Spot 633 nm
Temperature Coefficient of:							
Response (900 nm)	+0.03						%/°C
Response (350 nm)	−0.01						%/°C
Response (200 nm)	−0.13						%/°C
Shunt Resistance	−20						%/°C
Operating Temperature	−55 to +125 (BG)						°C
	−55 to +70 (BQ)						°C
Package Style	TO-5	TO-5	TO-8	TO-5	TO-8	TO-36	

Notes

1. Spectral range 185-1150 nm applies to units with BQ suffix, 250-1150 nm for units with BG suffix.
2. Applicable only to units with BQ suffix.

Typical Spectral Response

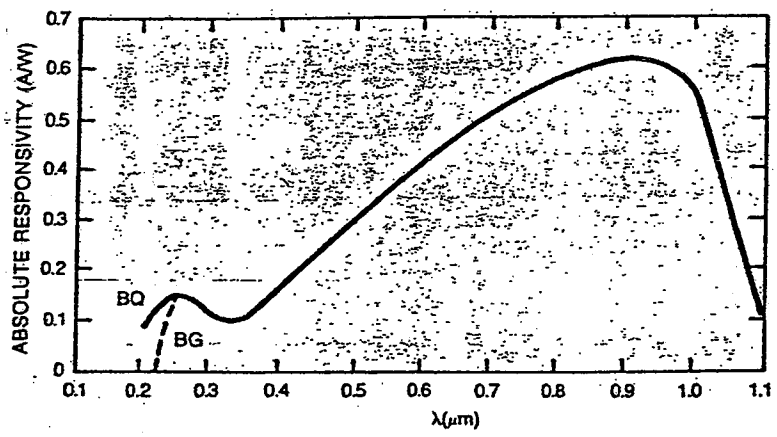

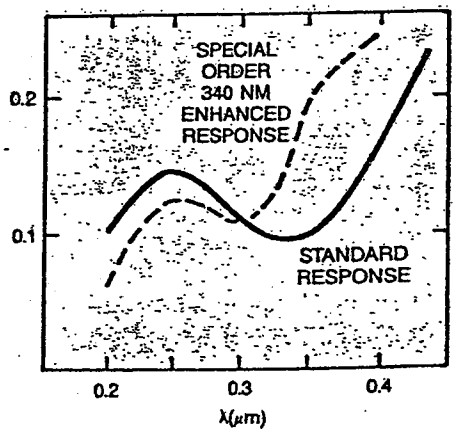

Mechanical Data and Pin Configurations

UV-040, 100, 215, 250, 360, 444

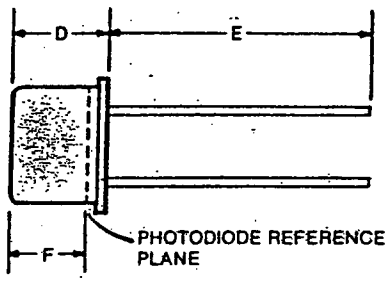

Dimension (mm)	040	100	215	250	360	444
A (Active Area)	1.0	2.5	5.5	4.6	6.0	11.3
B	8.3	8.3	12.3	8.3	12.6	27.8
C	9.0	9.0	13.8	9.0	14.6	31.8
D	4.2	4.2	4.6	4.2	5.7	7.1
E	>19	>19	>19	>19	>19	12.3
F	2.3	2.3	3.0	2.3	3.9	6.1
Pin Circle Radius	2.5	2.5	3.8	2.5	5.3	9.5
Window Thickness	1.0	1.0	1.0	1.0	1.0	1.6
Window Diameter	6.0	6.0	10.9	6.0	9.5	20.7

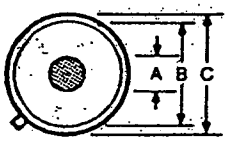

UV-100,444

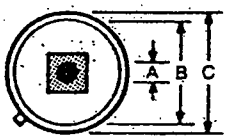

UV-040,215

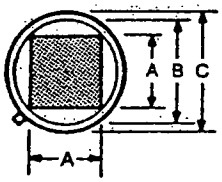

UV-250,360

Notes

1. Only UV-100 and UV-444 packages have apertures.
2. Only UV-040, UV-100, and UV-250 packages have tabs.
3. UV-250 and UV-360 active areas are square.

Typical deviation of responsivity with temperature

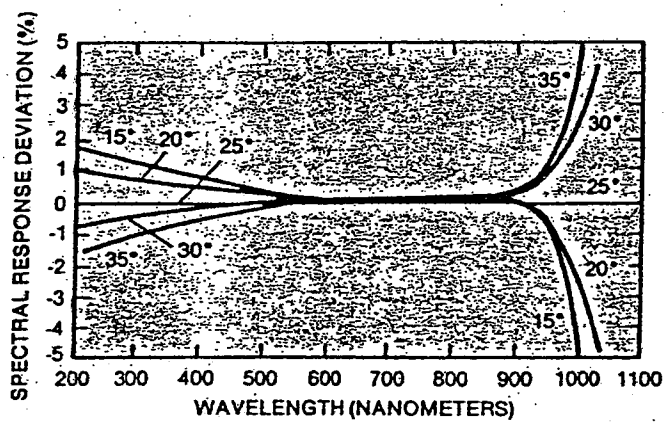

Typical shunt resistance change with temperature

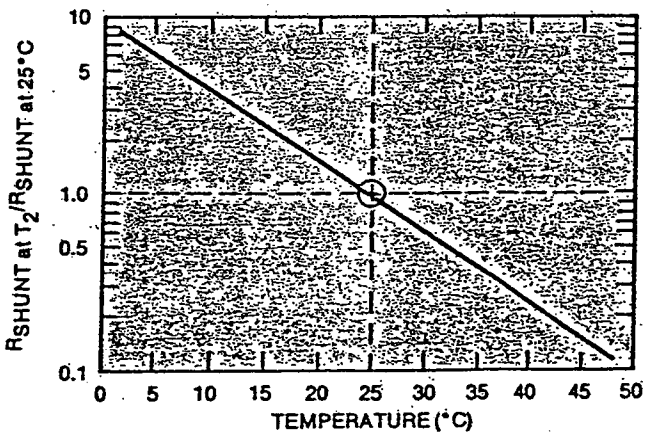

Glossary of Terms

1. **Breakdown Voltage (V_B)** — The voltage at which a semiconductor fails to withstand the voltage and ceases to act as an insulator. This point is generally defined as that voltage at which a predefined dark current is exceeded.

2. **Channel Impedance** — Photodiodes of guard ring construction have an impedance which appears between the active area and guard ring cathodes. The importance of the channel impedance is that it shunts the load resistor in the AC equivalent circuit, thereby restricting the maximum value of the load impedance that the designer may use in the operating circuit. The channel impedance is also a noise source which must be considered.

3. **Dark Current** — Photodiodes operating in the photoconductive or reverse biased mode will have some current flowing through the biasing circuit when no light is incident upon the photodiode. This dark current is a combination of surface and bulk leakage currents.

4. **Frequency Response** — The frequency at which the photocurrent is reduced to 0.707 (−3 dB) of the mid-band value is considered to be the frequency response limit. This definition may be used to describe both the upper frequency limit and, in the case of an AC coupled circuit, the lower frequency limit.

5. **Guard Ring** — Silicon photodiodes manufactured from P-type material utilize an additional cathode diffusion to reduce dark current induced noise caused by surface leakage. The surface leakage current is intercepted by the guard ring and shunted to ground, thus preventing this current from reaching the signal processing circuit.

6. **Junction Capacitance** — The junction capacitance of a silicon photodiode is analogous to the capacitance of a parallel plate capacitor having a voltage controlled plate separation. As such, the junction capacitance increases with an increase in active area and decreases with increasing bias voltage.

7. **Noise Current** — Photodiodes operating in the photovoltaic mode generate a thermal noise (Johnson noise) current that exhibits a flat noise vs. frequency spectrum from DC to approximately the photodiode cut-off frequency. The RMS value of the noise current is inversely proportional to the square root of the shunt resistance. Thermal noise is calculated by the formula:

$$i_t = \left(\frac{4kTdf}{R}\right)^{1/2}$$

where:
- k = Boltzmann's constant (1.38×10^{-23} joules/degree K)
- T = temperature (K)
- R = resistance (series, shunt, channel, or load)(ohms)
- df = noise equivalent bandwidth (Hertz)

Photodiodes operating in the photoconductive mode generate a noise current which is a combination of shot noise, excess noise (1/f), and thermal noise currents. Shot noise is calculated by the formula:

$$i_s = (2qI_d df)^{1/2}$$

where:
- q = electronic charge (1.6×10^{-19} coulombs)
- I_d = dark current (amps)
- df = noise equivalent bandwidth (Hertz)

8. **Noise Equivalent Power (NEP)** — A figure of merit which defines the minimum incident power required to generate a photocurrent equal to the total photodiode RMS noise current. NEP is calculated by the formula:

$$\text{NEP} = \frac{\text{Noise currents (amps) (RMS)}}{\text{Responsivity (amps/watt)}}$$

9. **Photoconductive (PC)** — The photoconductive or reverse biased p-n device is designed to detect high speed light pulses or the high frequency modulation of a continuous light beam. The photoconductive mode produces a high responsivity at the longer wavelengths, an extended frequency response due to lower junction capacitance, and series resistance time constant and a photocurrent that is linear with irradiance over an extended irradiance power range.

10. **Photovoltaic (PV)** — When a silicon p-n junction is operated with no external applied voltage, it is considered to be operating in the photovoltaic mode. Under this zero applied voltage condition and low levels of incident light, the p-n junction will generate a current proportional to the light power incident on the active surface. The photovoltaic operating mode results in low photodiode-generated shot noise, lower responsivity at the longer wavelengths, and lower frequency response due to higher junction capacitance and series resistance.

11. **Quantum Efficiency (QE)** — The number of electronic charges collected for each photon absorbed by the photodiode, expressed as a percentage, is the quantum efficiency. The quantum efficiency can be calculated by the formula:

$$QE = 124\% \ \frac{R}{\lambda}$$

where: R = responsivity (amperes/watt)
λ = wavelength (microns).

12. **Response Linearity** — The change in detector output versus the change in incident light power describes the response linearity. The low power limit is set by the detector noise where the noise current exceeds a predefined percentage of the signal. The high power limit is set by the self forward biasing conditions of the photodiode which limit the total amount of photocurrent that can be produced under the operating conditions.

13. **Responsivity** — The photocurrent produced per unit of incident light power at a specified wavelength is the photodiode responsivity. Responsivity is generally specified in amperes/watt (A/W).

14. **Rise Time (T_R)** — The amount of time to respond to an input step waveform is the rise time. The time is measured at the points which are 10% and 90% of the peak signal value.

15. **Series Resistance** — Photodiodes have an internal resistance through which the photocurrent flows. The photodiode series resistance is affected by the photodiode active area, silicon thickness, operating voltage, and the quality of electrode contacts.

16. **Shunt Resistance** — The dynamic resistance of a photovoltaic junction is defined by the slope of the dark I/V characteristic as it passes through zero volts. This resistance shunts the load resistance and the photocurrent source in the equivalent electrical circuit and is commonly referred to as the shunt resistance.

Basic Circuits

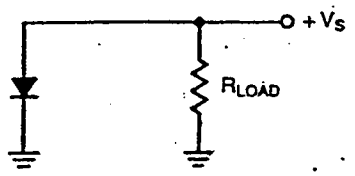

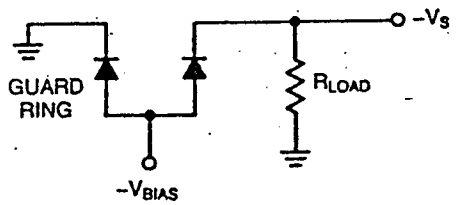

Load Resistor

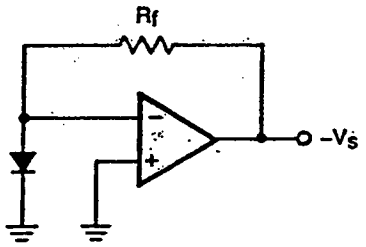

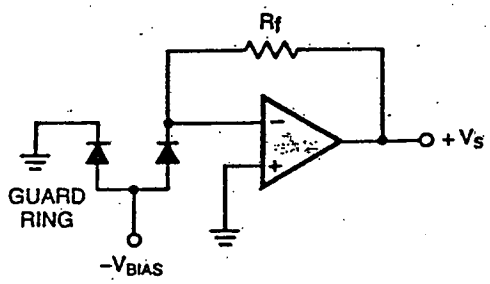

Operational Amplifier — Straight Feedback Loop

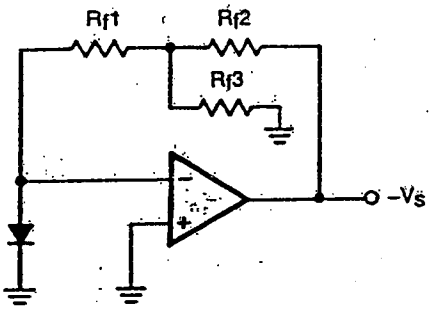

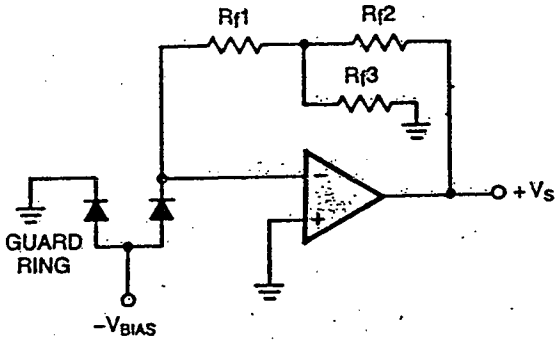

Operational Amplifier — T Feedback Loop

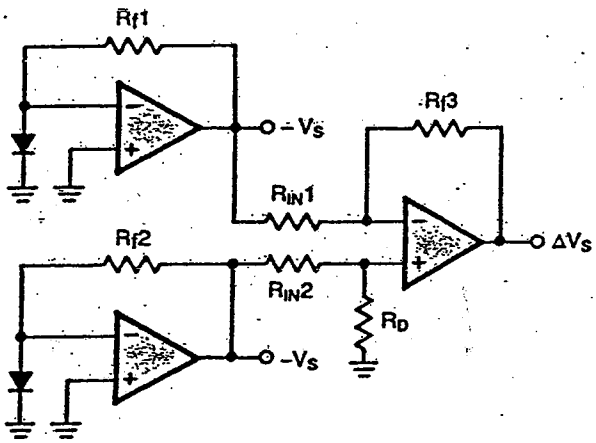

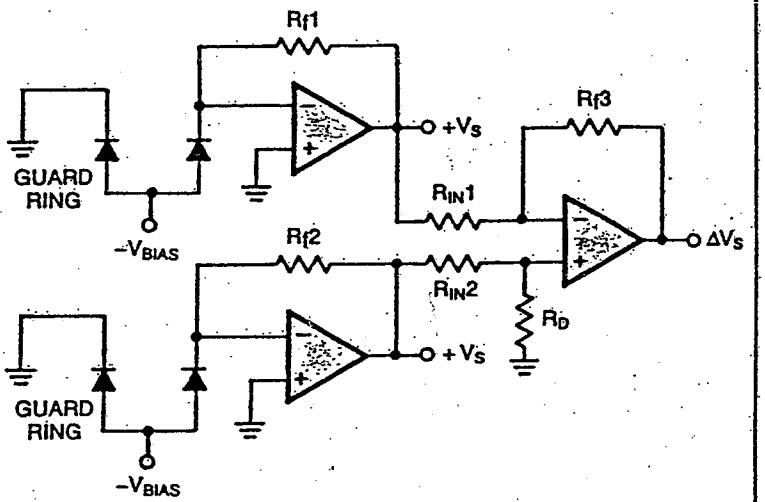

Differential Amplifier

Application Notes

1. Photo-Effect

When the junction of a semiconductor is illuminated and a connection is made to both sides of the junction, a current will flow during the period of illumination. This phenomenon is known as the photovoltaic effect, which is the operating mechanism for photovoltaic (PV) photodiodes and solar cells. In this case, there is no external bias applied and the cell generates an e.m.f. when illuminated.

If an external bias is applied in the reverse direction at the p-n junction, current will also flow under illumination. The current generated is composed of both the photo-induced current and the reverse leakage (dark) current. The reverse leakage current will remain constant for fixed bias and fixed temperature conditions. This is called the photoconductive (PC) mode.

In both modes of operation, PV and PC, the photocurrent will vary linearly with the intensity of the incident light.

2. Photovoltaic (PV) vs. Photoconductive (PC)

The photovoltaic detector is designed for low noise, low frequency applications. The PV frequency response, shunt resistance, and junction capacity are active area dependent. The equivalent noise current generated by the device at zero voltage is a virtually flat Johnson noise spectrum from DC to the cutoff frequency.

The photoconductive detector is designed to detect high speed light pulses or the high frequency modulation of a continuous light beam. The reverse voltage increases the junction field strength, which accelerates the electron/hole transit times. Reverse bias also reduces the junction capacity, thereby minimizing the capacitive loading effects on the frequency response. PC photodiodes may operate over frequencies from DC to over 1 GHz with rise times ranging from hundreds of picoseconds to tens of nanoseconds depending on operating conditions. The noise current generated by the PC photodiode is a combination of shot noise, excess noise, and, in the case of a guard ring structure device, Johnson noise. Shot noise is produced by the reverse bias current and exhibits a 1/f excess noise characteristic below 1 KHz. The Johnson noise is generated by the channel resistance between active area and guard ring diodes.

The design decision to use a PV or PC photodiode is predicated primarily on the frequency response requirements of the given application. Below 100 KHz, the PV photodiode provides better signal-to-noise performance than that obtained from an equivalent active area PC photodiode. Below 1 KHz, the PV photodiode is far superior in signal-to-noise performance.

3. Device Construction

All of the silicon photodiodes manufactured by EG&G Electro-Optics are of PIN construction. The P region is a layer which has been doped to a P+ level during a furnace diffusion process. The I region is the intrinsic bulk silicon which may be of either P or N type silicon. The N region is a layer which had been doped to a N+ level in another furnace diffusion process.

Figure 1 shows a cutaway view of a typical guard ring photodiode. The photodiode is fabricated from a P type silicon wafer of controlled thickness. A P+ diffusion is performed on the back surface to facilitate rear contacting. A N+ diffusion is performed on the front surface, using photo masking techniques, which accurately diffuses the active area and guard ring. Metal contacts are sputtered on the front and rear contact areas and the N+ diffusion is passivated.

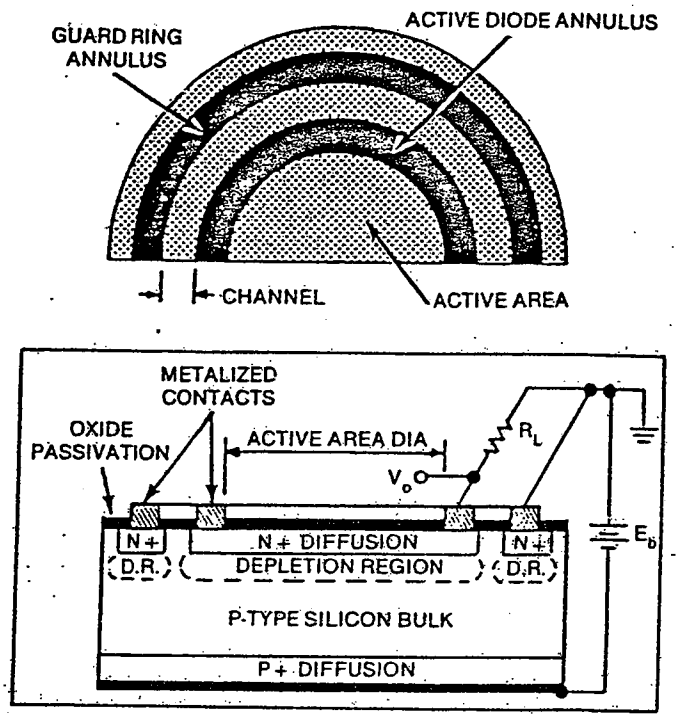

Figure 1. Guard ring planar diffused silicon photodiode.

The photodiode dark current is the sum of the reverse leakage through the bulk silicon and across the photodiode surface. The dark current leakage increases with increasing area. The surface leakage current increase is proportional to the square root of the active area while the bulk leakage current is directly proportional to the active area. Figure 2 shows the total dark current as a function of the area with and without the guard ring. Note that large area photodiodes do not have as significant a dark current reduction with the guard ring since a higher percentage of the dark current is due to bulk leakage. Under operating conditions where the active area and the guard ring are biased at the same potential, the surface leakage is shunted around the load resistor and flows through the guard ring to ground. In this manner, the much lower bulk leakage becomes the limiting source of shot noise current through the load resistor. Since the shot noise current of the detector varies directly as the square root of the leakage current, the total noise performance of the detector is greatly improved by the addition of a guard ring to detectors manufactured from P type material.

EG&G PHOTON DEVICES
35 CONGRESS STREET, P.O. BOX 5006, SALEM, MA 01970-6526
TEL: (617) 745-3200 TLX: 881-7405 EGGSA UW

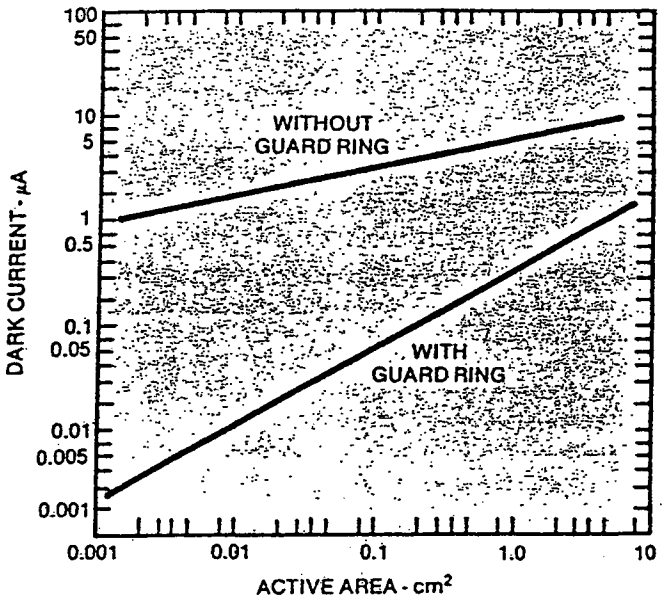

Figure 2. Photodiode dark current vs. active area.

Generally only detectors made of P type material are manufactured with guard rings due to the difference in the basic properties of the two materials. N type material does not have nearly as high a surface leakage as P type material; therefore guard rings typically are not used.

4. Photodiode Equivalent Circuits

The electrical equivalent circuits for N type and P type detectors are shown in Figures 3 and 4, respectively. The flow of photocurrent is in a direction so as to develop a load voltage which will forward bias the ideal diode. It is the development of this forward voltage across the ideal diode which determines the high power limit for linear response. Application of a voltage in the reverse direction across the ideal diode will extend the high power limit for linear response.

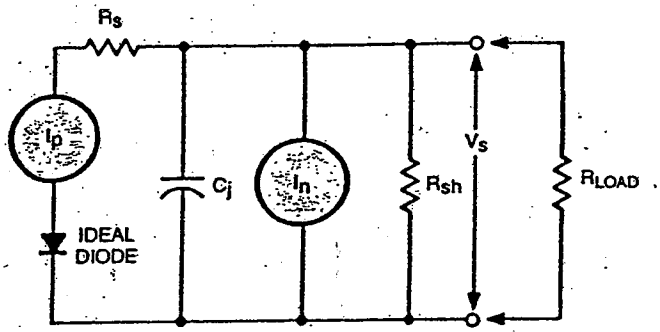

Symbols

I_p = Photocurrent generator
C_j = Junction capacitance
I_n = Noise current generator
R_{sh} = Shunt resistance
R_s = Series resistance
V_s = Signal voltage

Figure 3. N type material.

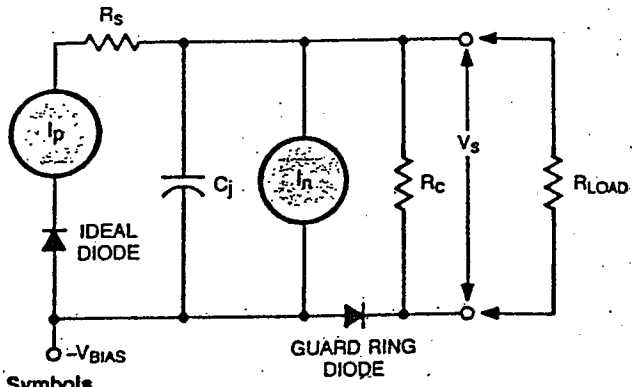

Symbols

I_p = Photocurrent generator
C_j = Junction capacitance
I_n = Noise current generator
R_c = Channel resistance
R_s = Series resistance
V_s = Signal voltage

Figure 4. P type material.

5. Silicon Photodiode Characteristics

Planar diffused photodiodes are usually fabricated from material having a range of resistivity from 10 to 10,000 ohm-cm. The resistivity of the silicon and the bias voltage determine the junction depletion depth, junction capacitance, responsivity profile, series resistance, response time, and dark current. A nomograph has been prepared that permits rapid determination of photodiode depletion depth and junction capacitance for a given resistivity, active area, and operating bias. Figure 5 is the nomograph that shows these parameters and their interdependence.

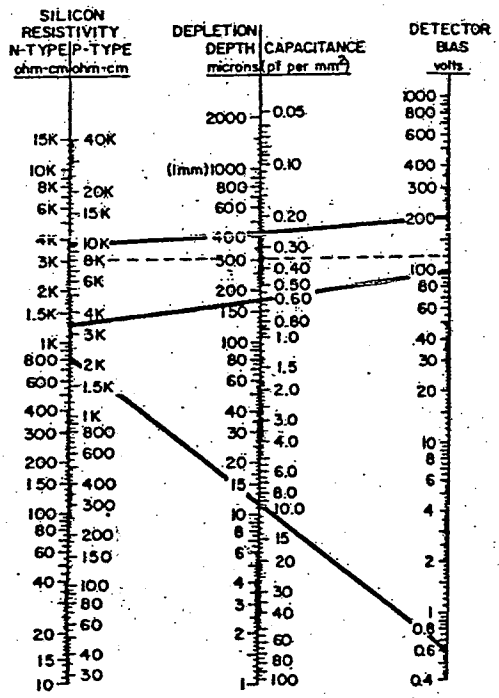

Figure 5. Resistivity/depletion depth/capacitance/bias voltage nomograph.

6. Detector Biasing

Photodiodes are designed to be operated at specific bias voltages which are dictated by the operating conditions. Whenever possible, the user should follow the recommendations of the device data sheet in order to achieve optimum performance. Circuit designers should be aware that, if a device is not operated at the recommended bias voltage, many of the operating charcteristics listed in the data sheet will change. The nomograph of Figure 5 shows some of the changes which are bias voltage dependent. The following is a list of parameters and the effect that an increase of bias voltage has on them:

A.	Dark current	Increases
B.	Noise current	Increases
C.	Junction capacitance	Decreases
D.	Series resistance	Decreases
E.	Channel resistance	Increases
F.	Depletion depth	Increases
G.	Infra-red responsivity	Increases
H.	Rise and fall time	Decreases

7. Capacitance

Junction capacitance, in conjunction with load impedance and series resistance, can produce a system RC time constant that will be in excess of the photodiode charge collection time. It is for this reason that the system designer should determine the value of the junction capacitance and its relative importance to the particular application.

The junction capacitance of a photodiode can be determined for various bias voltages using the nomograph of Figure 5 if the active area and the silicon resistivity are known. A straight line drawn from the proper value on the Resistivity scale to the operating voltage on the Detector Bias scale will intersect the Capacitance scale at some point. This capacitance constant multiplied by the photodiode active area, in square millimeters, will be the value of the photodiode junction capacitance in picofarads.

The voltage at which the junction capacitance becomes constant for increasing values of applied voltage is called the full depletion voltage. The full depletion voltage can be determined from the Figure 5 nomograph. A straight line drawn from the proper value on the Resistivity scale through a value on the Depletion Depth scale equal to the detector thickness will intersect the Detector Bias scale at the voltage at which full depletion occurs. The example shown on the nomograph illustrates a detector manufactured of 8 Kohm-cm, P type material, 300 microns thick. The full depletion bias voltage for this device is 120 volts.

8. Series Resistance

Series resistance is an important parameter to consider in high frequency applications. When the junction transit time is minimized, the limiting factor for high frequency operation is the RC time constant. This is the product of the junction capacitance and the sum of the series plus load resistances.

In an equivalent electrical diagram, the series resistance appears in the series with the photodiode junction impedance. The resistance of the undepleted bulk silicon can be calculated from the following formula:

$$R = \frac{\varrho}{A} L$$

where: ϱ = Resistivity of the silicon (ohm-cm)
L = Photodiode thickness less the depletion depth (cm)
A = Active area (sq cm)

In addition to the resistance of the undepleted bulk silicon, the resistance of electrode contacts must also be considered. Contact resistance may vary from 10 to 100 ohms, depending on the geometry of the contact. When choosing detectors for high speed applications, proper contact design is essential.

One resistance to the photocurrent which is often overlooked is the spreading resistance. This resistance appears between the point where the carriers are generated and the electrode contact where the photocurrent is collected. This resistance is difficult to quantify, as each case is different; however, this resistance is related to the distance the carriers must travel across the surface of the silicon. For optimum high speed performance, the active area should be as close to the illuminating spot size as possible.

9. Response Time

The photodiode response time is the root-mean-square sum of the charge collection time in the depletion region and the RC time produced by the series plus load resistance and junction plus stray capacitance. The charge collection time is bias voltage dependent and is equal to approximately one half the depletion depth divided by the carrier drift velocity. Photon energy absorbed outside the depletion region will produce carriers that are collected by diffusion and the response time of these carriers will be much slower than the carriers swept from the depletion region. Under certain biasing conditions, a photodiode can have a fast response time for short wavelengths and a slower response time for long wavelengths.

In the majority of applications, the designer will find that the limiting factor in photodiode response time will be the RC time. In a RC limited situation, the photodiode operating bandwidth will be equal to $1/(2\pi RC)$ or $0.159/RC$, and the rise time (10% to 90%) to a step waveform of radiation will be equal to 2.2 RC. The fall time from a step waveform will be equal to the RC time plus the carrier life time. Carrier life time produces a delay in the start of fall time due to the fact that photon generated carriers are still being swept out of the depletion region. The rise and fall times are generally equal for fully depleted photodiodes but are dissimilar when the photodiode is operated in the photovoltaic mode or at low bias voltages.

10. Spectral Response

The photodiode responsivity profile is directly related to the depletion depth obtained for a given operating bias voltage and silicon resistivity. The following equation is

EG&G PHOTON DEVICES
35 CONGRESS STREET SALEM, MA 01970
TEL (617) 745-3200 TWX: 310-681-7405

given to illustrate the dependence of the relative responsivity on the silicon resistivity.

$$I = I_0 (1 - e^{\delta t}) \frac{q}{hc} \lambda$$

where:
- I = Photocurrent (amps)
- I_0 = Maximum photocurrent for total photon absorption (amps)
- λ = Wavelength (microns)
- δ = Absorption coefficient of silicon at λ (cm^{-1})
- h = Planck's constant (6.624×10^{-27} ergs/second)
- c = Velocity of light (2.998×10^{8} meters/second)
- t = Depletion depth (cm)

At 1.06 microns, the absorption coefficient of silicon is approximately 35 cm^{-1}. The depletion depth obtained with 10 ohm-cm silicon with 90 volts bias is 1×10^{-3} cm as compared to 15×10^{-3} cm for 2500 ohm-cm silicon. Substituting these values into the efficiency equation indicates that the 10 ohm-cm photodiode will respond to 3.5% of the total 1.06 micron radiation but the 2500 ohm-cm photodiode will respond to 41% of the total 1.06 micron radiation. In both cases, surface reflection losses are assumed to be identical and are not included in the efficiency values. In order to complete the spectral response profile, it is necessary to consider the short wavelength response for the two photodiodes. At 0.45 micron, the absorption coefficient of silicon is approximately 3.4×10^{4} cm^{-1}. Computing the value of I will show that both detectors will respond to 100% of the 0.45 micron radiation. Reflection losses have been ignored in this case also.

Figure 6 presents typical relative spectral responses for the two cases previously described. The two responsivity curves have been normalized to the peak of the 2500 ohm-cm curve.

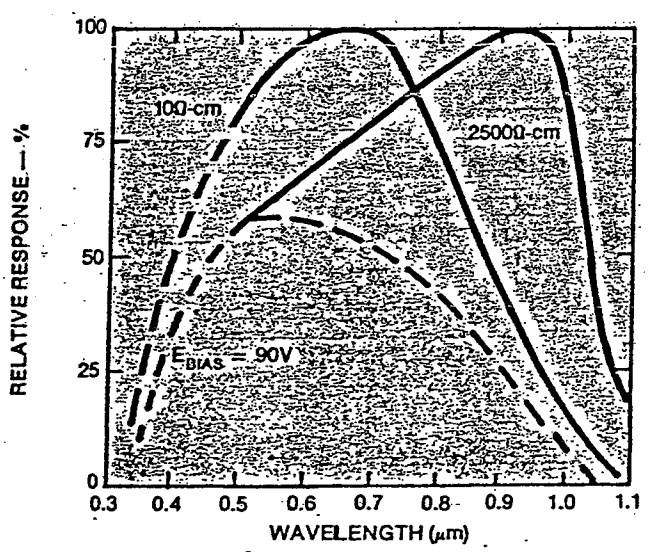

Figure 6. Relative spectral response.

The dashed portion of the responsivity curve for wavelengths below 0.50 micron is an approximation due to the difficulty in accurately determining the effects of the reflection losses and the front window absorption losses in this wavelength region. The front window is a term used to describe the front surface of the silicon in which the photons are absorbed but do not contribute to the photocurrent. The front window thickness for photodiodes without antireflective coatings is typically 0.20 micron. The absolute responsivity peak for the 2500 ohm-cm curve is 0.52 A/W. Manufacturers of planar diffused photodiodes have demonstrated the ability to improve monochromatic responsivity by 10% to 30% by the application of antireflective coatings to the detector active area.

Photodiodes of very high efficiency at long wavelengths can be produced using thick, very high resistivity silicon. Consider the case of a photodiode manufactured from 40,000 ohm-cm, P type silicon. Operating this device at 300 volts bias will result in a depletion depth of 0.1 cm. Calculating the value of I for 1.06 micron radiation will show that this photodiode will respond to 97% of the total 1.06 micron radiation. Reflection losses, again, have been ignored.

11. Quantum Efficiency

Figure 7 shows a typical spectral response curve for a UV enhanced photodiode operating at 0 volts bias. The spectral range is from 0.19 to 1.1 microns. The responsivity curve, for this device, typically peaks at 0.9 micron with a responsivity of approximately 0.62 A/W.

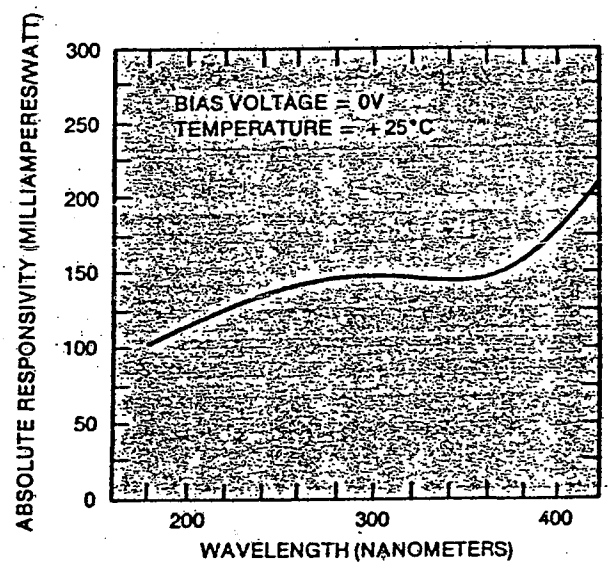

Figure 7. Typical spectral response - UV series.

Figure 8 is the quantum efficiency curve for the responsivity given in Figure 7. The quantum efficiency is calculated from the formula:

$$Q.E. = \frac{hc}{q} \times \frac{R}{\lambda} \times 100\% = \frac{S}{\lambda} \times 124\%$$

where:
- h = Planck's constant (6.624×10^{-27} ergs/second)
- c = Velocity of light (2.998×10^{8} meters/second)
- q = Electronic charge (1.6×10^{-19} coulombs)
- R = Responsivity (A/W)
- λ = Wavelength (microns)

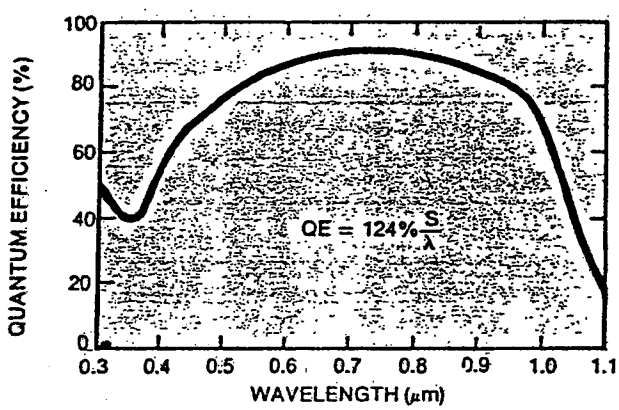

Figure 8. Typical quantum efficiency — UV series.

12. Noise — Photoconductive Mode

The noise current generated by a planar diffused photodiode operating in the reverse bias mode is a combination of shot noise, excess noise, and thermal (Johnson) noise.

Shot noise is generated by current flowing through the device. This current may be either the dark current or the photocurrent; however, the predominant shot noise generator is the dark current. The shot noise produced by the dark current can be calculated by the formula:

$$I_s = (2qI_D\,\Delta f)^{1/2}$$

where: q = Electronic charge (1.6×10^{-19} coulombs)

I_D = Dark current (amperes)

Δf = Noise equivalent bandwidth (hertz)

Below 1 KHz, the shot noise increases with a 1/f characteristic and is referred to as excess noise.

The thermal noise contribution is provided by the series resistance, load resistance, and, in the case of a guard ring device, the channel resistance. The thermal noise current is equal to:

$$I_t = \left(\frac{4kT\Delta f}{R}\right)^{1/2}$$

where: k = Boltzmann's constant (1.38×10^{-23} joules/°K)

T = Temperature (K)

Δf = Noise equivalent bandwidth (hertz)

R = Resistance: series, channel, or load (ohms)

The interrelation of these noise sources can be seen by referring to Figure 9, which is a noise model for a guard ring structured, planar diffused photodiode operating under reverse bias.

The designer is normally interested in the total noise present at the input to the preamplifier or, as shown in Figure 9, the total noise voltage, V_n, present across the load resistor.

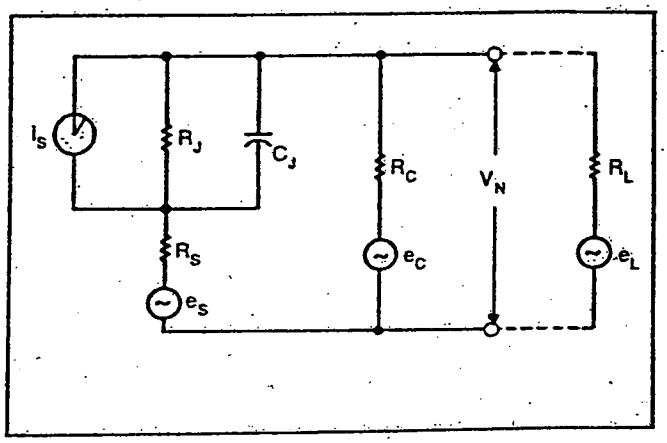

$$i_s = (2qI_D\,\Delta f)^{1/2}$$
$$e_C = (4kTR_C\,\Delta f)^{1/2}$$
$$e_S = (4kTR_S\,\Delta f)^{1/2}$$
$$e_L = (4kTR_L\,\Delta f)^{1/2}$$

Figure 9. Noise model for reverse biased, guard ring structured photodiode.

To simplify the analysis, it is assumed that $R_L < R_C$. If in practice R_L is significant with respect to R_C, then the designer can calculate their equivalent parallel resistance.

The total noise voltage present across R_L is the square root of the sum of the squared noise voltages as follows:

$$e_{n\ total} = (e_1^2 + e_2^2 + e_3^2)^{1/2}$$

where:

$$e_1 = \frac{e_S R_L}{[(R_L + R_S)^2 \frac{1}{\omega^2} C_{j2}]^{1/2}}$$

$$e_2 = \frac{e_L(1+\omega^2 C_{j2} R_{S2})^{1/2}}{[1+\omega^2 C_{j2}(R_L+R_S)^2]^{1/2}}$$

$$e_3 = \frac{i_S R_L}{[1+\omega^2 C_{j2}(R_L+R_S)^2]^{1/2}}$$

The preceding three equations relate the spot noise voltage at a specific operating frequency. The operating bandwidth of the individual noise generators (e_1, e_2, e_3) can be computed from the relationship: $f_{-3dB} = 0.159/RC$. This operating bandwidth can be converted to a noise bandwidth by multiplying f_{-3dB} by the factor 1.59, assuming a 6 dB/octave rolloff slope.

13. Noise — Photovoltaic Mode

The shunt resistance generates a thermal noise current that exhibits a flat noise vs. frequency spectrum from DC to approximately the photodiode cutoff frequency. The RMS value of the noise current is inversely proportional to the square root of the shunt resistance as shown in the following Johnson (thermal) noise formula:

$$i_{nt} = \left(\frac{4kT\,\Delta f}{R_{sh}}\right)^{1/2}$$

where: k = Boltzmann's constant (1.38×10^{-23} joules/°K)

T = Temperature (K)

Δf = Noise equivalent bandwidth (hertz)

R_{sh} = Shunt resistance (ohms)

14. Noise Equivalent Power (NEP)

In many photodiode applications, the designer is concerned with the minimum detectable power of the photodiode. The noise equivalent power (NEP) figure of merit defines the minimum incident power required to generate a photocurrent equal to the total photodiode noise current. In formula form, this would appear as:

$$\text{NEP} = \frac{\text{Noise current (Amps)}}{\text{Responsivity (Amps/Watt)}}$$

It should be noted that NEP is an ambiguous figure of merit if the test conditions are not specified. Experienced designers will qualify a value of NEP by specifying the test conditions in parenthetic notation as follows:

NEP (source wavelength, test frequency, noise bandwidth)

Example:

NEP (900 nm, 10 Hz, 1 Hz) = 3×10^{-15} Watts/Hz$^{1/2}$

Photodiode manufacturers generally specify NEP for the photodiode only, and do not consider the noise contribution from other sources in the circuit.

15. Response Linearity — Photoconductive Mode

The reverse biased photodiode signal current is linear over a wide range of irradiance. It is limited at high irradiance levels by the permissible power dissipation quoted for the device, providing that the load plus series resistances are not current limiting. At low irradiance levels, the signal linearity is limited by the shot noise current for the operating bandwidth, neglecting any measurement system noise.

Some general rules for determining maximum linear signal are:

$$e_{signal}\,(V) \le 0.3 \times V_{BIAS}$$

$$i_{signal}\,(A) \le \frac{0.3 \times V_{BIAS}}{R_S + R_L}$$

The photodiode will have a linear operating range of 7 to 9 decades when followed by a properly designed circuit. The range for 1% linearity is defined as being from 100 times the noise, 100:1 S/N, to the point at which the detector response deviates from the predicted response curve by 1%. Greater range can be achieved if larger deviations can be tolerated.

16. Response Linearity — Photovoltaic Mode

In low light level applications, the linearity limit is determined by the noise current for the operating noise bandwidth. At high irradiance levels, the limit is determined by the forward voltage which appears across the junction and the rate at which the carriers can be swept from the junction. The following formula for determining maximum linear photocurrent is based on empirical evaluations of photovoltaic photodiodes.

$$I_{pm} = \left(\frac{25 \times 10^{-3}}{R_S + R_L}\right) \log_e \left(\frac{P \times R_{sh}}{R_S + R_L}\right)$$

The active area dependency of the series and shunt resistances creates a singular linearity solution for each photodiode. Figure 10 is a graphical presentation of a 1% linearity equation for the various photodiode active areas normally encountered in instrument applications.

If photodiodes are used in conjunction with a load resistor, the response to incident light may become nonlinear well before the current levels shown in Figure 10 are reached. The linear range of a photodiode is also limited by the forward voltage generated across the diode junction by the photocurrent flowing through the series and load resistors. For linear response:

Load voltage $\le 100 \times 10^{-3}$ V

Linearity will also be affected if current densities are too high. The low field strength of photovoltaic diode junctions limits the rate at which the carriers can be swept from the junction. For linear response:

Current density $\le 50 \times 10^{-6}$ A/sq. mm of illuminated area

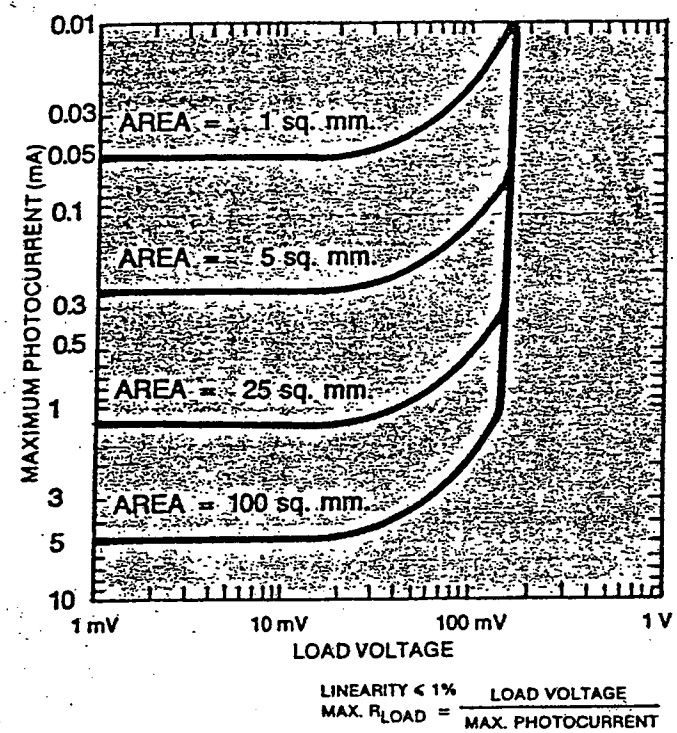

Figure 10. Maximum photocurrent for ≤1% linearity.

The maximum radiant power density for linear response can be calculated from the following formula:

$$\text{Maximum power density} = \frac{\text{Maximum current density}}{\text{Responsivity at } \lambda}$$

17. Response Uniformity

The uniformity of response is dependent upon the qualities of the window, the photodiode front surface, and the phodiode rear surface. In applications where the incident light is focused on the detector surface, the window should be clean but minor imperfections can be ignored. In applications where the light spot is small and from a collimated source, it is important that the window be of uniform quality.

In applications where the operating wavelength is less than approximately 900 nm, the quality of the diode front surface is most important. The front surface must be clean and free of contamination and any antireflective coatings must be uniform and free of holes. This is especially true in applications where there is no protective window. The response uniformity is inversely proportional to the illuminated area; therefore, surface condition is critical in situations where a small light spot is used. A high quality protodiode should exhibit response uniformity of better than ±1% with a spot size ≥0.13 mm.

At wavelengths longer than approximately 900 nm, photons start to penetrate the silicon, deep enough to reach the back surface. The rear surface is partially reflective and its condition is a factor in long wavelength applications.

In applications where all of the light energy must be kept within the photodiode active area, the ideal spot size is the active area dimension minus the beam movement dimension. In the case of a photodiode with an active area diameter of 2.54 mm and a beam movement of 1 mm, the ideal spot size for the most uniform response would be 1.54 mm.

18. Angular Response

The responsivity of a photodiode is quoted for incident radiation that is normal to the plane surface of the photodiode active area. When the angle of incidence varies from the normal angle of incidence, the photodiode response will decrease by a factor that approximates the cosine of the incident angle. The angular response is wavelength dependent and is greatly affected by the active area reflectivity. Figure 11 shows the typical deviation from a true cosine response for a planar diffused, oxide passivated photodiode for two wavelengths of incident radiation. Reflections from package surfaces will also affect angular response.

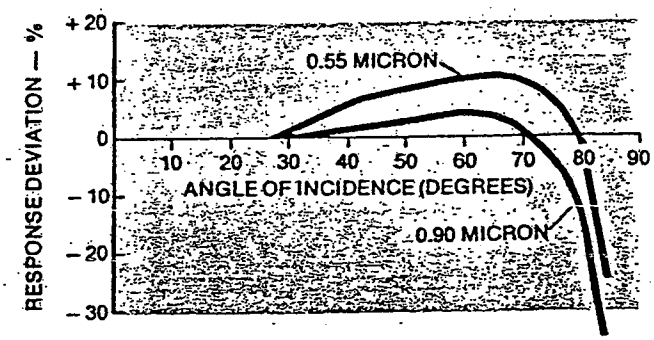

Figure 11. Typical deviations (%) from true cosine response vs. angle of incidence.

19. Responsivity vs. Temperature

Photodiode responsivity is temperature dependent. The responsivity temperature coefficient value is wavelength dependent. Typically, the temperature coefficient for wavelengths shorter than 700 nm is negative; at wavelengths longer than 700 nm, the temperature coefficient is positive. Figure 12 is a table of responsivity temperature coefficient vs. wavelength data for two photodiode types.

EG&G PHOTON DEVICES
35 CONGRESS STREET, P.O. BOX 5006, SALEM, MA 01970-8526
TEL: (617) 745-3200 TLX: 681-7405 EGGSA UW

Wavelength (Nanometers)	Temperature Coefficient[1] (%/°C)	Temperature Coefficient[2] (%/°C)
200	—	−0.18
250	—	−0.16
300	—	−0.14
350	—	−0.10
400	−0.14	0
450	−0.06	+0.009
500	−0.003	+0.018
550	−0.002	+0.027
600	−0.001	+0.036
650	−0	+0.045
700	0	+0.055
750	+0.003	+0.064
800	+0.010	+0.072
850	+0.015	+0.090
900	+0.030	+0.22
950	+0.060	+0.30
1000	+0.30	+0.51
1060	+1.01	+1.51

1. SGD series at 90 V bias
2. UV series at 0 V bias

Figure 12. Typical responsivity temperature coefficients.

The equation to calculate the photodiode responsivity at a different temperature is:

$$\text{Responsivity 2} = \text{Responsivity 1} \times \left(1 + \frac{\text{Temp. coef. (\%/°C)}}{100}\right)^{T_2 - T_1}$$

where: Responsivity 1 = Known responsivity at λ
Temp. Coef. = Photodiode temperature coefficient at λ
T_2 = New temperature
T_1 = Starting temperature

20. Photodiode/Operational Amplifier Combination: Linearity

The operational amplifier, when used as a current to voltage converter, creates a unique solution to the linearity limitations imposed on photodiodes by the terminating load impedance. In this transimpedance configuration, the photodiode views a load impedance as shown in the following equation:

$$Z_a = \frac{R_f}{A[1 + (\omega R_f C_f)^2]^{1/2}}$$

This equation shows that at low frequencies the apparent photodiode load impedance is very low but it increases with increasing frequency. With the availability of open-loop amplifier gains that exceed 10^5 at DC, it is evident that photodiode signal gain can be accomplished over a reasonable frequency range without the loss of response linearity. A good approximation of the photodiode/operational amplifier response linearity can be determined by the substitution of Z_a for R_L in the linearity equations for both photovoltaic and photoconductive modes.

It is important to remember that operational amplifiers do not have the same dynamic range as a silicon photodiode and that the linearity range may be limited by the amplifier. If an amplifier has an RMS noise voltage of 1 mV at the output and a maximum output of 13 V (±15 V supply), then this is a maximum range of just over 4 decades. If the output signal voltage is limited to 100 mV, 100:1 S/N) at the low end and 10 V at the high end, this is only 2 decades of linear output signal voltage. This linear range limitation makes the proper choice of feedback resistor value an important design consideration.

21. Operational Amplifier Transimpedance

When used in conjunction with a silicon photodiode, an operational amplifier is used in the transimpedance mode as a current-to-voltage converter. In this mode, the photocurrent, or dark current, is converted to a voltage by an impedance in the feedback loop. When operating at DC, the output signal voltage is proportional to the feedback resistor value and can be calculated from the formula:

$$E_{out} = I_{in} \times R_f$$

This formula does not consider any offset voltages. This subject is covered in Section 23.

The term "gain" does not apply to the transimpedance mode of operation. Gain is the ratio of the amplifier output to the amplifier input and both terms must be the same: volts/volts; amps/amps; watts/watts. In the transimpedance mode, the input and output terms are different; therefore, the term "gain" does not apply.

It should be noted that the formula for E_{out} does not reflect the closed loop "gain peaking" that can occur because of the summation of the open loop gain and the related phase angle with the transimpedance and its associated phase angle. If the open loop gain and feedback gain are added algebraically and compared to the sum of the respective phase angles, it may become evident that a sum positive gain will occur at the frequency where the sum phase angle crosses 180 degrees. This situation of positive gain at 180 degrees phase angle is generally referred to as "gain peaking" and most designers recognize this situation as being the basis for amplifier instability.

The cause of gain peaking in photodiode/op-amp combinations is the total capacity presented at the amplifier input which must be driven in the closed loop configuration by the output voltage through the feedback impedance. The solution to gain peaking is to add a small amount of capacitance across the feedback resistor so as to modify the closed loop gain/phase angle relationship. Figure 13 depicts gain peaking in a typical photodiode/op-amp combination where the detector is a large area, photovoltaic photodiode. The curves show the results of adding small amounts of capacitance across the feedback resistor.

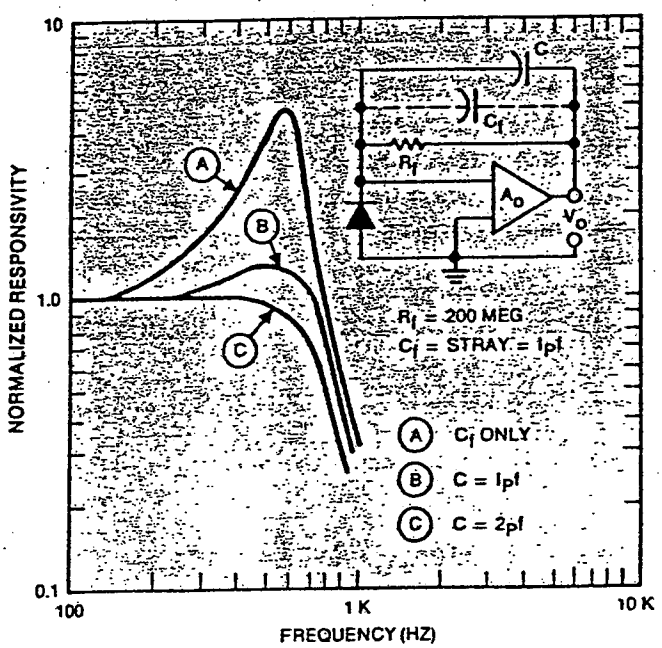

Figure 13. Gain peaking in photodiode/op-amp circuit.

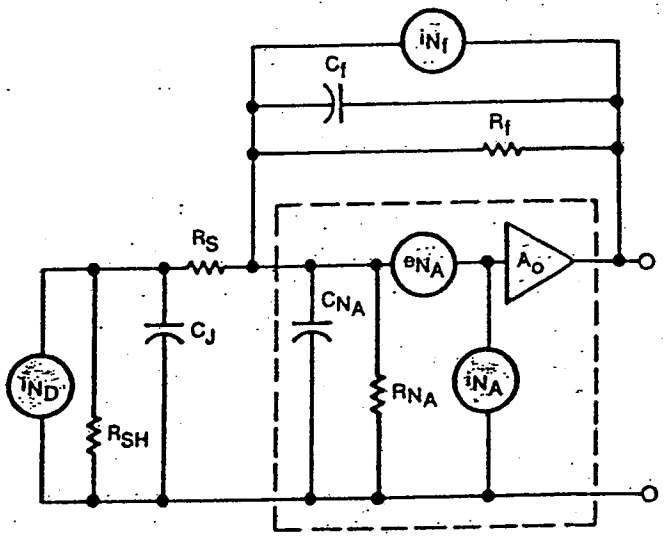

SYMBOLS

A_o = NOISELESS AMPLIFIER WITH FREQUENCY DEPENDENT GAIN

i_{N_f} = JOHNSON NOISE CURRENT OF FEEDBACK RESISTOR

i_{N_D} = JOHNSON NOISE CURRENT OF PHOTOVOLTAIC PHOTODIODE (DUE TO SHUNT RESISTANCE)

i_{N_A} = AMPLIFIER INPUT NOISE CURRENT — FREQUENCY DEPENDENT

e_{N_A} = AMPLIFIER INPUT NOISE VOLTAGE — FREQUENCY DEPENDENT

R_{N_A} = AMPLIFIER INPUT RESISTANCE

C_{N_A} = AMPLIFIER INPUT CAPACITY

Figure 14. Photodiode/op-amp electrical model.

22. Photodiode/OP-AMP Noise Characteristics

The various noise generators which contribute to the total output noise voltage of a photodiode/op-amp combination are shown in Figure 14. For large area photovoltaic detectors, the output noise voltage at frequencies greater than 50 Hz is determined by the amplifier noise voltage generator, the photodiode impedance, and the feedback impedance. In most cases, gain peaking of the noise voltage will occur but this can be controlled as previously discussed. From 10-50 Hz, the total noise voltage is affected by the combination of photodiode noise current, amplifier input noise current, and the value of feedback resistance. Below 10 Hz, the magnitude of the 1/f characteristic of the amplifier noise current will tend to control the magnitude of the output noise. Figure 15 is a plot of the output noise voltage for a large area photovoltaic detector coupled to a typical operational amplifier. Note in Figure 15 how the noise performance is improved by the addition of a 2 picofarad feedback capacitance.

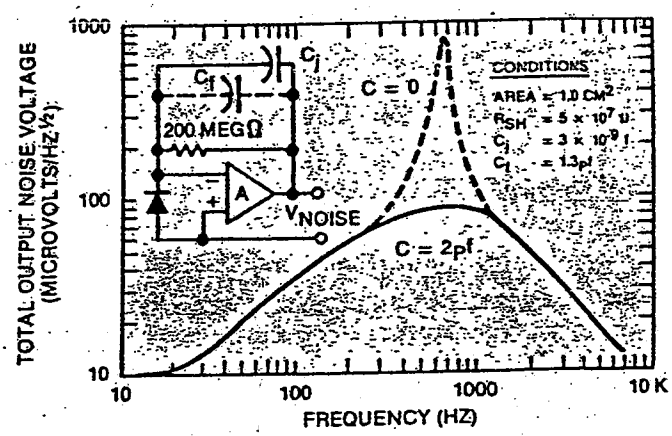

Figure 15. Total output noise vs. frequency.

EG&G PHOTON DEVICES
35 CONGRESS STREET, P.O. BOX 5006, SALEM, MA 01970-6526
TEL: (617) 745-3200 TLX: 681-7405 EGGSA UW

Smaller active area photodiodes with larger shunt resistance and lower junction capacitance will produce a lower noise and extend the gain peaking to a higher frequency.

As gain peaking is determined by the individual characteristics of feedback impedance, amplifier gain/phase angle, and photodiode source impedance, it becomes difficult to define an accurate total noise equation. A reasonable solution is to neglect gain peaking, which can be compensated, and to define the total noise by its contributing sources. The following equation is derived from Figure 14, where the various noise generators are identified. This provides a good approximation of the total noise present at the output of the photodiode/op-amp combination.

$$e_{n_T} = Z_f \left[\frac{(e_{n_A})^2}{Z_s} + i_{n_A}^2 + i_{n_{sh}}^2 + i_{n_f}^2 \right]^{1/2}$$

where: $Z_f = R_f(1 + \omega^2 C_{f2} R_{f2})^{1/2}$

$Z_s = R_{sh} / (1 + \omega^2 C_{j2} R_{sh2})^{1/2}$

$i_{n_{sh}} = \left(\frac{4KT\,\Delta f}{R_{sh}}\right)^{1/2}$

$i_{n_f} = \left(\frac{4KT\,\Delta f}{R_f}\right)^{1/2}$

In applications involving large area photodiodes, the amplifier input noise voltage generator is the major contributor to the total output noise voltage. Therefore, it is important, in these applications, to select an operational amplifier that has a minimum value of input noise voltage. Conversely, in applications involving small area photodiodes, the optimum noise performance is obtained with an operational amplifier having a very low value associated with the input noise current generator.

23. Amplifier Output Offset Voltage

The DC offset voltage present at the output terminal of a photodiode/op-amp combination is a function of feedback resistance, shunt resistance for a PV photodiode, and dark current for a PC photodiode. The equation for determining DC output offset voltage is:

$$e_{offset} = (V_{offset} + \Delta V_{offset})\left(1 + \frac{R_f}{R_{sh}}\right) + [(i_B + i_D) \times R_f]$$

where: V_{offset} = Amplifier input offset voltage (volts)

ΔV_{offset} = Amplifier input offset voltage drift (V/°C)

R_f = Feedback resistor (ohms)

R_{sh} = Photodiode shunt resistance (ohms)

i_B = Amplifier input bias current (amperes)

i_D = Photodiode dark current (amperes)

This equation has three terms, R_{sh}, i_B, and i_D, which have a nonlinear dependence on temperature. When calculating DC offset voltages for temperatures other than those given in the data sheet presented earlier in this catalog, it is important to consider the temperature effects.

The equation to calculate shunt resistance at a different temperature is:

$$R_{sh2} = R_{sh1} / 2^{(T_2 - T_1)/6}$$

where: R_{sh1} = Known shunt resistance at temperature T_1 (ohms)

T_1 = Starting temperature (degrees C)

T_2 = New temperature (degrees C)

The equation to calculate either photodiode dark current or amplifier input bias current at different temperature is:

$$i_{B2} = i_{B1} / 2^{(T_2 - T_1)/10}$$

$$i_{D2} = i_{D1} / 2^{(T_2 - T_1)/10}$$

where: i_{B1} = Known input bias current at temperature T_1 (amperes)

i_{D1} = Known dark current at temperature T_1 (amperes)

T_1 = Starting temperature (degrees C)

T_2 = New temperature (degrees C)

Optics (Hecht) Addison Wesley (1987, 2nd Ed.)

8.3.3 Polaroid

In 1928 Edwin Herbert Land, then a 19-year-old undergraduate at Harvard College, invented the first dichroic sheet polarizer, known commercially as *polaroid J-sheet*. It incorporated a synthetic dichroic substance called *herapathite*, or *quinine sulfate periodide*.* Land's own retrospective account of his early work is rather informative and makes fascinating reading. It is particularly interesting to follow the sometimes whimsical origins of what is now, no doubt, the most widely used group of polarizers. The following is an excerpt from Land's remarks:

> In the literature there are a few pertinent high spots in the development of polarizers, particularly the work of William Bird Herapath, a physician in Bristol, England, whose pupil, a Mr. Phelps, had found that when he dropped iodine into the urine of a dog that had been fed quinine, little scintillating green crystals formed in the reaction liquid. Phelps went to his teacher, and Herapath then did something which I [Land] think was curious under the circumstances; he looked at the crystals under a microscope and noticed that in some places they were light where they overlapped and in some places they were dark. He was shrewd enough to recognize that here was a remarkable phenomenon, a new polarizing material [now known as herapathite]....
>
> Herapath's work caught the attention of Sir David Brewster, who was working in those happy days on the kaleidoscope.... Brewster, who invented the kaleidoscope, wrote a book about it, and in that book he mentioned that he would like to use herapathite crystals for the eyepiece. When I was reading this book, back in 1926 and 1927, I came across his reference to these remarkable crystals, and that started my interest in herapathite.

Land's initial approach to creating a new form of linear polarizer was to grind herapathite into millions of submicroscopic crystals, which were naturally needle-shaped. Their small size lessened the problem of the scattering of light. In his earliest experiments the crystals were aligned nearly parallel to each other by means of magnetic or electric fields. Later Land found that they would be mechanically aligned when a viscous colloidal suspension of the herapathite needles was extruded through a long narrow slit. The resulting *J*-sheet was effectively a large flat dichroic crystal. The individual submicroscopic crystals still scattered light a bit, and as a result, *J*-sheet was somewhat hazy. In 1938 Land invented *H-sheet*, which is now probably the most widely used linear polarizer. It does not contain dichroic crystals but is instead a molecular analogue of the wire grid. A sheet of clear polyvinyl alcohol is heated and stretched in a given direction, its long hydrocarbon molecules becoming aligned in the process. The sheet is then dipped into an ink solution rich in iodine. The iodine impregnates the plastic and attaches to the straight long-chain polymeric molecules, effectively forming a chain of its own. The conduction electrons associated with the iodine can move along the chains as if they were long thin wires. The component of **E** in an incident wave that is parallel to the molecules drives the electrons, does work on them, and is strongly absorbed. The transmission axis of the polarizer is therefore perpendicular to the direction in which the film was stretched.

Each separate miniscule dichroic entity is known as a *dichromophore*. In *H*-sheet the dichromophores are of molecular dimensions, so scattering represents no problem. *H*-sheet is a very effective polarizer across the

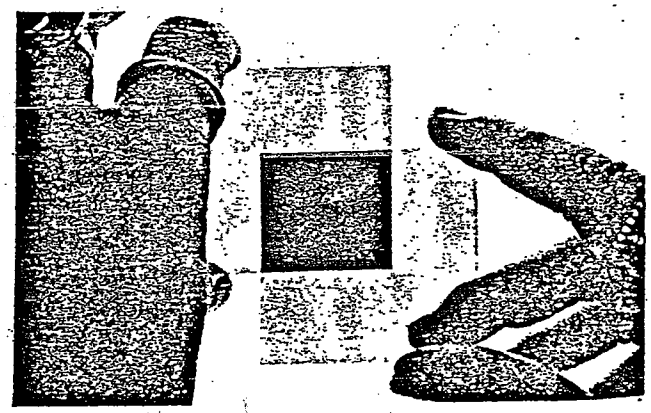

Figure 8.14 A pair of crossed polaroids. Each polaroid appears gray because it absorbs roughly half the incident light. (Photo by E.H.)

* E. H. Land, "Some Aspects of the Development of Sheet Polarizers," *J. Opt. Soc. Am.* 41, 957 (1951).

entire visible spectrum but is somewhat less so at the blue end. When a bright white light is viewed through a pair of crossed *H*-sheet polaroids, as in Fig. 8.14, the *extinction* color will be a deep blue as a result of this leakage. *HN*-50 would be the designation of a hypothetical, ideal *H*-sheet having a *neutral color* (*N*) and transmitting 50% of the incident natural light while absorbing the other 50%, which is the undesired polarization component. In practice, however, about 4% of the incoming light will be reflected back at each surface (antireflection coatings are not generally used), leaving 92%. Half of this is presumably absorbed, and thus we might contemplate an *HN*-46 polaroid. Actually, large quantities of *HN*-38, *HN*-32, and *HN*-22, each differing by the amount of iodine present, are produced commercially and are readily available (Problem 8.7).

Many other forms of polaroid have been developed.* *K-sheet*, which is humidity- and heat-resistant, has as its dichromophore the straight-chain hydrocarbon polyvinylene. A combination of the ingredients of *H*- and *K*-sheets leads to *HR-sheet*, a near-infrared polarizer.

Polaroid vectograph is a commercial material designed to be incorporated in a process for making three-dimensional photographs. The stuff never was successful at its intended purpose, but it can be used to produce some rather thought-provoking, if not mystifying, demonstrations. Vectograph film is a water-clear plastic laminate of two sheets of polyvinyl alcohol arranged so that their stretch directions are at right angles to each other. In this form there are no conduction electrons available, and the film is not a polarizer. Using an iodine solution, imagine that we draw an *X* on one side of the film and a *Y* overlapping it on the other. Under natural illumination the light passing through the *X* will be in a $\mathcal{P}$-state perpendicular to the $\mathcal{P}$-state light coming from the *Y*. In other words, the painted regions form two crossed polarizers. They will be seen superimposed on each other. Now, if the vectograph is viewed through a linear polarizer that can be rotated, either the *X*, the *Y*, or both will be seen. Obviously, more imaginative drawings can be made (one need only remember to make the one on the far side backward).

* See *Polarized Light: Production and Use*, by Shurcliff, or its more readable little brother, *Polarized Light*, by Shurcliff and Ballard.

8.4 BIREFRINGENCE

Many crystalline substances (i.e., solids whose atoms are arranged in some sort of regular repetitive array) are *optically anisotropic*. In other words, their optical properties are not the same in all directions within any given sample. The dichroic crystals of the previous section are but one special subgroup. We saw there that if the crystal's lattice atoms were not completely symmetrically arrayed, the binding forces on the electrons would be anisotropic. Earlier, in Fig. 3.25(b) we represented the isotropic oscillator using the simple mechanical model of a spherical charged shell bound by identical springs to a fixed point. This was a fitting representation for *optically isotropic* substances (amorphous solids, such as glass and plastic, are usually, but not always, isotropic). Figure 8.15 shows another charged shell, this one bound by springs of differing stiffness (i.e., having different spring constants). An electron that is displaced from equilibrium along a direction parallel to one set of "springs" will evidently oscillate with a different characteristic frequency than it would were it displaced in some other direction. As we have pointed out previously (Section 3.5.2), light propagates through a transparent substance by exciting the electrons within the medium. The electrons are driven by the **E**-field and they reradi-

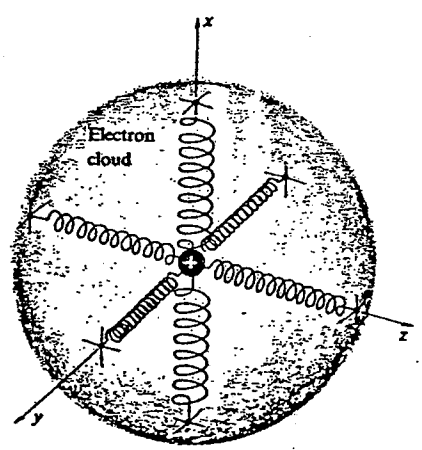

Figure 8.15 Mechanical model depicting a negatively charged shell bound to a positive nucleus by pairs of springs having different stiffness.

Optics Hecht (Addison-Wesley (1987, 2nd Ed.)

10.2 FRAUNHOFER DIFFRACTION

10.2.1 The Single Slit

Return to Fig. 10.8, where now the point of observation is very distant from the coherent line source and $R \gg D$. Under these circumstances $r(y)$ never deviates appreciably from its midpoint value R, so that the quantity $(\mathcal{E}_L/R)$ at P is essentially constant for all elements dy. It follows from Eq. (10.9) that the field at P due to the differential segment of the source dy is

$$dE = \frac{\mathcal{E}_L}{R} \sin(\omega t - kr)\, dy, \tag{10.10}$$

where $(\mathcal{E}_L/R)\, dy$ is the amplitude of the wave. Notice that the phase is much more sensitive to variations in $r(y)$ than is the amplitude, so that we will have to be more careful about introducing approximations into it. We can expand $r(y)$, in precisely the same manner as was done in Problem (9.13), to make it an explicit function of y; thus

$$r = R - y \sin\theta + (y^2/2R)\cos^2\theta + \cdots, \tag{10.11}$$

where θ is measured from the xz-plane. The third term can be ignored so long as its contribution to the phase is insignificant even when $y = \pm D/2$; that is, $(\pi D^2/4\lambda R)\cos^2\theta$ must be negligible. This will be true for all values of θ when R is adequately large. We now have the **Fraunhofer condition**, where the distance r is linear in y: the distance to the point of observation and therefore the phase can be written as a linear function of the aperture variables. Substituting into Eq. (10.10) and integrating leads to

$$E = \frac{\mathcal{E}_L}{R} \int_{-D/2}^{+D/2} \sin[\omega t - k(R - y\sin\theta)]\, dy, \tag{10.12}$$

and finally

$$E = \frac{\mathcal{E}_L D}{R} \frac{\sin[(kD/2)\sin\theta]}{(kD/2)\sin\theta} \sin(\omega t - kR). \tag{10.13}$$

To simplify the appearance of things let

$$\beta = (kD/2)\sin\theta, \tag{10.14}$$

so that

$$E = \frac{\mathcal{E}_L D}{R}\left(\frac{\sin\beta}{\beta}\right)\sin(\omega t - kR). \tag{10.15}$$

The quantity most readily measured is the irradiance (forgetting the constants) $I(\theta) = \langle E^2 \rangle$ or

$$I(\theta) = \frac{1}{2}\left(\frac{\mathcal{E}_L D}{R}\right)^2 \left(\frac{\sin\beta}{\beta}\right)^2, \tag{10.16}$$

where $\langle \sin^2(\omega t - kR)\rangle = \frac{1}{2}$. When $\theta = 0$, $\sin\beta/\beta = 1$ and $I(\theta) = I(0)$, which corresponds to the *principal maximum*. *The irradiance resulting from an idealized coherent line source in the Fraunhofer approximation* is then

$$I(\theta) = I(0)\left(\frac{\sin\beta}{\beta}\right)^2 \tag{10.17}$$

or, using the *sinc function* (Section 7.9 and Table 1 of the Appendix),

$$I(\theta) = I(0)\,\mathrm{sinc}^2\,\beta.$$

There is symmetry about the y-axis, and this expression holds for θ measured in any plane containing that axis. Notice that since $\beta = (\pi D/\lambda)\sin\theta$, when $D \gg \lambda$, the irradiance drops extremely rapidly as θ deviates from zero. This arises from the fact that β becomes very large for large values of length D (a centimeter or so when using light). The phase of the line source is equivalent, by way of Eq. (10.15), to that of a point source located at the center of the array, a distance R from P. Finally, a relatively long coherent line source ($D \gg \lambda$) can be envisioned as a single point emitter radiating predominantly in the forward, $\theta = 0$, direction; in other words, its emission resembles a circular wave in the xz-plane. In contrast, notice that if $\lambda \gg D$, β is small, $\sin\beta \approx \beta$, and $I(\theta) \approx I(0)$. The irradiance is then constant for *all* θ, and the line source resembles a point source emitting spherical waves.

We can now turn our attention to the problem of Fraunhofer diffraction by a slit or elongated narrow rectangular hole (Fig. 10.9). An aperture of this sort might typically have a width of several hundred λ and a length of a few centimeters. The usual procedure to follow in the analysis is to divide the slit into a series of long differential strips (dz by ℓ) parallel to the y-axis,

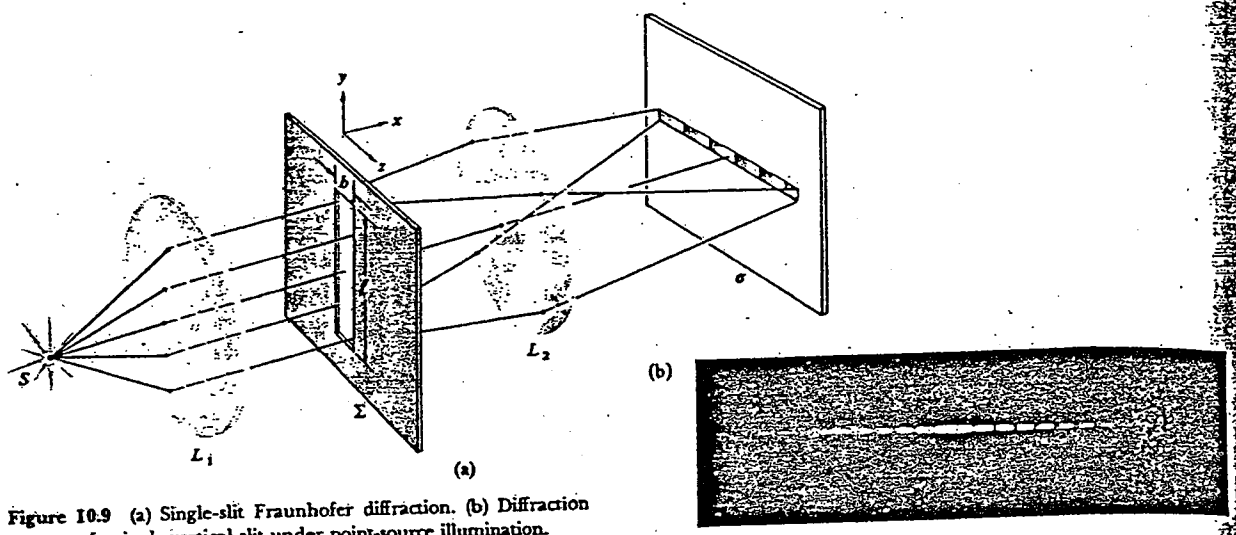

Figure 10.9 (a) Single-slit Fraunhofer diffraction. (b) Diffraction pattern of a single vertical slit under point-source illumination.

as shown in Fig. 10.10. We immediately recognize, however, that each strip is a long coherent line source and can therefore be replaced by a point emitter on the z-axis. In effect, each such emitter radiates a circular wave in the ($y = 0$ or) xz-plane. This is certainly reasonable, since the slit is long and the emerging wavefronts are practically unobstructed in the slit direction. There will thus be very little diffraction parallel to the edges of the slit. The problem has been reduced to that of finding the field in the xz-plane due to an infinite number of point sources extending across the width of the slit along the z-axis. We then need only evaluate the integral of the contribution dE from each element dz in the Fraunhofer approximation. But once again, this is equivalent to a coherent line source, so that the complete solution for the slit is, as we have seen,

$$I(\theta) = I(0)\left(\frac{\sin\beta}{\beta}\right)^2, \qquad (10.17)$$

provided that

$$\beta = (kb/2)\sin\theta \qquad (10.18)$$

and θ is measured from the xy-plane (see Problem 10.3). Note that here the line source is short, $D = b$, β is not large, and although the irradiance falls off rapidly, higher-order subsidiary maxima will be observable. The extrema of $I(\theta)$ occur at values of β that cause $dI/d\beta$ to be zero, that is,

$$\frac{dI}{d\beta} = I(0)\frac{2\sin\beta(\beta\cos\beta - \sin\beta)}{\beta^3} = 0. \qquad (10.19)$$

The irradiance has minima, equal to zero, when $\sin\beta = 0$, whereupon

$$\beta = \pm\pi, \pm 2\pi, \pm 3\pi, \ldots. \qquad (10.20)$$

It also follows from Eq. (10.19) that when

$$\beta\cos\beta - \sin\beta = 0$$

$$\tan\beta = \beta. \qquad (10.21)$$

The solutions to this transcendental equation can be determined graphically, as shown in Fig. 10.11. The points of intersection of the curves $f_1(\beta) = \tan\beta$ with the straight line $f_2(\beta) = \beta$ are common to both and so satisfy Eq. (10.21). Only one such extremum exists between adjacent minima (10.20), so that $I(\theta)$ must have subsidiary maxima at these values of β ($\pm 1.4303\pi$, $\pm 2.4590\pi$, $\pm 3.4707\pi, \ldots$).

There is a particularly easy way to appreciate what's happening here with the aid of Fig. 10.12. We envision every point in the aperture emitting rays in all directions in the xz-plane. The light that continues to propagate directly forward in Fig. 10.12(a) is the undiffracted beam, all the rays arrive on the viewing screen in phase,

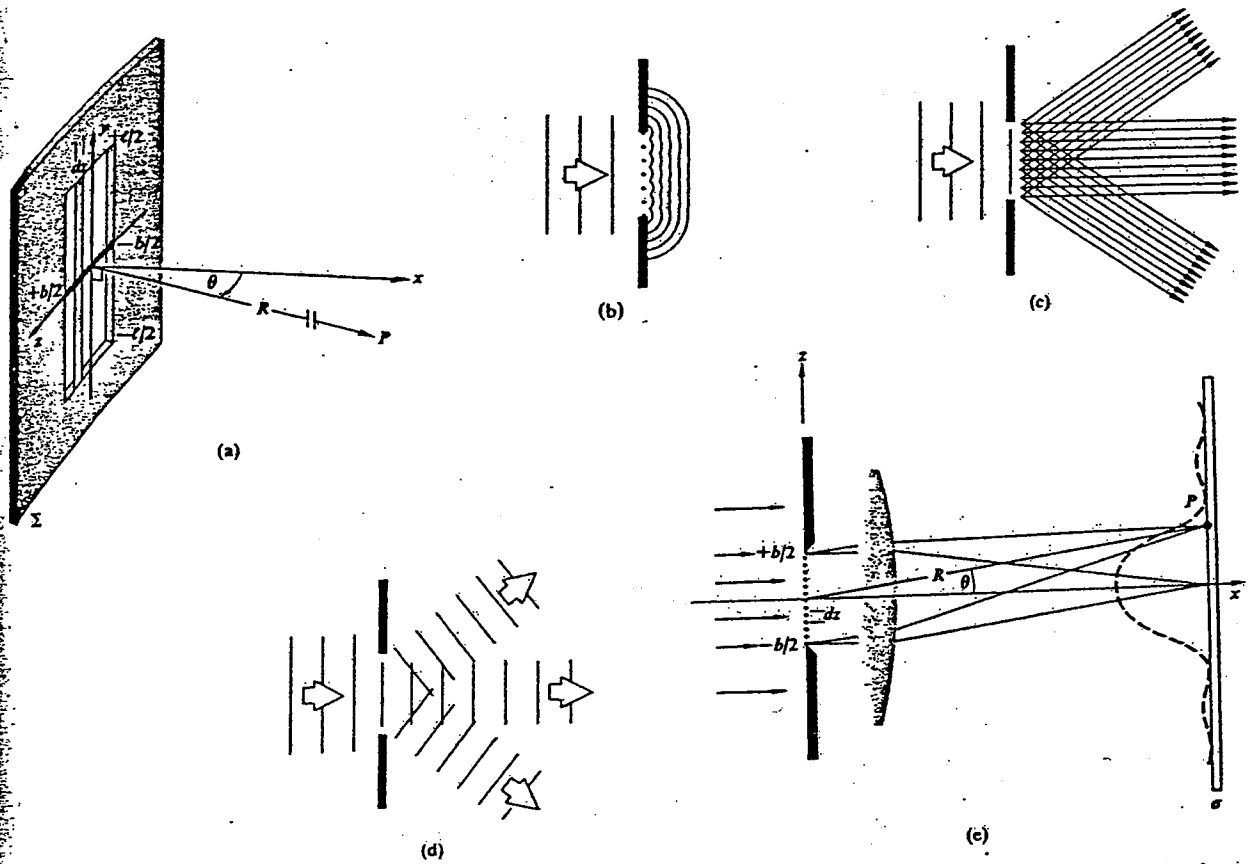

Figure 10.10 (a) Point P on σ is essentially infinitely far from Σ. (b) Huygens wavelets emitted across the aperture. (c) The equivalent representation in terms of rays. Each point emits rays in all directions. The parallel rays in various directions are seen. (d) These ray bundles correspond to plane waves, which can be thought of as the three-dimensional Fourier components. (e) A single slit illuminated by monochromatic plane waves.

and a central bright spot will be formed by them. If the screen is not actually at infinity, the rays that converge to it are not quite parallel but with it at infinity, or better still, with a lens in place, the rays are as drawn. Figure 10.12(b) shows the specific bundle of rays coming off at an angle θ_1 where the path-length difference between the rays from the very top and bottom, $b \sin \theta_1$, is made equal to one wavelength. A ray from the middle of the slit will then lag $\frac{1}{2}\lambda$ behind a ray from the top and exactly cancel it. Similarly, a ray from just below center will cancel a ray from just below the top, and so on; all across the aperture ray-pairs will cancel, yielding a minimum. The irradiance has dropped from its high central maximum to the first zero on either side at $\sin \theta_1 = \pm\lambda/b$.

As the angle increases further, some small fraction of the rays will again interfere constructively, and the irradiance will rise to form a subsidiary peak. A further increase in the angle produces another minimum, as shown in Fig. 10.12(c), when $b \sin \theta_2 = 2\lambda$. Now imagine the aperture divided into quarters. Ray by ray, the top quarter will cancel the one beneath it, and the next, the

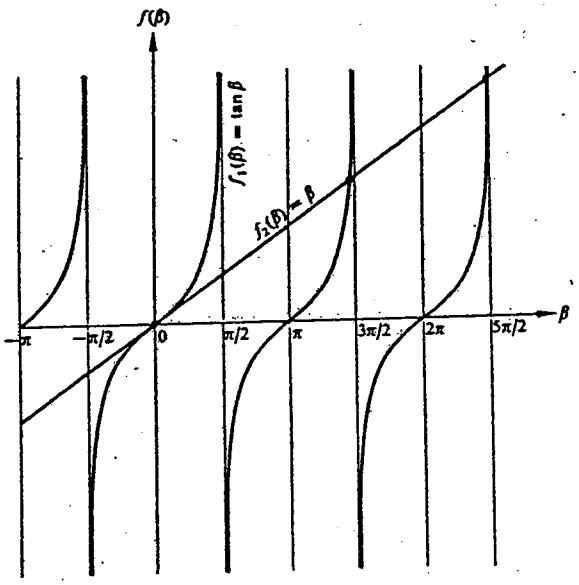

Figure 10.11 The points of intersection of the two curves are the solutions of Eq. (10.21).

third, will cancel the last quarter. Ray-pairs at the same locations in adjacent segments are $\lambda/2$ out of phase and destructively interfere. In general then, zeros of irradiance will occur when

$$b \sin \theta_m = m\lambda,$$

where $m = \pm 1, \pm 2, \pm 3, \ldots$, which is equivalent to Eq. (10.20), since $\beta = m\pi = (kb/2) \sin \theta_m$.

We should inject a note of caution at this point: one of the frailties of the Huygens–Fresnel principle is that it does not take proper regard of the variations in amplitude, with angle, over the surface of each secondary wavelet. We will come back to this when we consider the *obliquity factor* in Fresnel diffraction, where the effect is significant. In Fraunhofer diffraction the distance from the aperture to the plane of observation is so large that we need not be concerned about it, provided that θ remains small.

Figure 10.13 is a plot of the flux density, as expressed by Eq. (10.17). Envision some point on the curve, for example, the third subsidiary maximum at $\beta =$

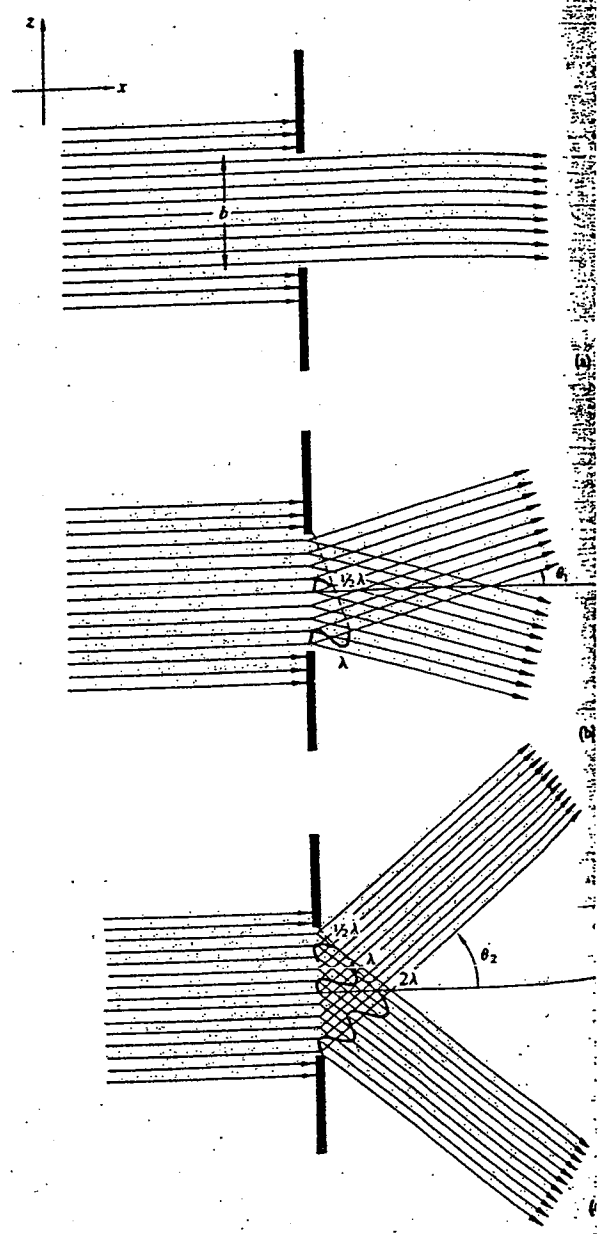

Figure 10.12 The diffraction of light in various directions. Here the aperture is a single slit, as in Fig. 10.10.

3.4707π; since $\beta = (\pi b/\lambda)\sin\theta$, an increase in the slit width b requires a decrease in θ, if β is to be constant. Under these conditions the pattern shrinks in toward the principal maximum, as it would if λ were decreased. If the source emits white light, the higher-order maxima show a succession of colors trailing off into red with increasing θ. Each different colored light component has its minima and subsidiary maxima at angular positions characteristic of that wavelength (Problem 10.6). Indeed, only in the region about $\theta = 0$ will all the constituent colors overlap to yield white light.

The point source S in Fig. 10.9 would be imaged at the position of the center of the pattern, if the diffracting screen Σ were removed. Under this sort of illumination, the pattern produced with the slit in place is a series of dashes in the yz-plane of the screen σ, much like a spread-out image of S [Fig. 10.9(b)]. An incoherent line source (in place of S) positioned parallel to the slit, in the focal plane of the collimator L_1, will broaden the pattern out into a series of bands. Any point on the line source generates an independent diffraction pattern, which is displaced, with respect to the others, along the y-direction. With no diffracting screen present, the image of the line source would be a line parallel to the original slit. With the screen in place the line is spread out, as was the point image of S (Fig. 10.14). Keep in mind that it's the small dimension of the slit that does the spreading out.

The single-slit pattern is easily observed without the use of special equipment. Any number of sources will do (e.g., a distant street light at night, a small incandescent lamp, sunlight streaming through a narrow space

Figure 10.13 The Fraunhofer diffraction pattern of a single slit.

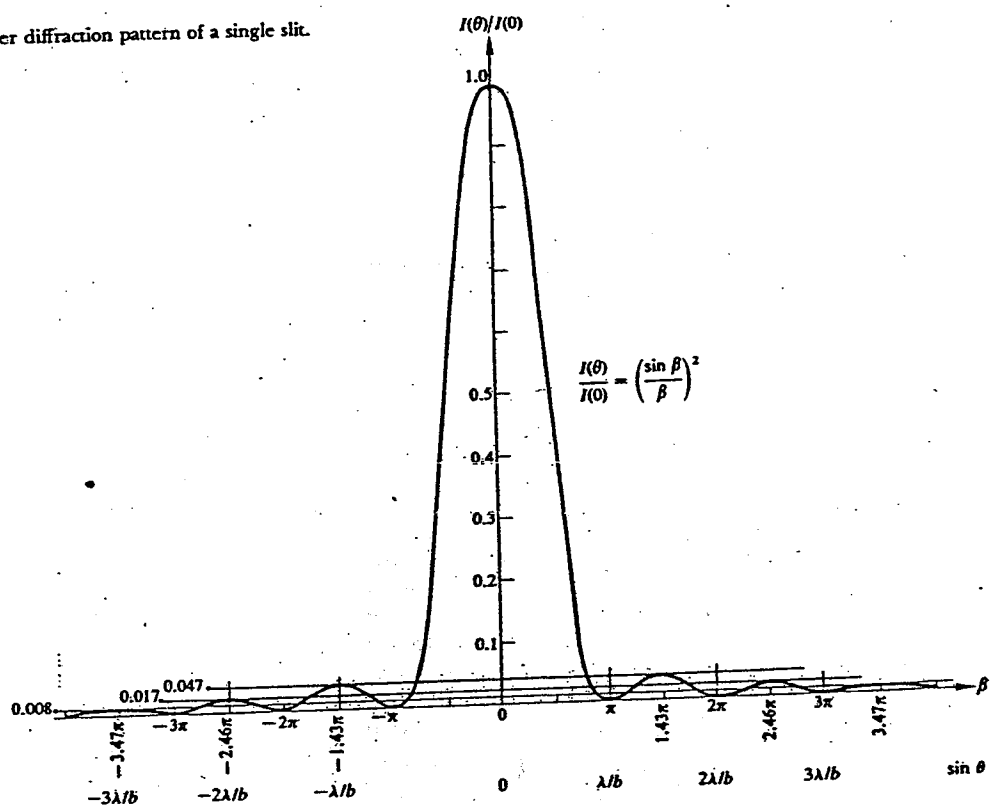

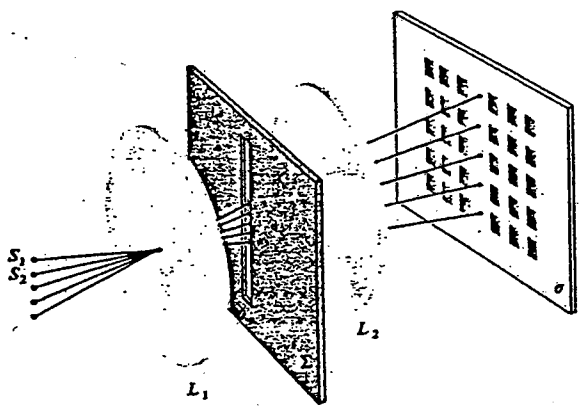

Figure 10.14 The single-slit pattern with a line source. See first photograph of Fig. 10.17.

in a window shade); almost anything that resembles a point or line source will serve. Probably the best source for our purposes is an ordinary clear, *straight-filament* display bulb (the kind in which the filament is vertical and about 3 inches long). You can use your imagination to generate all sorts of single-slit arrangements (e.g., a comb or fork rotated to decrease the projected space between the tines, or a scratch across a layer of india ink on a microscope slide). An inexpensive vernier caliper makes a remarkably good variable slit. Hold the caliper close to your eye with the slit, a few thousandths of an inch wide, parallel to the filament of the lamp. Focus your eye beyond the slit at infinity, so that its lens serves as L_2.

10.2.2 The Double Slit

It might at first seem from Fig. 10.10 that the location of the principal maximum is always to be in line with the center of the diffracting aperture; this, however, is not generally true. The diffraction pattern is actually centered about the axis of the lens and has exactly the same shape and location, regardless of the slit's position, as long as its orientation is unchanged and the approximations are valid (Fig. 10.15). All waves traveling parallel to the lens axis converge on the second focal point of L_2; this then is the image of S and the center of the diffraction pattern. Suppose now that we have two long slits of width b and center-to-center separation a (Fig. 10.16). Each aperture, by itself, would generate the same single-slit diffraction pattern on the viewing screen σ. At any point on σ, the contributions from the two slits overlap, and even though each must be essentially equal in amplitude, they may well differ significantly in phase. Since the same primary wave excites the secondary sources at each slit, the resulting wavelets will be coherent, and interference must occur. If the primary plane wave is incident on Σ at some angle θ_i (see Problem 10.3), there will be a constant relative phase difference between the secondary sources. At normal incidence, the wavelets are all emitted in phase. The interference fringe at a particular point of observation is determined by the differences in the optical path lengths traversed by the overlapping wavelets from the two slits. As we will see, the flux-density distribution (Fig. 10.17) is the result of a rapidly varying double-slit interference system modulated by a single-slit diffraction pattern.

To obtain an expression for the optical disturbance at a point on σ, we need only slightly reformulate the single-slit analysis. Each of the two apertures is divided into differential strips (dz by ℓ), which in turn behave like an infinite number of point sources aligned along

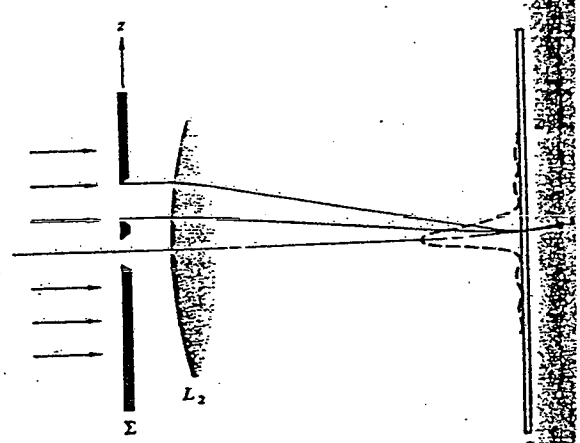

Figure 10.15 The double-slit setup.

Week 2 Notes

Photomultiplier Ratings and Characteristics (Cont'd)

Spectral Response (See Page 3)	RCA Type No.	No. Of Stages and Cage Structure[a]	Max. Rating[b] Supply Voltage V	Typical Characteristics at specified operating supply voltage, voltage distribution, and 22° C. Operating Supply Voltage and Distribution[c] V	Responsivity[d] Radiant[e] Anode Typ. A/W	Radiant[e] Cathode Typ. mA/W	Luminous[f] Anode Min. A/lm	Luminous[f] Anode Typ. A/lm	Luminous[f] Cathode Min. μA/lm	Luminous[f] Cathode Typ. μA/lm	Anode Dark Current @ Anode Luminous Responsivity nA@A/lm	Anode Pulse Rise Time[g] <ns	Outline Drawing	Remarks[h]
2"-Diameter Head-On Types (Cont'd)														
35CT	8575/V1	12 I	3000	2000 S	1.4×10^6	97	175/23^k	1230/160^k	77/10^k	85/11^k	1 @ 200	2.5	26	An 8575 supplied with an AJ2132 adapter making it interchangeable with type 56AVP. Dynode emitting surfaces, BeO.
35CT	8575/V2	12 I	3000	2000 S	1.4×10^6	97	175/23^k	1230/160^k	77/10^k	85/11^k	1 @ 200	2.5	26	An 8575 supplied with an AJ2144 socket rather than an AJ2145 type. Dynode emitting surfaces, BeO.
35CT	C31057	12 I	3000	2000 S	1.4×10^6	97	175/23^k	1230/160^k	77/10^k	85/11^k	1 @ 200	2.5	25	A ruggedized 8575 with flying leads. Design tested for S, V, and A. Dynode emitting surfaces, BeO.
35CT	C31057A	12 I	3000	2000 S	1.4×10^6	97	175/23^k	1230/160^k	77/10^k	85/11^k	1 @ 200	2.5	25	Variant of C31057 that is 100% tested for S and V. Dynode emitting surfaces, BeO.
35CT	C31057B	12 I	3000	2000 S	1.4×10^6	97	175/23^k	1230/160^k	77/10^k	85/11^k	1 @ 200	2.5	25	Variant of 8575 having base attached to flying leads. Dynode emitting surfaces, BeO.
35CT	4507	12 I	2500	1500 V	1.8×10^5	97	19/2.5^k	160/21^k	73/9.5^k	85/11^k	0.2 @ 50	2.5	27	A bialkali photocathode type having a spherical-section faceplate. Dynode emitting surfaces, BeO.
35CT	4501/V3	12 I	2500	2500[m] S	Has a minimum tritium (H^3) efficiency[n] of 58% and a typical E^2/BP figure of merit of 155 at the tritium end point (TEP) voltage.								27	Variant of 4507 designed specifically for liquid scintillation counting systems. Dynode emitting surfaces, BeO.
35CT	8850	12 I	3000	2000 T	1.4×10^6	97	115/15^k	1230/160^k	77/10^k	85/11^k	0.6 @ 200	2.5	26	Premium QUANTACON type for photon counting applications. Has high-gain GaP first dynode emitting surface followed by BeO dynode emitting surfaces in succeeding stages.
35JT	4501/V4	12 I	2500	1700[m] S	Has a minimum tritium (H^3) efficiency[n] of 59% and a typical E^2/BP figure of merit of 205 at the tritium end point (TEP) voltage.								27	Variant of 4501/V3 having improved liquid scintillation counting characteristics. Dynode emitting surfaces, BeO.
35JT	C31000M	12 I	3000	2000 T	1.4×10^6	97	115/15^k	1230/160^k	77/10^k	85/11^k	0.6 @ 200	2.5	26	UV-variant of 8850. Has high-gain GaP first dynode emitting surface followed by BeO dynode emitting surfaces in succeeding stages.
40AT	C31000AJ	12 I	2500	2000 S	4.9×10^5	71	250/25^k	650/65^k	60/6^k	95/9.5^k	3 @ 250	2.5	26	Has "high-temperature" bialkali photocathode permitting operation at temperatures as high as 150° C. Dynode emitting surfaces, BeO.
50AT (S-20)	4463	10 V	2500	2000 E	1.1×10^4	68	12	25	120	160	4.8 @ 12	10	31	Variant of 8053 having a multialkali photocathode for red and near IR systems. Dynode emitting surfaces, BeO.
50AT (S-20)	7265	14 I	3000	2400 W	3.1×10^6	64	800	7200	100	150	50 @ 1000	3	28	Variant of 6810A having a multialkali photocathode. Dynode emitting surfaces, BeO.
50AT (S-20)	7326	10 I	2400	1800 E	3.8×10^4	64	12.5	88	120	150	3 @ 20	2.5	28	Variant of 7265 having 10 stages. Dynode emitting surfaces, BeO.
50CT	C31000A	12 I	3000	2000 S	2.7×10^5	77	200	700	120	200	5 @ 200	2.5	26	Variant of 8575 having a multialkali photocathode. Dynode emitting surfaces, BeO.

Spectral Response Characteristics and Data

RCA has changed its pure-numeric notation for specifying spectral-response characteristics to a more orderly system. The new designations are alphanumeric combinations that are based on (1) the photocathode material, (2) the window material, and (3) the photocathode operating mode. As illustrated below, the first two digits (Column I) in the designation indicate the photocathode material; the following alpha character (Column II), the window material; and the next alpha character (Column III), the photocathode operating mode. Where required, the letter "X" is used as a suffix to the designation to indicate an extended response in the red or near infrared.

Column I
10 = AgOCs
15 = AgBiOCs
20 = CsSb
25 = CsBi
30 = CsTe
35 = KCsSb (Bialkali)
40 = NaKSb (High Temperature Bialkali)
50 = NaKCsSb (Multialkali)
51 = NaKCsSb (ERMA I)
52 = NaKCsSb (ERMA II)
53 = NaKCsSb (ERMA III)
60 = GaAs
71 = InGaAs (Type I)
72 = InGaAs (Type II)
73 = InGaAs (Type III)

Column II
A = 0080 (Lime Glass) or 7056 (Borosilicate Glass)
C = 7740 (Pyrex)
E = 9741 (UV-Transmitting Glass)
G = 9823 (UV-Transmitting Glass)
J = SiO_2 (Fused Silica)
M = UV-Grade Sapphire
P = LiF

Column III
D = Dormer-Window Type
R = Reflection Type
T = Transmission Type

Column IV
X = Extended Response

Examples:

Tube type 931A has a spectral response that was previously designated as 102 (S-4). This tube type has a CsSb photocathode, a 0080 window, and a reflection type photocathode. Its new designation is 20AR.

Similarly, a tube type having a CsSb photocathode, a 0080 window, and a transmission type photocathode is designated 20AT. This response was previously designated 107 (S-11).

Selected Spectral Response Curves

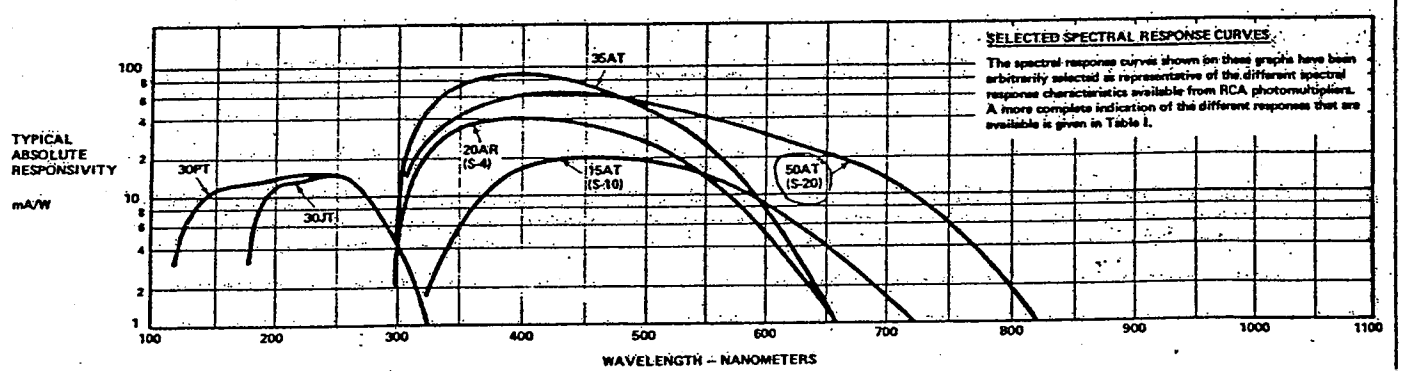

Typical Ultraviolet and Visible Spectral Response Characteristics

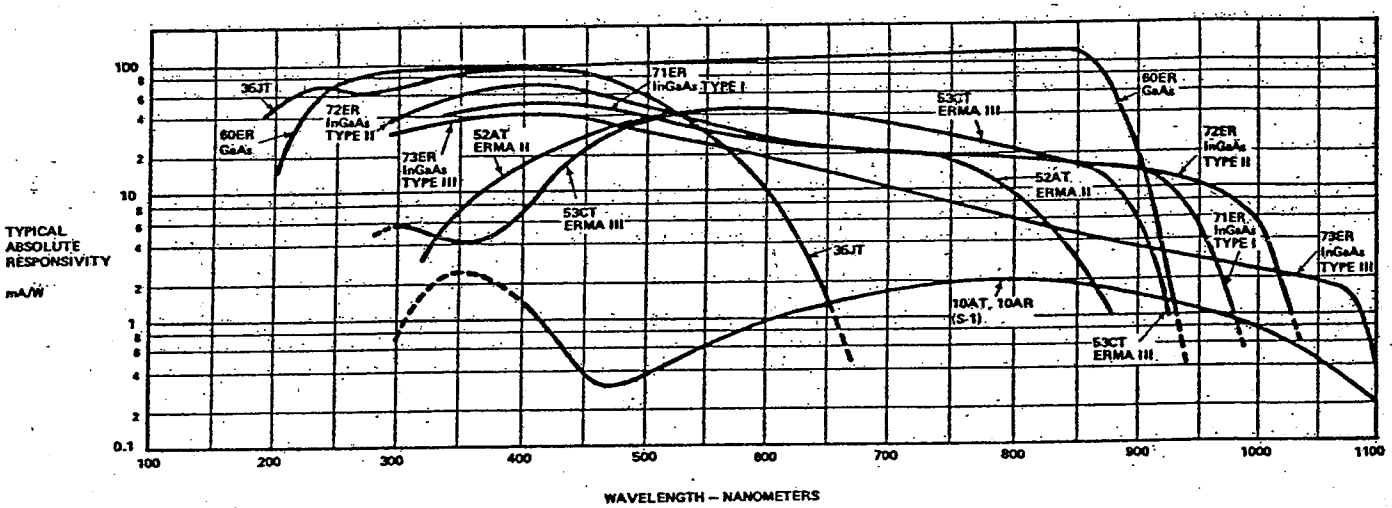

Typical "Broadband" Spectral Response Characteristics

Voltage-Distribution Considerations

No. Of Stages	Distribution Code	Voltage Distribution K, Dy1, Dy2, Dy3, – – – – P
5	A	4, 2, 2, 2, 1, 1.7♦, and 0.37▲
6	B	2, 1, 1, 1, 1, 1, and 1
	C	1.2, 1.2, 1.7, 1, 1, 1, and 1.
9	D	1, 1, 1, 1, 1, 1, 1, 1, 1, and 1
10	E	2, 1, 1, 1, 1, 1, 1, 1, 1, 1, and 1
	F	2, 1, 1, 1, 1, 1, 1, 1, 1, 1, and 0.75
	G	1.2, 1.2, 1.7, 1, 1, 1, 1, 1, 1, 1, and 1
	H	1.1, 1.2, 1.7, 1, 1, 1, 1, 1, 1, 1, and 1
	I	1.7, 1.3, 1.3, 1, 1, 1, 1, 1, 1, 1, and 1
	J	1.8, 1.4, 1.5, 1.2, 1, 1, 1, 1, 1, 1, and 1
	K	2, 1.4, 1, 1, 1, 1, 1, 1, 1, 1, and 1
	L	3, 1, 1, 1, 1, 1, 1, 1, 1, 1, and 1
11	M	1, 1.4, 1, 1, 1, 1, 1, 1, 1, 1, 1, and 1
	N	150■, 1, 1, 1, 1, 1, 1, 1, 1, 1, 2, and 1
	P	1, 1, 1, 1, 1, 1, 1, 1, 1, 1, 1, and 1
12	Q	1.2, 1.2, 1.7, 1, 1, 1, 1, 1, 1, 1, 1, 1, and 1
	R	2, 1.4, 1, 1, 1, 1, 1, 1, 1, 1, 1, and 1
	S	4, 1, 1.4, 1, 1, 1, 1, 1, 1, 1, 1, 1, and 1
	T	6, 1, 1.4, 1, 1, 1, 1, 1, 1, 1, 1, 1, and 1
	U	660★, 1, 1.4, 1, 1, 1, 1, 1, 1, 1, 1, 1, and 1
	V	2, 1, 1.4, 1, 1, 1, 1, 1, 1, 1, 1, 1, and 1
14	W	2, 1, 1, 1, 1, 1, 1, 1, 1, 1, 1, 1.25, 1.5, 1.75, and 2
	X	3, 1, 1, 1, 1, 1, 1, 1, 1, 1, 1, 1, 1, 1, and 1

♦Between dynode No.5 and suppressor grid

▲Between suppressor grid and ground

■150 volts

★660 volts

K, cathode; Dy, dynode; and P, anode

The voltage distributions specified for the individual tube types are typical average distributions which are used to measure the tabulated characteristic values.

Interstage voltages for the tube electrodes may be supplied by individual sources but are usually obtained from resistive voltage-divider networks placed across the high-voltage supply. The power ratings of the individual resistors making up the network should be approximately twice that of the calculated dissipation values for circuit safety reasons. Resistors having tolerances of about 5% are satisfactory in most systems for circular-cage and focused in-line photomultipliers. Resistors having 10% tolerances may be used with venetian-blind tubes.

The voltage-divider arrangement should be located so that it will not affect tube operating temperature. Head-on type photomultipliers sometimes use zener diodes between cathode and dynode No.1 to provide constant voltage when tube sensitivity is varied by adjustment of supply voltage.

An important consideration is that the voltage-divider current should be maintained at a value of at least 10 times that of the expected average value of anode current. If this consideration is not observed, deviation from linearity and limitations on anode-current response to pulsed light may occur. The latter effect may be reduced by connecting capacitors between the tube socket terminals for the last 3 or 4 dynode stages and anode return. The values of the capacitors will depend upon the shape and the amplitude of the anode-current pulse, and the time duration of the pulse, or train of pulses. When the output pulse is assumed to be rectangular in shape, the following formula applies:

$$C = 100 \frac{i \cdot t}{V}$$

where C is in farads, i is the amplitude of the anode current in amperes, V is the voltage across the capacitor in volts, and t is the time duration of the pulse in seconds.

This formula applies for the anode-to-final dynode capacitor. The factor 100 is used to limit the voltage change across the capacitor to 1% maximum during a pulse. Capacitor values for preceding stages should take into account the smaller values of dynode currents in these stages. Conservatively, a factor of approximately 2 per stage is used. Capacitors are not required across those dynode stages where the dynode current is less than 1/10 of the current through the voltage-divider network.

Typical Voltage-Divider Arrangement for Fast Pulse Response and High Peak Current Systems. Anode Return at Ground Potential.

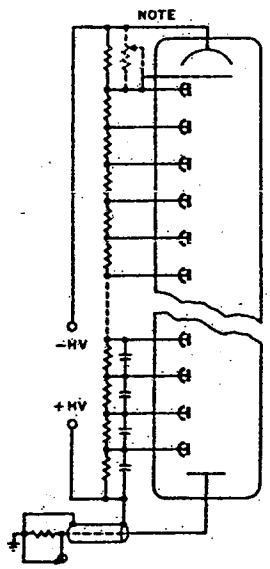

Typical Voltage-Divider Arrangement for Scintillation Counting Systems. Photocathode at Ground Potential.

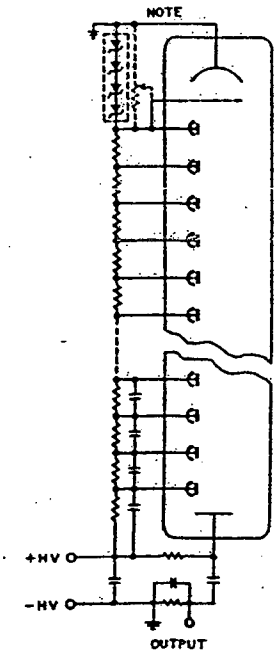

Note: In modern photomultipliers, the focusing electrode is normally connected to dynode No.1. In older tube types, the focusing electrode may be connected to the arm of a potentiometer, between cathode and dynode No.1, to permit adjustment for maximum anode current.

Dimensional Outlines and Basing Diagrams for Photomultipliers (Cont'd)

26

8575
8575/V1
8575/V2
8850
8852
C31000A
C31000M★
C31000AJ

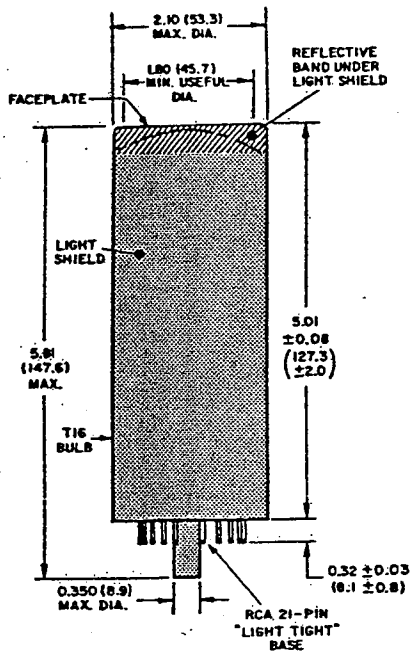

Basing, Bottom View

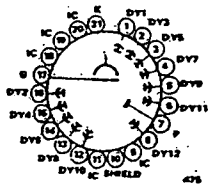

Socket
For types 8575, 8850, 8852, C31000A, C31000M, and C31000AJ — RCA AJ2145 (Supplied with tube)
RCA AJ2144

For type 8575/V2 — RCA AJ2144 (Supplied with tube)

For type 8575/V1 — Not required. Type supplied with RCA AJ2132 socket adapter.

Magnetic Shield
RCA AJ2252

Socket Adapters
For types 8575, 8850 — RCA AJ2132

Auxiliary Photomultiplier Assemblies
For types 8575, 8575/V2, C31000A, and C31000AJ — RCA AJ2207A
RCA AJ2208

For types 8850, 8852, and C31000M — RCA AJ2209A

★Overall length for C31000M is 6.43" (163.3 mm) max., seated height is 5.70" ± 0.08" (144.8 mm ± 2 mm).

27

4501/V3
4501/V4
4507
8853

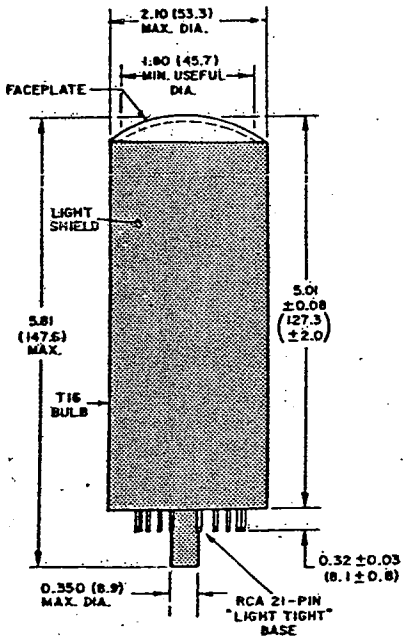

Basing, Bottom View

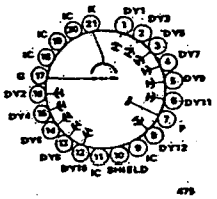

Socket
RCA AJ2145 (Supplied with tube)
RCA AJ2144

Magnetic Shield
RCA AJ2252

Auxiliary Photomultiplier Assemblies
For types 4501/V3, 4501/V4 — RCA AJ2208

For type 8853 — RCA AJ2209A

Construction and Operating Characteristics

INTRODUCTION

The photomultiplier tube (or PMT) is a photosensitive device consisting of a photoemissive cathode (photocathode) followed by focusing electrodes, an electron multiplier and an electron collector (anode) in a vacuum tube, as shown in Figure 1.

When light enters the photocathode, the photocathode emits photoelectrons into the vacuum. These photoelectrons are then directed by the focusing electrode voltages towards the electron multiplier where electrons are multiplied by the process of secondary emission. The multiplied electrons are collected by the anode as an output signal.

Because of secondary-emission multiplication, photomultiplier tubes are uniquely sensitive among photosensitive devices currently used to detect radiant energy in the ultraviolet, visible, and near infrared regions. The photomultiplier tube also features fast time response and low noise.

This section describes the prime features of photomultiplier tube construction and basic operating characteristics.

Figure 1: Cross-Section of Head-On Type PMT

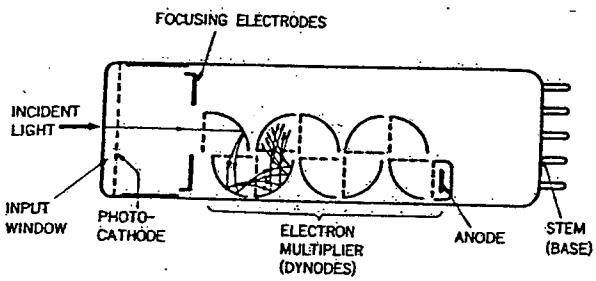

CONSTRUCTION

The photomultiplier tube generally has a photocathode in either a side-on or a head-on configuration. The side-on type receives incident light through the side of the glass bulb, while, in the head-on type, it is received through the end of the glass bulb. In general, the side-on type photomultiplier tube is relatively low priced and widely used for spectrophotometers and general photometric systems. Most of the side-on types employ an opaque photocathode (reflection-mode photocathode) and a circular-cage structure electron multiplier which has good sensitivity and high amplification at a relatively low supply voltage.

The head-on type (or the end-on type) has a semitransparent photocathode (transmission-mode photocathode) deposited upon the inner surface of the entrance window. The head-on type provides better uniformity than the side-on type having a reflection-mode photocathode. Other features of head-on types include a choice of photosensitive area from tens of square milimeters to hundreds of square centimeters.

Variants of the head-on type having a hemispherical window have been developed for high energy physics experiments where a large diameter and good angular light acceptability are important.

Figure 2: External Appearance

a) Side-On Type b) Head-On Type

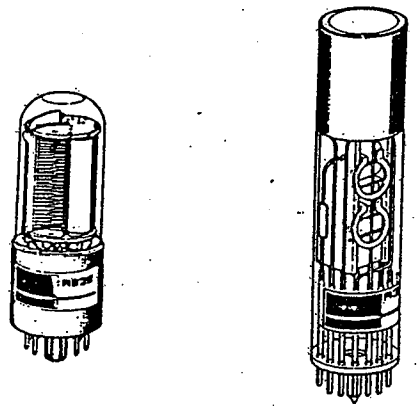

Figure 3: Types of Photocathode

a) Reflection Mode b) Transmission Mode

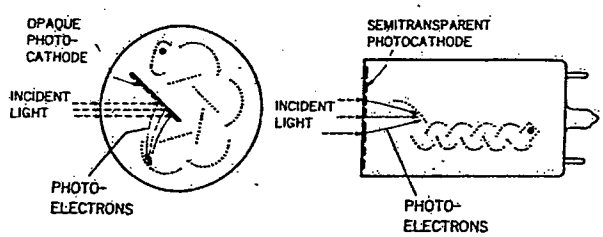

ELECTRON MULTIPLIER

The superior sensitivity (high gain and high S/N ratio) of photomultiplier tubes is due to the use of a low-noise electron multiplier which amplifies electrons by a cascade secondary emission process. The electron multiplier consists of from several up to 15 stages of electrodes called dynodes.

There are several principal types in use today.

1) Circular-cage type

The circular cage is generally used for the side-on type of photomultiplier tube. The prime features of the circular-cage are its compactness and fast response.

2) Box-and-grid type

This type consists of a train of quarter cylindrical dynodes and is widely used in head-on type photomultiplier tubes because of its relatively easy dynode design and better uniformity, although time response may be a problem in some applications.

3) Liner focused type

Since this type features fast response time, it is widely used in applications where time resolution and pulse linearity are important.

4) Venetian blind type

The venetian blind type has a large dynode area and is primarily used for tubes with large photocathode areas. It offers better uniformity and a larger output current. This structure is usually used when time response is not a prime consideration.

5) Proximity mesh type

In addition to good uniformity and high pulse linearity, this type provides high immunity to magnetic fields. Also, it has position-sensitive capability when used with multiple anodes.

6) Microchannel plate (MCP)

The MCP has much faster time response than the other discrete dynodes. It also features good immunity magnetic fields and two-dimensional detection ability when multiple anodes are used.

Recently hybrid dynodes combining two of the above dynodes have been developed. These hybrid dynodes are desi gned to provide the merits of each dynode.

Figure 4: Types of Electron Multipliers

(a) Circular-Cage Type

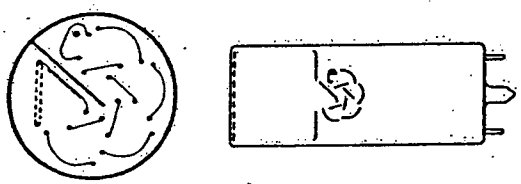

(b) Box-and-Grid Type

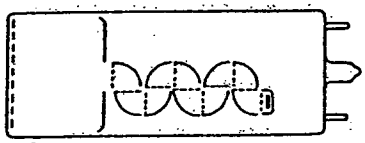

(c) Linear Focused Type

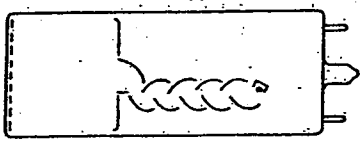

(d) Venetian Blind Type

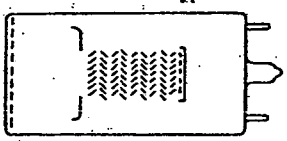

(e) Proximity mesh type

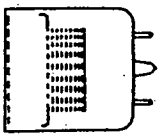

(f) MCP

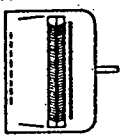

SPECTRAL RESPONSE

The photocathode of photomultiplier tubes converts energy of incident light into electrons. The conversion efficiency (photocathode sensitivity) varies with the wavelength of incident light. This relationship between photocathode sensitivity and wavelength is called the spectral response characteristic. Figure 5 shows a typical spectral response of the bialkali photomultiplier tube. The spectral response range is determined on the long wavelength side by the photocathode material and on the short wavelength side by the window material. Typical spectral response characteristics for various types of photomultiplier tubes are shown on the inside back cover.

In this catalog, the long-wavelength cutoff of spectral response characteristics is defined as the wavelength at which the cathode radiant sensitivity becomes 1% of the maximum sensitivity for bialkali and Ag-O-Cs photocathodes, and 0.1% of the maximum sensitivity for multialkali photocathodes. Spectral response characteristics shown inside the back cover are typical curves for representative tube types. Typical radiant sensitivity for individual tube types is listed in their characteristic tables. But actual data may be different from tube to tube.

Figure 5: Typical Spectral Response of Bialkali Photocathode (R878, etc.)

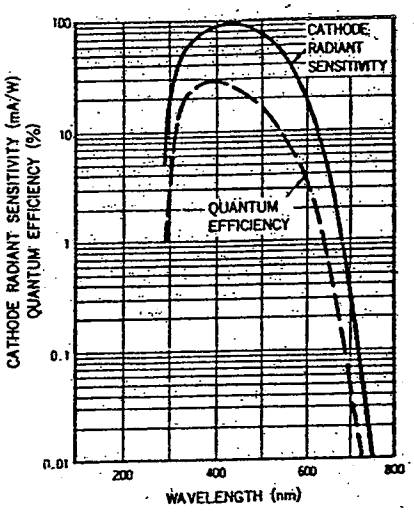

Photocathode Materials

The photocathode is a photoemissive surface usually

consisting of alkali metals with very low work functions. The photocathode materials most commonly used in photomultiplier tubes are as follows:

1) Ag-O-Cs

The transmission-mode photocathode using this material is designated S-1. It is sensitive from the visible to infrared radiation beyond 1000 nm. Since it has high adverse dark emission, tubes of this photocathode are chiefly used for detection in the infrared region with the photocathode cooled.

2) Sb-Cs

This is a widely used photocathode and has a spectral response in the ultraviolet to visible range. Mainly used for reflection-mode photocathodes.

3) Bialkali (Sb-Rb-Cs, Sb-K-Cs)

These have a spectral response range similar to the Sb-Cs photocathode, but have higher sensitivity and lower noise than Sb-Cs. They also have a favorable blue sensitivity for scintillator flashes, thus they are frequently used for scintillation counting.

4) High temperature bialkali, low noise bialkali (Na_2K-Sb)

This is particularly useful at higher operating temperatures since it can withstand up to 175°C. A major application is in the oil well logging industry. At room temperatures, it operates with very low dark current. Thus it can also be useful for photon counting applications.

5) Multialkali (Na-K-Sb-Cs)

The multialkali photocathode has a high, wide spectral response from the ultraviolet to near infrared region. It is widely used for broad-band spectrophotometers and photon counting applications. The long wavelength response can be extended out to 930 nm by special photocathode processing.

6) GaAs (Cs)

GaAs activated in cesium is also used as a photocathode. The spectral response of this photocathode usually covers a wider range than multialkali, ultraviolet to 930 nm, and is very flat.

7) InGaAs

This new photocathode has more extended sensitivity in infrared than GaAs. Also, in the range between 900 and 1000 nm, InGaAs has much higher S/N ratio than Ag-O-Cs.

8) Cs-Te, Cs-I

These materials are sensitive to vacuum UV and UV rays but not to visible light and are therefore called solar blind. Cs-Te is quite insensitive to wavelengths longer than 320 nm and Cs-I to those longer than 200 nm.

Window Materials

The window materials commonly used in photomultiplier tubes are as follows:

1) Borosilicate glass

This is the most frequently used material. It transmits radiation from the infrared to approximately 300 nm. It is not suitable for detection in the ultraviolet region.

For scintillation counting applications, the low-noise borosilicate glass (so called K free glass) may be used. It contains very low potassium (^{40}K) which can cause unwanted background counts.

2) UV-transmitting glass (UV glass)

This glass transmits ultraviolet radiation well, as the name implies, and is used as widely as borosilicate glass. The UV cutoff is approximately 185 nm.

3) Synthetic silica

This material transmits ultraviolet radiation down to 160 nm. Since silica has a different thermal expansion coefficient from Kovar, which is used for the tube leads, it is not suitable for the stem material of the tube. Borosilicate glass is used for the stem, then a graded seal using glasses with gradually different thermal expansion coefficient are connected to the fused silica window.

4) Sapphire glass

The sapphire glass made of Al_2O_3 crystal has an intermediate transmittance in the ultraviolet region between UV glass and synthetic silica. But, at wavelengths shorter than 150 nm, it has higher transmittance than synthetic silica. Since the sapphire glass does not require graded seal, the overall length of tubes can be shortened.

5) MgF_2 (magnesium fluoride)

The crystals of alkali halide are superior in transmitting ultraviolet radiation, but deliquescence is a common problem. Among them, MgF_2 has low deliquescence and transmits ultraviolet radiation down to 115 nm.

Figure 8: Typical Transmittance of Various Window Materials

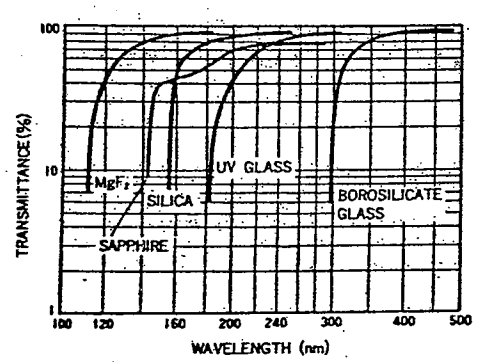

As stated above, spectral response range is determined by the photocathode and window materials. It is important to select an appropriate combination which will suit your applications.

RADIANT SENSITIVITY AND QUANTUM EFFICIENCY

As Figure 5 shows, spectral response is usually expressed in terms of radiant sensitivity and quantum efficiency.

Radiant sensitivity is the photoelectric current from the photocathode divided by the incident radiant power at a given wavelength, expressed in A/W (amperes per watt).

Quantum efficiency (QE) is defined as the ratio of the number of incident photons to resulting photoelectrons emitted from the photocathode. It is customary to present quantum efficiency as a percent. Quantum efficiency and radiant sensitivity have the following relationship at a given wavelength.

$$QE = \frac{S \times 1240}{\lambda} \times 100\ (\%)$$

where S is the radiant sensitivity in A/W at the given wavelength and λ is the wavelength in nm (nanometers).

LUMINOUS SENSITIVITY

Since the measurement of spectral response characteristic of a photomultiplier tube requires a sophisticated system and time, it is not practical to provide customers with spectral response characteristics of each tube ordered. Instead, a value of cathode or anode luminous sensitivity is commonly used.

The cathode luminous sensitivity is the photoelectric current from the photocathode per incident light flux (10^{-5} to 10^{-2} lumen) from a tungsten filament lamp operated at a distribution temperature of 2856K. The anode luminous sensitivity is the anode output current (amplified by the secondary emission process) per incident light flux (10^{-10} to 10^{-5} lumen) on the photocathode. Although the same tungsten lamp is used, the light flux and the applied voltage are adjusted to an appropriate level. These parameters are particularly useful when comparing tubes having the same or similar spectral response range. Hamamatsu final test sheets accompanying the tubes usually indicate these parameters except for tubes with CsI or CsTe photocathodes which are not sensitive to tungsten lamp light. (Radiant sensitivity at a specific wavelength is listed for those tubes instead.)

Both the cathode and anode luminous sensitivities are expressed in units of A/lm (amperes per lumen). Note that the lumen is a unit used for luminous flux in the visible region and therefore these values may be meaningless for tubes which are sensitive beyond the visible region. For those tubes, the blue sensitivity or red/white ratio is often used.

BLUE SENSITIVITY AND RED/WHITE RATIO

For simple comparison of spectral response of photomultiplier tubes, cathode blue sensitivity and red/white ratio are often used.

The cathode blue sensitivity is the photoelectric current from the photocathode produced by a light flux of a tungsten lamp at 2856K passing through a blue filter (Corning CS No. 5-58 polished to half stock thickness). Since the light flux, once transmitted through the blue filter cannot be expressed in lumens, blue sensitivity is usually presented in A/lm-b (amperes per lumen-blue). The blue sensitivity is a very important parameter in scintillation counting since scintillators produce emissions in the blue region of the spectrum, and may dominate energy resolution.

The red/white ratio is used for photomultiplier tubes with a spectral response extending to the near infrared region. This parameter is defined as the quo-

Figure 7: Typical Human Eye Response and Spectral Distribution of 2856K Tungsten Lamp

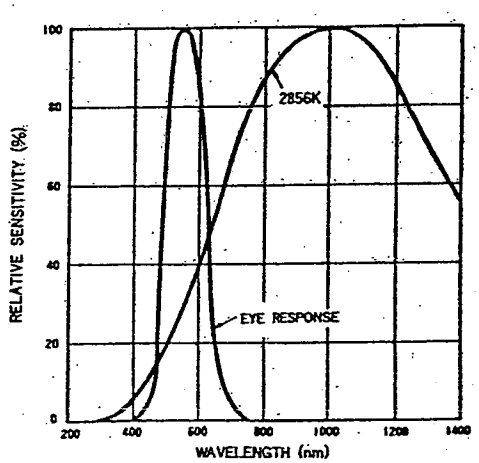

Figure 8: Transmittance of Filters

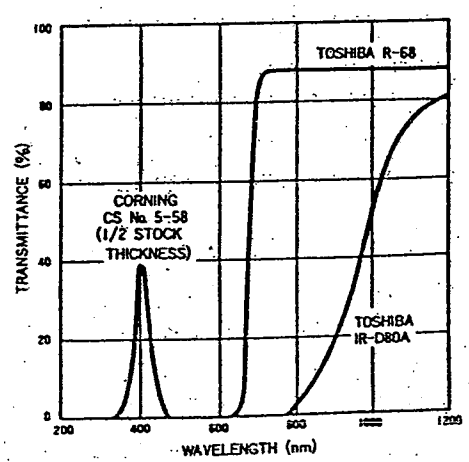

tient of the cathode sensitivity measured with a light flux of a tungsten lamp at 2856K passing through a red filter (Toshiba IR-D80A for the S-1 photocathode or R-68 for others) divided by the cathode luminous sensitivity with the filter removed.

CURRENT AMPLIFICATION (GAIN)

Photoelectrons emitted from a photocathode are accelerated by an electric field so as to strike the first dynode and produce secondary electron emissions. These secondary electrons then impinge upon the next dynode to produce additional secondary electron emissions. Repeating this process over successive dynode stages, a high current amplification is achieved. A very small photoelectric current from the photocathode can be observed as a large output current from the anode of the photomultiplier tube.

Current amplification is simply the ratio of the anode output current to the photoelectric current from the photocathode. Ideally, the current amplification of a photomultiplier tube having n dynode stage and an average secondary emission ratio δ per stage is δ^n. While the secondary electron emission ratio δ is given by

$$\delta = A \cdot E^{\alpha}$$

where A is constant, E is interstage voltage, and α is a coefficient determined by the dynode material and geometric structure. It usually has a value of 0.7 to 0.8.

When a voltage V is applied between the cathode and the anode of a photomultiplier tube having n dynode stages, current amplification, G, becomes

$$G = \delta^n = (A \cdot E^{\alpha})^n = \left\{ A \left(\frac{V}{n+1} \right)^{\alpha} \right\}^n$$

$$= \frac{A^n}{(n+1)^{\alpha n}} \cdot V^{\alpha n} = K \cdot V^{\alpha n} \quad \text{(K: constant)}$$

Figure 9: Typical Current Amplification vs. Supply Voltage

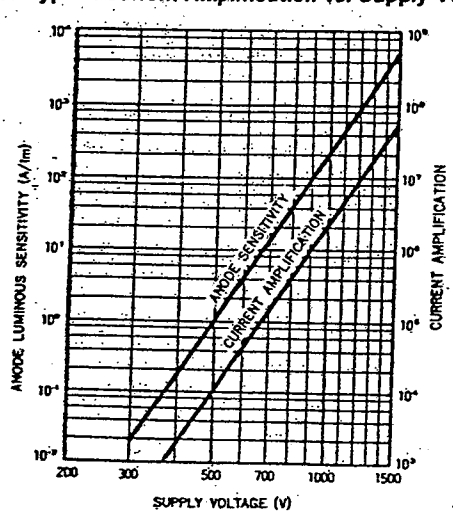

Since generally photomultiplier tubes have 9 to 12 dynode stages, the anode output varies directly with the 6th to 10th power of the change in applied voltage. The output signal of the photomultiplier tube is extremely susceptible to fluctuations in the power supply voltage, thus the power supply should be very stable and exhibit minimum ripple, drift and temperature coefficient. Regulated high voltage power supplies designed with this consideration are available from Hamamatsu (see page 69).

ANODE DARK CURRENT

A small amount of current flows in a photomultiplier tube even when the tube is operated in complete darkness. This output current, called the anode dark current, and the resulting noise are critical factors in determining the lower limit of light detection. Figure 10 shows that dark current is greatly dependent on the supply voltage.

Other sources of dark current may be categorized as follows:

1) Thermionic emission of electrons

Since the materials of the photocathode and dynodes have very low work functions, they emit thermionic electrons even at room temperature. Most of dark currents originate from the thermionic emissions, especially from the photocathode and, if so, become multiplied by the dynodes. Cooling the tube is most useful in applications where low dark current is essential such as in photon counting.

Figure 10: Typical Dark Current vs. Supply Voltage

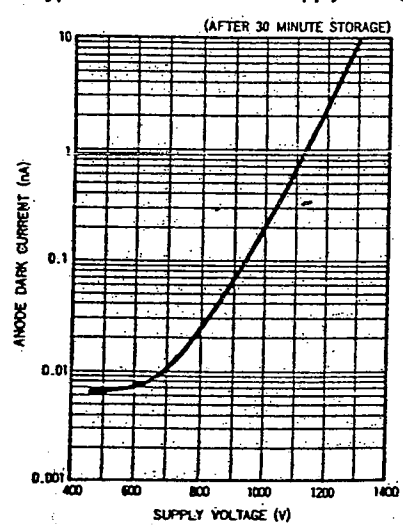

Figure 11 shows the relationship between dark current and temperature for various photocathodes. Photocathodes which have high sensitivity in the red to infrared region, especially S-1, show higher dark current at room temperature.

Figure 11: Temperature Characteristics of Dark Current

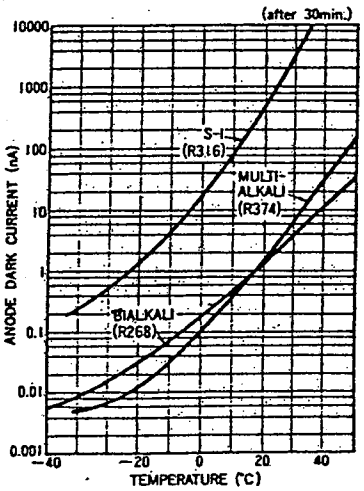

Hamamatsu provides thermoelectric coolers designed for various sizes of photomultiplier tubes (see page 68).

2) Ionization of residual gases

Residual gases inside a photomultiplier tube can be ionized by the flow of photoelectrons. When these ions strike the photocathode or earlier stages of dynodes, secondary electrons may be emitted, thus resulting in relatively large output noise pulse. These noise pulses are usually observed as afterpulses following the primary signal pulses and may be a problem in detecting short light pulses. Present photomultiplier tubes are designed to minimize afterpulses.

3) Glass scintillation

When electrons deviating from their normal trajectories strike the glass envelope, scintillations may occur and a dark pulse may result. To eliminate this type of dark pulse, photomultiplier tubes may be operated with the anode at high voltage and the cathode at ground potential. Here it is useful to coat the glass bulb with a conductive paint (HA Coating) connected to the cathode (see page 13).

4) Ohmic leakage

Ohmic leakage resulting from imperfect insulation of the glass stem base and socket may be another source of dark current. This is predominant when the photomultiplier tube is operated at a low voltage or low temperature. The flatter slopes in Figure 10 and 11 are mainly due to ohmic leakage.

Contamination consisting of dirt and humidity on the surface of the tube may contribute to ohmic leakage, and therefore should be avoided.

5) Field emission

[illegible] near the maximum rating value, electrons may be emitted from electrodes by the strong electric field and may cause dark pulses. It is therefore recommended that the tube be operated at 200 to 300 volts lower than the maximum rating.

The anode dark current decreases with time after the tube is placed in darkness. In this catalog, anode dark currents are measured after 30 minutes storage in darkness.

ENI (EQUIVALENT NOISE INPUT)

ENI is an indication of the photon-limited signal-to-noise ratio. It refers to the amount of light in watts necessary to produce a signal-to-noise ratio of unity in the output of a photomultiplier tube. The value of ENI is given by:

$$ENI = \frac{\sqrt{2q \cdot Idb \cdot G \cdot \Delta f}}{S} \quad \text{(watts)}$$

where q = electronic charge (1.60×10^{-19} coul.)
Idb = anode dark current in amperes after 15-hour storage in darkness
G = current amplification
Δf = bandwidth of the system in hertz (usually 1 hertz)
S = anode radiant sensitivity in amperes per watt at the wavelength of interest

For the tubes listed in this catalog, the value of ENI may be calculated by the above equation. Usually it has a value between 10^{-15} and 10^{-16} watts.

EFFECT BY MAGNETIC FIELD

Most photomultiplier tubes are affected by the presence of magnetic fields. Magnetic fields may deflect electrons from their normal trajectories and cause a loss of gain. The extent of the loss of gain depends on the type of photomultiplier tube and its orientation in the magnetic field. Figure 12 shows

Figure 12: Typical Effects by Magnetic Fields Perpendicular to Tube Axis

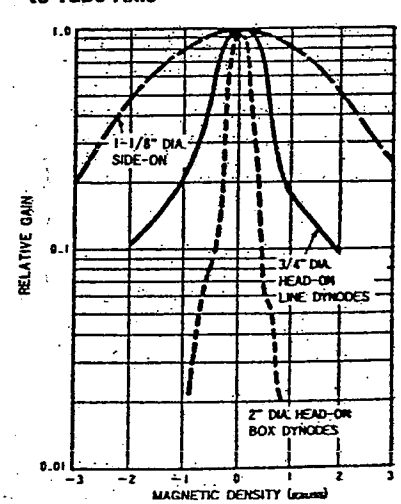

typical effects of magnetic fields on some types of photomultiplier tubes. In general, tubes having a long path from the photocathode to the first dynode are very sensitive to magnetic fields. Therefore head-on types, especially large diameter tubes, tend to be more adversely influenced by magnetic fields.

When a tube has to be operated in magnetic fields, it may be necessary to shield the tube with a magnetic shield case. (Hamamatsu provides a variety of magnetic shield cases. See page 68.) To express the effect of a magnetic shield case, the magnetic shielding factor is used, which is the ratio of the strength of the magnetic field outside the shield case, H_{out}, to that inside the shield case, H_{in}. It is determined by the permeability μ, the thickness t and inner diameter D of the shield case, as follows.

$$\frac{H_{out}}{H_{in}} \simeq \frac{3\mu t}{4D}$$

It should be noted that the magnetic shielding effect decreases towards the edge of the shield case as shown in Figure 13. It is suggested to cover the tube with a shield case longer than the tube length by at least half the tube diameter.

Figure 13: Edge Effect of Magnetic Shield Case

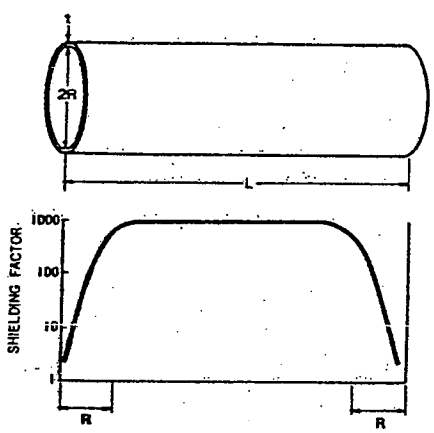

Recently proximity mesh made of non-magnetic material has been introduced as an alternate dynode in photomultiplier tubes. These tube types (see page 56) exhibit much higher immunity to external magnetic fields than the photomultiplier tubes with other dynodes. Also triode and tetrode tubes (see page 56) are useful for applications where the measured amount of light is large.

SPATIAL UNIFORMITY

Although the focusing electrodes of a photomultiplier tube are designed so that electrons emitted from the photocathode or dynodes are collected efficiently by the first or following dynodes, some electrons may deviate from their desired trajectories and collection efficiency is degraded. The collection efficiency varies with the position on the photocathode from which the photoelectrons are emitted and influences the spatial uniformity of a photomultiplier tube. The spatial uniformity is also determined by the photocathode surface uniformity itself.

In general, head-on type photomultiplier tubes provide better spatial uniformity than side-on types because of the photocathode to first dynode geometry. Tubes especially designed for gamma camera applications have excellent spatial uniformity.

Figure 14: Examples of Spatial Uniformity
(a) Head-On Type (b) Side-On Type
(R1306 for γ camera)

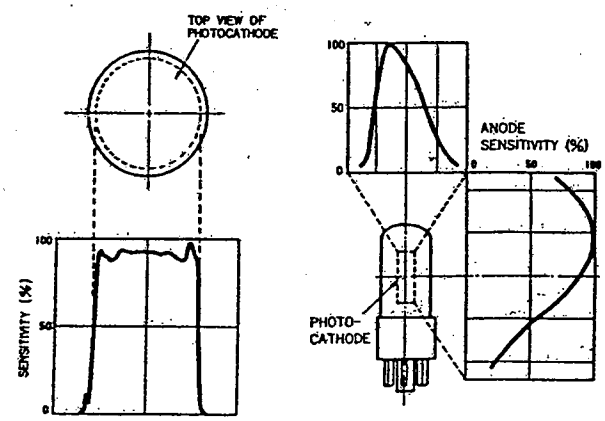

TEMPERATURE CHARACTERISTICS

As discussed earlier, by decreasing ambient temperature of a photomultiplier tube, dark current originating from thermionic emission can be reduced. Sensitivity of the photomultiplier tube also varies with the temperature. In the ultraviolet to visible region, the temperature coefficient of sensitivity has a negative

Figure 15: Typical Temperature Coefficients of Anode Sensitivity

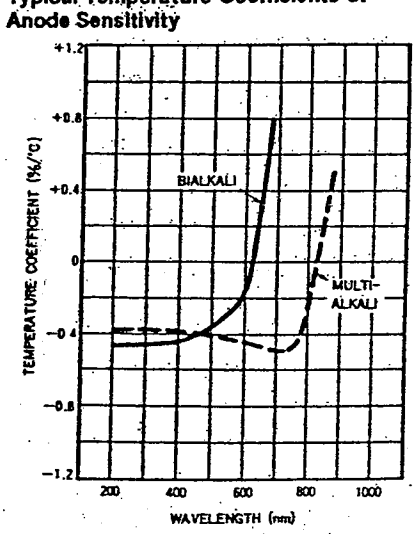

value, while near the long wavelength cutoff it has a positive value. Figure 15 shows typical temperature coefficients around room temperature for multialkali and bialkali photocathodes. Since the temperature coefficient change is large near the long wavelength cutoff, temperature control may be required in some applications.

DRIFT (ANODE CURRENT INSTABILITY)

While operating a photomultiplier tube continuously over a long period, anode output current of the photomultiplier tube may vary slightly with time, although operating conditions have not changed. This instability of anode output current is called drift. Figure 16 shows general drift curves. Drift is primarily caused by damage to the last dynode by heavy electron bombardment. The operating stability of a photomultiplier tube depends on the magnitude of the anode current and not so much on the applied voltage, and therefore the use of lower anode current is desirable. When stability is of prime importance, the use of average anode current of 1 μA or less is recommended.

Figure 16: Examples of Drift

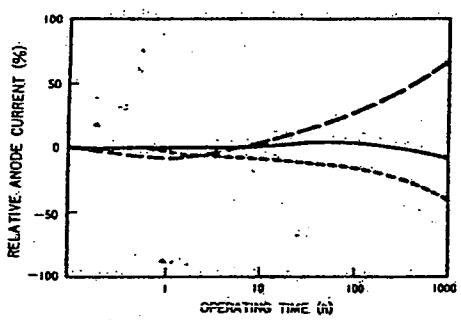

HYSTERESIS

Photomultiplier tubes exhibit a temporary instability in anode output current for several seconds to several tens of seconds after voltage and light are applied, i.e., sensitivity may overshoot or undershoot before reaching a stable value. This instability is called hysteresis and may be a problem in spectrophotometry and other applications.

Figure 17: Hysteresis Measurement

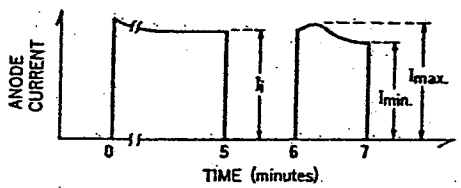

$$\text{HYSTERESIS} = \frac{I_{max} - I_{min}}{I_{\bar{}}} \times 100\ (\%)$$

Hysteresis is mainly caused by electrons being deviated from their planned trajectories and electrostatically charging the dynode support ceramics and glass bulb. When the applied voltage is changed as the light input changes, marked hysteresis can occur.

To eliminate hysteresis, many Hamamatsu side-on photomultiplier tubes employ "anti-hysteresis design" in which the dynode support ceramics are coated with chromium and maintained at the cathode potential in order to repulse stray electrons.

TIME RESPONSE

In application where the incident light is in the form of pulses, the anode output signal should reproduce a waveform faithful to the incident pulse waveform. This reproducibility is related to the anode pulse rise time and the electron transit time.

As illustrated in Figure 18, the anode pulse rise time is defined as the time to rise from 10% to 90% of the peak amplitude when the whole photocathode is illuminated by a delta function light pulse (pulse width less than 50 ps). The electron transit time is the time interval between the arrival of a delta function light pulse (pulse width less than 1ns) at the photocathode and the instant when the anode output pulse reaches its peak amplitude. The electron transit time has a fluctuation between individual light pulses. This fluctuation is called transit time spread (T.T.S.) and defined as the FWHM of the frequency distribution of electron transit times. The T.T.S. is an important factor in time-resolving measurement.

Those parameters are affected by the dynode structure and applied voltage. In general, tubes of the linear focused or circular cage structure exhibit better time response than tubes of the box-and-grid or venetian blind structure. Figure 19 shows typical time response characteristics vs. applied voltage for types R268 (1-1/8" dia. head-on, 11-stage, box-and-grid type) and 931A (1-1/8" dia. side-on, 9-stage, circular cage type).

Figure 18: Anode Pulse Rise Time and Electron Transit Time

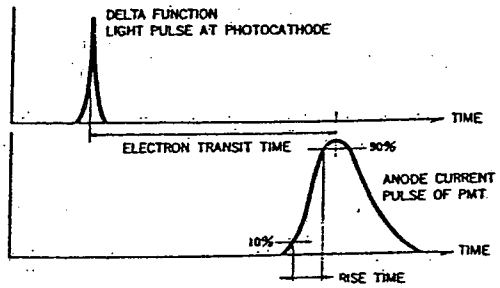

Figure 19: Transit Time Spread (T.T.S.)

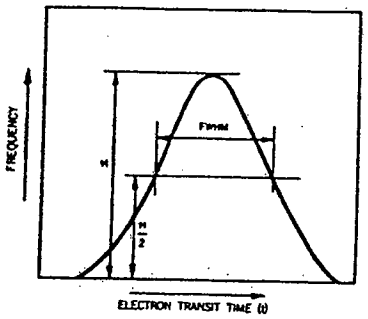

Figure 20: Time Response Characteristics vs. Supply Voltage

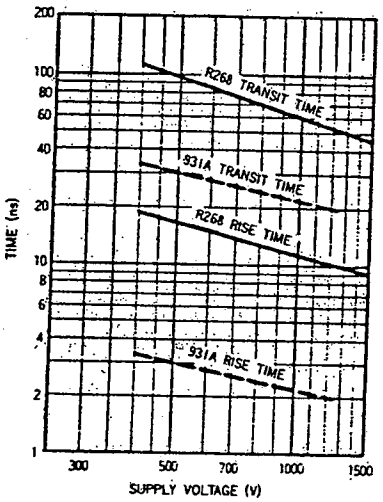

VOLTAGE-DIVIDER CONSIDERATION

Interstage voltages for the dynodes of a photomultiplier tube are usually supplied by a voltage-divider network consisting of series-connected resistors. Schematic diagrams of typical voltage-divider networks are illustrated in Figure 21. Circuit (a) is a basic arrangement and (b) is for high-current pulse operations. Figure 22 shows the response of a photomultiplier tube using the voltage-divider (a) as a function of the input light flux. Deviation from linearity (over-response, region A) is caused by an increase in dynode voltage resulting from the redistribution of the voltage loss between the last dynode and the anode. As the input light level is increased, the anode output current begins to saturate near the value of the current flowing through the voltage divider (region C) due to the extension of voltage losses to the last few stages. Therefore, the upper limit of dynamic range of the photomultiplier tube is determined by the voltage-divider current. To prevent this problem, it is suggested that the voltage-divider current be maintained at at least 20 times the anode output current required from the photomultiplier tube.

Figure 21: Schematic Diagrams of Voltage-Divider Networks

(a) Basic arrangement for DC operation

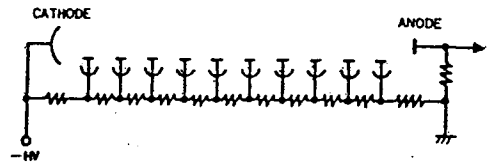

(b) For pulse operation

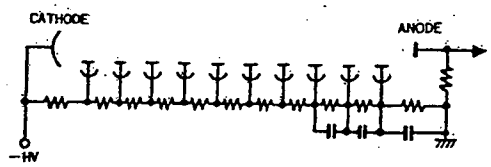

Figure 22: Response of a PMT Using Voltage Divider (a)

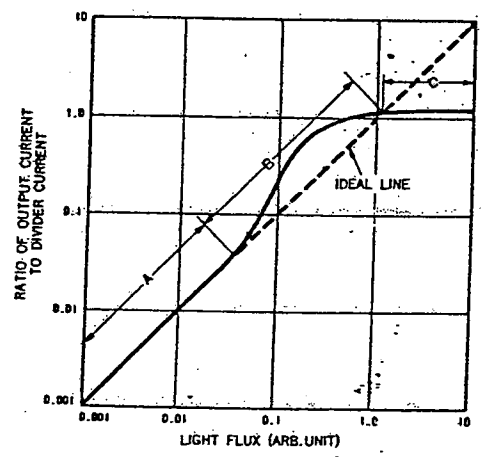

Generally high output current is required in applications where the input light is in the form of pulses. In order to maintain dynode potentials at a constant value during pulse durations and obtain high peak currents, large capacitors are used as shown in Figure 20 (b). The capacitor values depend on the output charge. If linearity of better than 1% is needed, the capacitor value between the last dynode and the anode should be at least 100 times the output charge per pulse, as follows:

$$C > 100 \frac{I \cdot t}{V} \quad \text{(farads)}$$

where I is the peak output current in amperes, t is the pulse width in seconds, and V is the voltage across the capacitor in volts.

Hamamatsu provides socket assemblies incorporating voltage-divider networks. They are compact, rugged, and carefully engineered to minimize electric leakage. (See page 66.)

Ground Polarity and HA Coating

The general technique used for voltage divider circuits is to ground the anode with a high negative voltage applied to the cathode. This scheme eliminates the potential difference between the external circuit and the anode, facilitating the connection of such circuits as ammeters or current-to-voltage conversion operational amplifiers to the photomultiplier tube. However, when a grounded anode configuration is used, bringing a grounded metallic holder or magnetic shield case near the bulb of the tube can cause electrons to strike the inner bulb wall, resulting in the generation of noise. Also, for head-on type photomultiplier tubes, if the faceplate or bulb near the photocathode is grounded, the slight conductivity of the glass material causes a current to flow between the photocathode (which has a high negative potential) and ground. This may cause electrolysis of the photocathode, leading to the danger of significant deterioration. For this reason, when designing the housing for a photomultiplier tube and when using an electrostatic or magnetic shield case, extreme care is required.

In addition, when using foam rubber or similar material to mount the tube in its housing, it is essential that material having sufficiently good insulation properties be used. This problem can be solved by applying a black conductive layer around the bulb and connecting to the cathode potential (called HA Coating), as shown in Figure 24. However, in scintillation counting, it is often impossible to use this technique, since the grounded scintillator is in intimate contact with the photomultiplier tube. In such cases, it is recommended that the cathode be grounded, as shown in Figure 23, with a high positive voltage applied to the anode. Using this scheme, a coupling capacitor C is used to separate the high positive voltage applied to the anode from the signal, making it impossible to obtain a DC signal output.

Figure 23: Cathode Ground Scheme

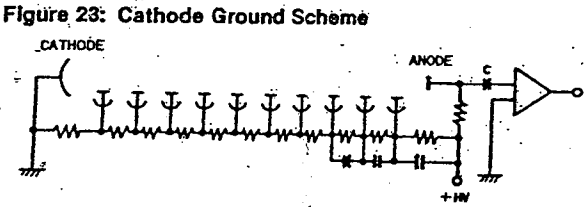

Figure 24: HA Coating

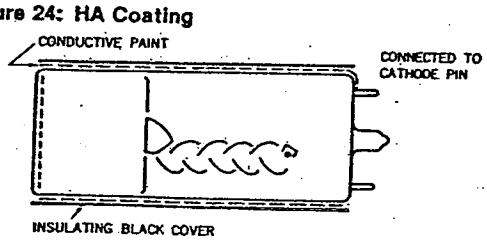

LOAD RESISTANCE

Since the output of a photomultiplier tube is a current signal and the type of external circuit to which photomultiplier tubes are usually connected has voltage inputs, a load resistance is used to perform a current-voltage transformation. This section describes considerations to be made when selecting this load resistance. Since for low output current levels, the photomultiplier may be assumed to act as virtually an ideal constant-current source, the load resistance can be made arbitrarily large, thus converting a low-level current output to a high-level voltage output. In practice, however, using very large values of load resistance creates the problems of deterioration of frequency response and output linearity described below.

Figure 25: Output Circuit for PMT

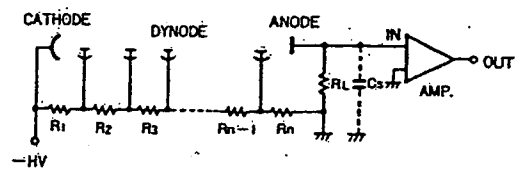

If, in the circuit of Figure 25, we let the load resistance be R_L and the total of the capacitance of the photomultiplier tube anode to all other electrodes, including such stray capacitance as wiring capacitances be C_S, the cutoff frequency f_C is expressed by the following relationship.

$$f_C = \frac{1}{2\pi C_S R_L}$$

From this relationship, it can be seen that, even if the photomultiplier tube and amplifier have very fast response, response will be limited to the cutoff frequency f_C of the output circuit. Anode effect of large load resistance is on linearity of the output current with respect to intensity of incident light. If the load resistance is made large, at high current levels the voltage drop across R_L becomes large, causing the potential difference between the last dynode stage and the anode to drop. This increases the effect of the space charge and lowers the efficiency of the anode in collecting electrons. In effect, the output becomes saturated above a certain current, resulting in a loss of linearity.

Figure 26: Amplifier Internal Resistance

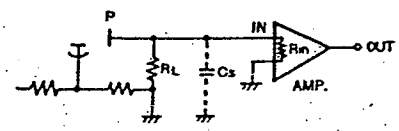

In Figure 26, let us consider the effect of the internal resistance of the amplifier. If the load resistance is R_L and the input impedance of the amplifier is R_{in}, the combined parallel output resistance of the photomultiplier tube, R_O, is given by the following relationship.

$$R_O = \frac{R_L \cdot R_{in}}{R_L + R_{in}}$$

This value of R_O, less than the value of R_L, is then the effective load resistance of the photomultiplier tube. If, for example, $R_L = R_{in}$, the effective load resistance is 1/2 that of R_L alone. From this we see that the upper limit of the load resistance is actually the input resistance of the amplifier and that making the load resistance much greater than this value does not have significant effect. While the above description assumed the load and input impedances to be purely resistive, in practice, stray capacitances, input capacitance, and stray inductances influence phase relationships. Therefore, as frequency is increased these circuit elements must be considered as compound impedances rather than pure resistances.

From the above, three guides can be derived for use in selection of the load resistance:

1) In cases in which frequency response is important, the load resistance should be made as small as possible.
2) In cases in which output linearity is important, the load resistance should be chosen such that the output voltage is below several volts.
3) The load resistance should be less than the approximate input impedance of the external amplifier.

HIGH-SPEED OUTPUT CIRCUIT

For the detection of high-speed and pulsed light signals, a coaxial cable is used to make the connection between the photomultiplier tube and the electronic circuit, as shown in Figure 27. Since commonly used cables have characteristic impedances of 50 Ω or 75 Ω, this cable must be terminated in a pure resistance equivalent to the characteristic impedance to provide impedance matching and ensure distortion-free transmission for the signal waveform. If a matched transmission line is used, the impedance of the cable as seen by the photomultiplier tube output will be the characteristic impedance of the cable, regardless of the cable length, and no distortion will occur in signal waveforms.

If proper matching at the signal receiving end is not achieved, the impedance seen at the photomultiplier tube output will be a function of both frequency and cable length, resulting in significant waveform distortion. Such mismatched conditions can be caused by the connectors used as well, so that the connector to be used should be chosen with regard given to the frequency range to be used, to provide a match to the coaxial cable.

When a mismatch at the signal receiving end occurs, all of the pulse energy from the photomultiplier tube is not dissipated at the receiving end, but is partially reflected back to the photomultiplier tube. While this reflected energy will be fully dissipated at the photomultiplier tube if an impedance match has been achieved at the tube, if this is not the case, since the photomultiplier tube itself acts as an open circuit, the energy will be reflected and, thus, returned to the signal-receiving end. Since part of the pulse makes a round trip in the coaxial cable and is again input to the receiving end, this reflected signal is delayed with respect to the main pulse and results in waveform distortion (so called ringing phenomenon). To prevent this phenomenon, in addition to providing impedance matching at the receiving end, it is necessary to provide a resistance matched to the cable impedance at the photomultiplier tube end as well. If this is done, it is possible to virtually eliminate the ringing caused by an impedance mismatch, although the output pulse height of the photomultiplier tube is reduced to one-half of the normal level by use of this impedance matching resistor.

Figure 27: High-Speed Output Circuit

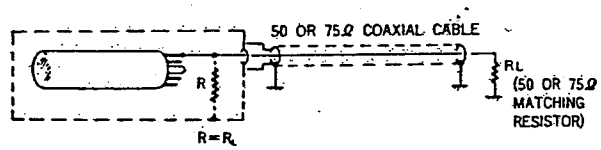

In Figure 28, let us consider waveform observation of high-speed pulses using an oscilloscope. This type of operation requires a low load resistance. Since, however, there is a limit to the oscilloscope sensitivity, an amplifier is required.

For cables to which a matching resistor has been connected, there is an advantage that the cable length does not affect the characteristics of the cable. However, since the matching resistance is very low compared to the usual load resistance, the output voltage becomes too small. While this situation can be remedied with an amplifier of high gain, the inherent noise of such an amplifier can itself be detrimental to measurement performance. In such cases, the photomultiplier tube can be brought as close as possible to the amplifier and a load resistance as large as possible should be used (consistent with preservation of frequency response), to achieve the desired input voltage.

Figure 28: Waveform Observation Using Oscilloscope

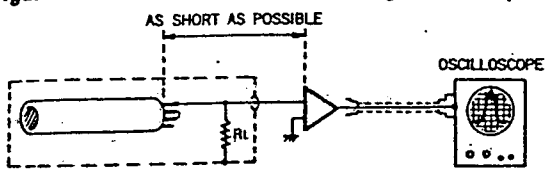

It is relatively simple to implement a high-speed amplifier using a wideband video amplifier or pulse-type ICs. Recent improvements in the availability of a variety of types of such ICs and price reductions have made this possible. There are, however, various problems concerned with characteristics (particularly noise performance) when using ICs, such problems requiring sufficient care in measurement system design.

As the pulse repetition frequency increases, baseline shift creates one reason for concern. This occurs because the DC signal component has been eliminated from the signal circuit by coupling with a capacitor which does not pass DC. If this occurs, the reference zero level observed at the last dynode stage is not the actual zero level. Instead, the apparent zero level is the time-average of the positive and negative fluctuations of the signal waveform. This will vary as a function of the pulse density, and is known as baseline shift. Since the height of the pulses above this baseline level is influenced by the repetition frequency, this phenomenon is of concern when observing waveforms or discriminating pulse levels.

OPERATIONAL AMPLIFIERS

In cases in which a high-sensitivity ammeter is not available, the use of an operational amplifier will enable measurements to be made using an inexpensive voltmeter. This technique relies on converting the output current of the photomultiplier tube to a voltage signal. The basic circuit is as shown in Figure 29, for which the output voltage, V_O, is given by the following relationship.

$$V_O = -R_f \cdot I_p$$

This relationship is derived for the following reason. If the input impedance of the operational amplifier is extremely large, and the output current of the photomultiplier tube is allowed to flow into the input terminal of the amplifier, most of the current will flow through R_f, and subsequently to the operational amplifier output circuit. Therefore, the output voltage, V_O, is given by the expression $-R_f \times I_p$. When using such an operational amplifier it is, of course, not possible to increase the output voltage without limit, the actual maximum output being approximately equal to the operational amplifier power supply voltage. At limitations are placed by the operational amplifier offset current (I_{OS}), the quality of R_f, and other factors such as the insulation materials used.

Figure 29: Current-Voltage Transformation Using Operational Amplifier

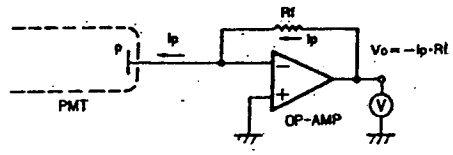

If the operational amplifier has an offset current (I_{OS}), the above-described output voltage becomes $V_O = -R_f (I_p + I_{OS})$, the offset current component being superimposed on the output. Also, the magnitude of temperature drift may create a problem. In general, a metallic film resistor is used for the resistance R_f, and for high resistance values, a vacuum-sealed type is used. Carbon resistors, with their highly temperature-dependent resistance characteristics, are not suitable for this application. When inputting such extremely low level currents as 100 pA and below, in addition to the considerations described above, the materials used in the circuit implementation require care as well. For example, materials such as bakelite are not suitable, more suitable materials being Teflon, polystyrol, or steatite. In addition, low-noise cables should be used, since general-purpose coaxial cables exhibit noise due to mechanical changes.

Figure 30: Frequency Compensation of Operational Amplifier

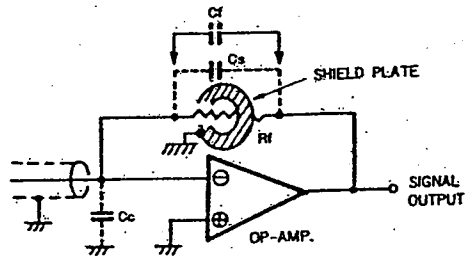

In Figure 30, if a capacitance C_f (including any stray capacitances) exists in parallel to the resistance R_f, the circuit exhibits a time constant of ($R_f \times C_f$), so that response speed is limited to this time constant. This is a particular problem if R_f is made large. Stray capacitance can be reduced by passing R_f through a hole in a shield plate. When using coaxial signal input cables, since the cable capacitance C_C and R_f are in the feedback loop, oscillations may occur and noise may be amplified. While the method of avoiding this is to connect C_f in parallel to R_f, to reduce gain at high frequencies, this, as described above, creates a

APPENDIX

1) Photon Counting

Photon counting is one effective way to use a photomultiplier tube for measuring very low light. It is widely used in astronomical photometry and fluorescence spectroscopy. In the usual application, a number of photons enters the photomultiplier tube and creates an output pulse train like (a) in Figure 31. The actual output obtained by the measurement circuit is a DC with fluctuation as shown at (b).

Figure 31: Overlapping Output Pulses

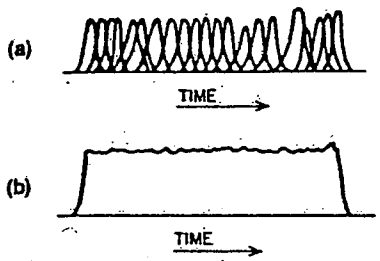

When the light intensity becomes so low that the incident photons are separated as shown in Figure 32. This condition is called single photon event. The number of output pulses is in direct proportion to the amount of incident light and this pulse counting method has advantages in S/N ratio and stability over the DC method averaging all the pulses. This pulse counting technique is the photon counting method.

Figure 32: Single Photon Event

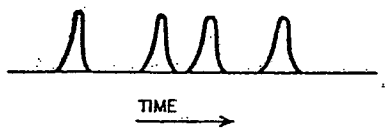

Since the photomultiplier tube output contains a variety of noise pulses in addition to the signal pulses representing photoelectrons as shown in Figure 33, simply counting the pulses without some form of noise elimination will not result in an accurate measurement. The most effective approach to noise elimination is to investigate the height of the output pulses.

Figure 33: Output Pulse and Discrimination Level

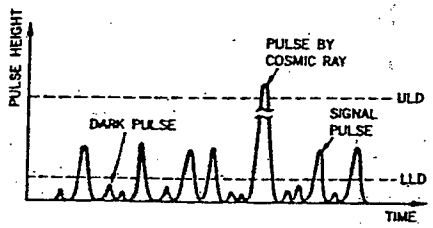

A typical pulse height distribution (PHD) of output of photomultiplier tubes is shown in Figure 34. In this PHD, the lower level discrimination (LLD) is set at the valley and the upper level discrimination (ULD) at the foot. Most pulses smaller than the LLD are noise and pulses larger than the ULD result from cosmic rays, etc. Therefore, by counting pulses between the LLD and ULD, accurate light measurements are made possible. In the PHD, Hm is the mean height of pulses. It is recommended that the LLD be set at 1/3 of Hm and the ULD at triple Hm.

Considering the above, clear definition of the peak and valley in the PHD is a very significant characteristic for photomultiplier tubes for use in photon counting. All of Hamamatsu photomultiplier tubes selected for photon counting are supplied with such PHD data.

Figure 34: Typical Pulse Height Distribution

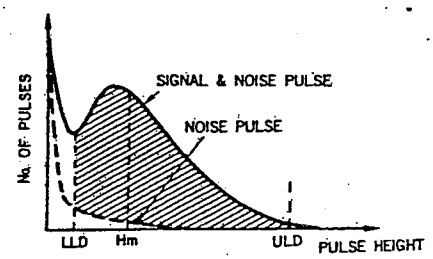

2) Scintillation Counting

Scintillation counting is one of the most common and effective methods in detecting radiation particles. It uses a photomultiplier tube coupled to a scintillator which produces light by incidence of radiation particles.

Figure 35: Diagram of Scintillation Detector

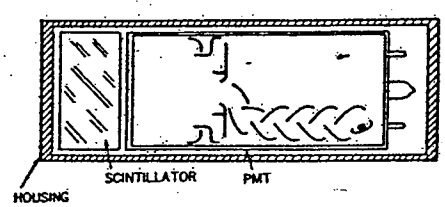

In radiation particle measurements, there are two parameters that should be measured. One is the energy of individual particles and the other is the amount of particles. When radiation particles enter the scintillator, it produces light flashes in response to each particle. The amount of flash is proportional to the energy of the incident particle and individual light flashes are detected by the photomultiplier tube. Consequently, the output pulses obtained from the photomultiplier tube contain information on both the energy and amount of pulses, as shown in Figure 36.

By analyzing these output pulses using a multichannel analyzer (MCA), a pulse height distribution (PHD) or energy spectrum as shown in Figure 37 is obtained. From the PHD, the amount of incident particles at various energy levels can be measured. For the PHD, it is very important to have distinct peaks at each energy level. This is evaluated as pulse height resolution and is the most significant characteristic in radiation particle measurements. Figure 38 shows the definition of pulse height resolution for a ^{137}Cs source.

Figure 36: Incident Particles and PMT Output

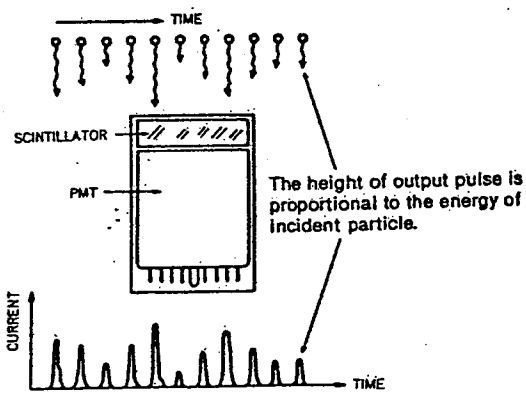

Figure 37: Pulse Height Distribution (Energy Spectrum)

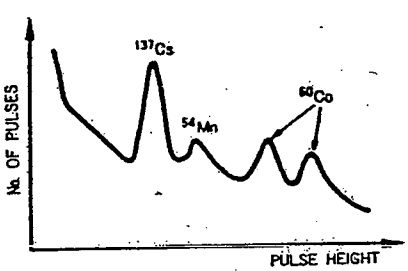

Figure 38: Definition of Pulse Height Resolution

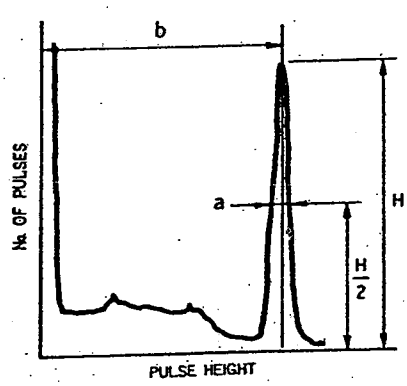

$$\text{Pulse Height Resolution} = \frac{a}{b} \times 100\ (\%)$$

Figure 39: Spectral Response of PMT and Spectral Emission of NaI (Tl) Scintillator

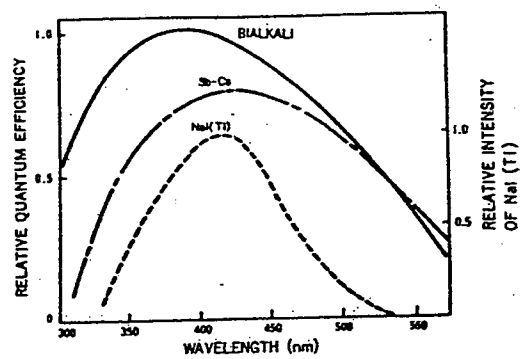

Pulse height resolution is mainly determined by the quantum efficiency of the photomultiplier tube in response to the scintillator emission. It is necessary to choose the tube whose spectral response matches the scintillator emission. For thallium-activated sodium iodide, NaI(Tl) which is the most popular scintillator, head-on type photomultiplier tubes with a bialkali photocathode are widely used. Hamamatsu has a 30-page catalog "Photomultiplier Tubes for Scintillation Counting and High Energy Physics" available from our sales office.

BASING DIAGRAM SYMBOLS

All basing diagrams show terminals viewed from the base end of the tube.

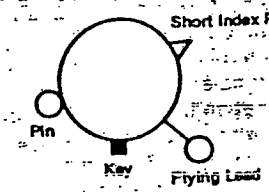

DY : Dynode
G (F) : Grid (Focusing Electrode)
ACC : Grid (Accelerating Electrode)
K : Photocathode
P : Anode
SH : Shield
IC : Internal Connection (Do not use)
NC : No Connection (Do not use)

Typical Photocathode Spectral Response

	Curve Codes	Photocathode Materials	Window Materials	Spectral Response: Range (nm)	Peak Wavelength: of Radiant Sensitivity (nm)	Peak Wavelength: of Q.E. (nm)	PMT Examples
Semitransparent Photocathode (Transmission Mode)							
○	100M	Cs-I	MgF2	115 – 200	140	130	R1081, R972, R1459, R2050
○	200S	Cs-Te	Synthetic silica	160 – 320	210	200	R1893, R759, R821, R431S
○	200M	Cs-Te	MgF2	115 – 320	210	200	R1080, R1460
/	201S	Cs-Te	Synthetic silica	160 – 320	240	220	R2078
/	201A	Cs-Te	Sapphire	150 – 320	250	220	R1689-01
○	300K (S-11)	Sb-Cs	Borosilicate	300 – 650	440	410	6199, 7696
○	400K	Bialkali	Borosilicate	300 – 650	420	390	R647, R1213, R268, R580, R329, R878, R1306, R1213, R1250, R1635, R3082, etc.
○	400U	Bialkali	UV glass	185 – 650	420	390	R750, R269
○	400S	Bialkali	Synthetic silica	160 – 650	420	390	R760, R292, R331, R585, R2059, R2496, R3172, etc.
○	401K	High temp. bialkali	Borosilicate	300 – 650	375	360	R1281, R1288, R1282, R1044, R1640, R1317-05, R1519-01, R1705
/	402K	Bialkali	Borosilicate	300 – 650	375	360	R1645U, R1564U, R2286U, R2287U, R2024U, R2809U, etc.
○	403U	Low noise bialkali	UV glass	185 – 680	375	320	R2693
○	500K (S-20)	Multialkali	Borosilicate	300 – 850	420	360	R1894, R1617, R1387, R550, R1513, R1925, PM55, R649
○	500U	Multialkali	UV glass	185 – 850	420	290	R1463, R1464, R374, R1508, R453, R567, R1104, R2027
○	500S	Multialkali	Synthetic silica	160 – 850	420	280	R376, R375, R562, R2368
○	501K	Multialkali	Borosilicate	300 – 900	650	600	R1333, R669, R1017, R649, R2066, R2228
○	700K (S-1)	Ag-O-Cs	Borosilicate	400 – 1200	800	780	R632, R316, R568, 7102, R1767
Opaque Photocathode (Reflection Mode)							
○	150M	Cs-I	MgF2	115 – 195	120	120	R1259
○	250S	Cs-Te	Synthetic silica	160 – 320	200	200	R1657, R427, R166, R166UH
○	250M	Cs-Te	MgF2	115 – 320	200	190	R1220
○	350K (S-4)	Sb-Cs	Borosilicate	300 – 650	400	350	R906, 931A, 1P21, R105, R105UH
○	350U (S-5)	Sb-Cs	UV glass	185 – 650	340	270	R1414, R300, R212, 1P28, R444, R212UH
○	350S (S-19)	Sb-Cs	Synthetic silica	160 – 650	340	210	R306, R106, R106UH
○	351U (Ext'd S-5)	Sb-Cs	UV glass	185 – 700	450	235	1P28A
/	451U	Bialkali	UV glass	185 – 730	340	320	R372
/	452U	Bialkali	UV glass	185 – 750	350	315	R905
/	453K	Bialkali	Borosilicate	300 – 650	400	360	931B
/	453U	Bialkali	UV glass	185 – 650	400	330	R1516
/	454K	Bialkali	Borosilicate	300 – 680	450	430	R1785
/	455U	Bialkali	UV glass	185 – 680	420	400	R1784
/	456U	Low noise bialkali	UV glass	185 – 680	375	320	R1527, R2371, R2371-02
/	457U	Bialkali	UV glass	300 – 680	450	450	R2752
/	550U	Multialkali	UV glass	185 – 850	530	250	R1546, R1547, R500, R889
/	550S	Multialkali	Synthetic silica	160 – 850	530	250	R1503
○	551U	Multialkali	UV glass	185 – 870	330	280	R446
○	551S	Multialkali	Synthetic silica	160 – 870	330	280	R456
○	552U	Multialkali	UV glass	185 – 900	400	260	R928
○	552S	Multialkali	Synthetic silica	160 – 900	400	215	R955
/	554U	Multialkali	UV glass	185 – 900	450	370	R1477
/	555U	Multialkali	UV glass	185 – 850	400	320	R777
/	556U	Multialkali	UV glass	185 – 930	420	320	R936
/	557U	Multialkali	UV glass	185 – 900	420	400	R1913
/	558K	Multialkali	Borosilicate	300 – 800	530	510	R1923
/	559U	Multialkali	UV glass	185 – 810	330	280	R508
○	650U	GaAs(Cs)	UV glass	185 – 930	300 – 700	300	R636
○	650S	GaAs(Cs)	Synthetic silica	160 – 930	300 – 700	280	R943-02
/	651U	GaAs(Cs)	UV glass	185 – 910	350	270	R666, R666S
○	750K	Ag-O-Cs	Borosilicate	400 – 1100	730	730	R406
/	850U	InGaAs (Cs)	UV glass	185 – 1010	400	330	R2658

○ : Spectral response curves are shown on page 77.

Semitransparent Photocathode

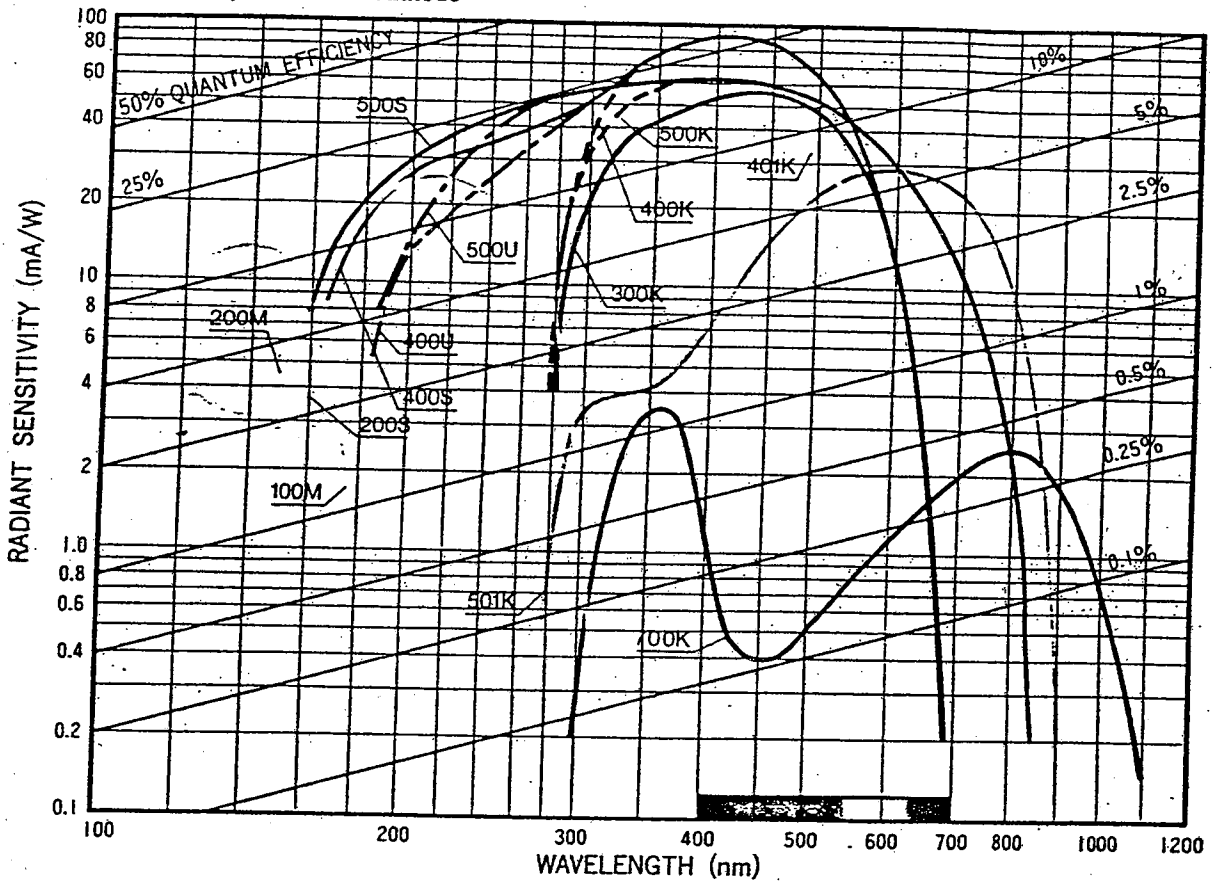

Opaque Photocathode

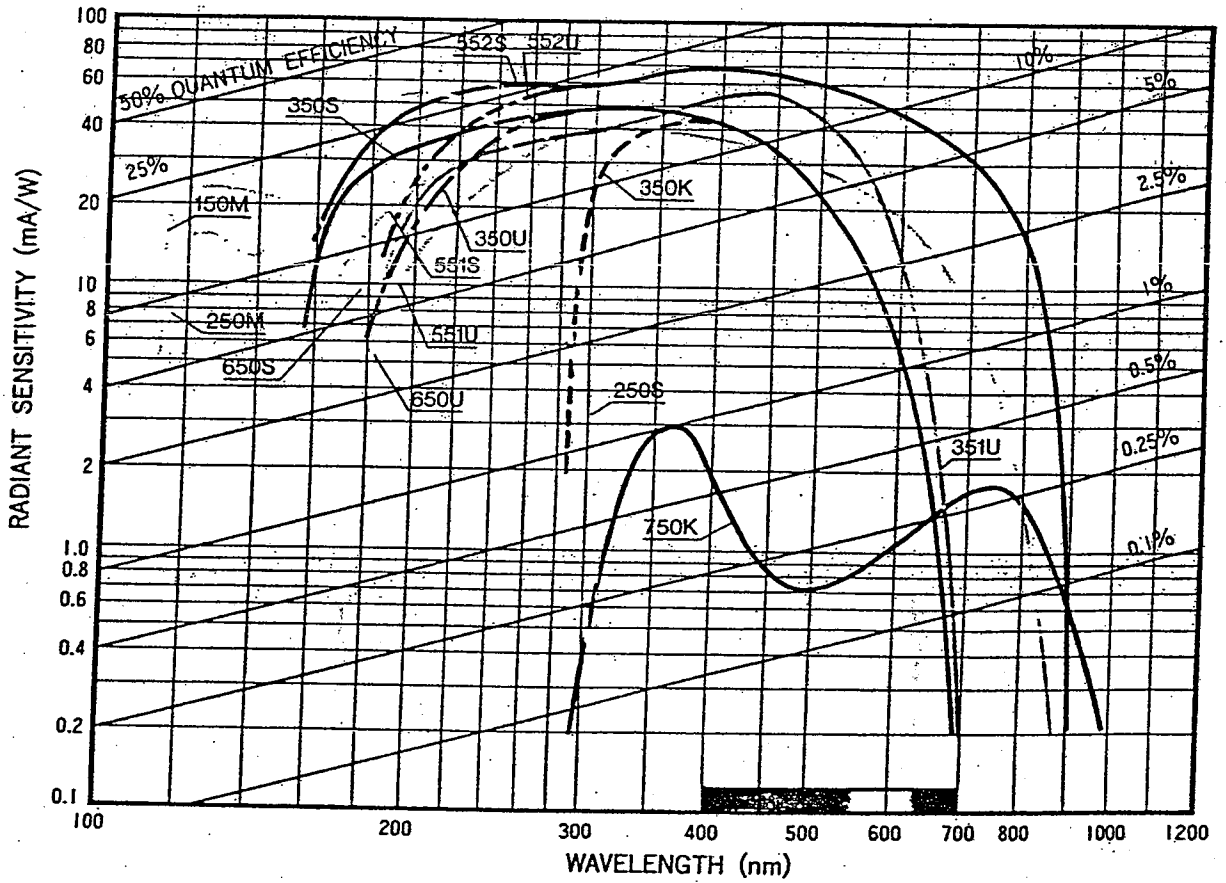

From Laser Electronics by Verdeyen

10.5.2 Helium-Neon Laser

The energy-level diagram for the helium-neon system is shown in Fig. 10.11 together with some common laser transitions shown as solid lines. For instance, the very common "red" laser line at 6328 Å is a transition from the $3s_2$

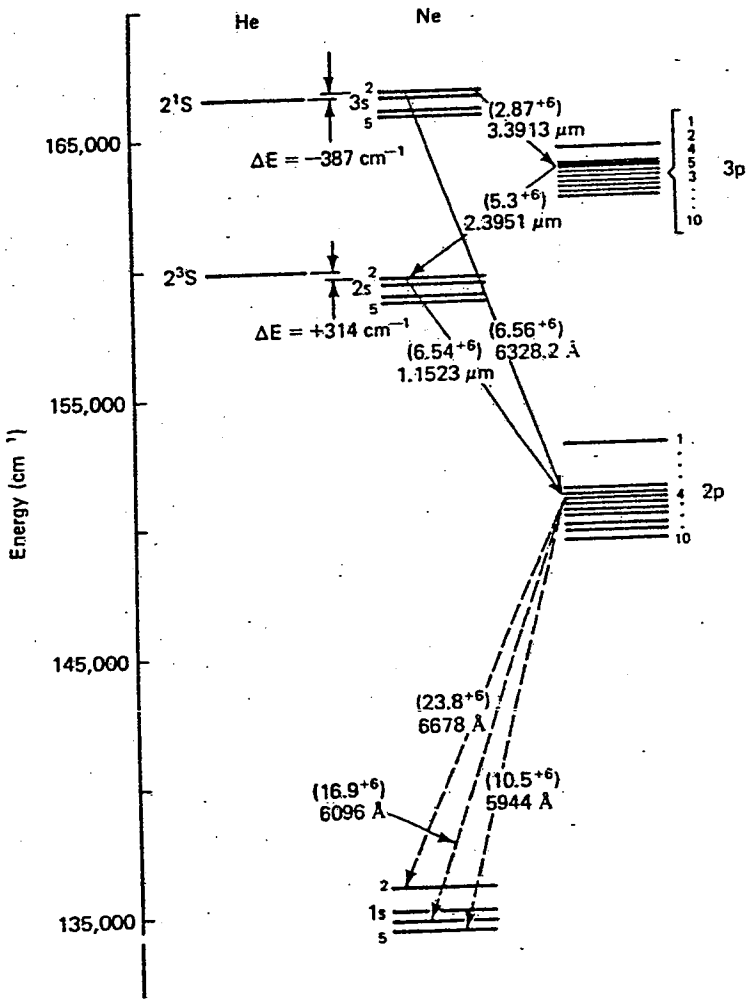

Figure 10.11 Energy-level diagram for the helium-neon laser. The solid line represents the common laser line; the dashed lines are spontaneous. The numbers in parentheses are the A coefficients.

Note: Spectroscopic notation for Ne is not the "standard" one that you have encountered.

to $2p_4$ state.* The numbers
this figure, as dashed lines
laser level, $2p_4$, down to t
These latter transition
rest of the $2p$ states, give n
A coefficients (the numbers
transitions are quite large c
trates an important point re
scheme of a laser was disc
for a laser; rather, it is the
strong ones, that are prime
To illustrate this poin
two states of interest in the
out of the two states and t
Chemistry and Physics (CR
and none of the $2p_4 \rightarrow 1s_2$
of the fact that the A coeff

However, as we will see,
transitions; hence, they do
states empties the lower le
A typical helium-nec
in diameter, and filled wi
pressure prescription of (1

$$p \cdot d \sim 0.36$$

Typical currents through t
operation.
Such a prescription
charge, a subject to be dis
need only the experimenta

1. The electron tempera
to number density o

*The spectroscopic notat
notation, as used in Fig. 10.11,
it did not work! Nevertheless, th
and letters are names of the stat
†The word "temperature"
it is not! But it is a reasonable

n-neon system is shown in Fig.
itions shown as solid lines. For
328 Å is a transition from the $3s_2$

e

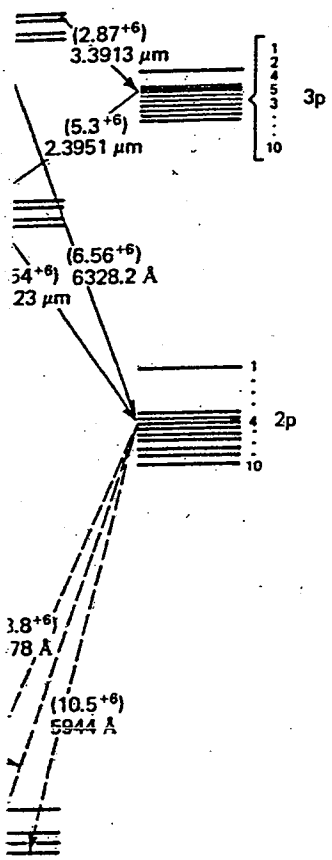

eon laser. The solid line represents the
The numbers in parentheses are the A

to $2p_4$ state.* The numbers in parentheses are the A coefficients. Also shown in this figure, as dashed lines, are the spontaneous decay routes from the lower laser level, $2p_4$, down to the $1s$ states.

These latter transitions, $2p_4 \rightarrow 1s_{2,4,5}$, and many others originating at the rest of the $2p$ states, give neon signs their characteristic red color. Note that the A coefficients (the numbers in parentheses in Fig. 10.11) for these spontaneous transitions are quite large compared with that of the laser transition. This illustrates an important point referred to in Chapter 8, where a generalized pumping scheme of a laser was discussed. We do *not* look for strong spontaneous lines for a laser; rather, it is the weak lines, which terminate on the upper states of the strong ones, that are prime candidates for a laser.

To illustrate this point further, consider the data given in Table 10.5 for the two states of interest in the 6328-Å transition. Here we list the many transitions out of the two states and their relative intensities as listed in the *Handbook of Chemistry and Physics* (CRC Press). *All* the $3s \rightarrow 2p_{1-8}$ transitions have lased, and none of the $2p_4 \rightarrow 1s_{2-5}$ have oscillated (in CW operation). This is in spite of the fact that the A coefficient is in the numerator of the laser gain equation:

$$\gamma_0(\nu) = A_{21}\frac{\lambda^2}{8\pi}g(\nu)\left(N_2 - \frac{g_2}{g_1}N_1\right) \tag{10.5.1}$$

However, as we will see, it is difficult to obtain an inversion on the $2p \rightarrow 1s$ transitions; hence, they do not lase. But the rapid spontaneous decay of the $2p$ states empties the lower level of the $3s \rightarrow 2p$ laser transitions.

A typical helium-neon laser is a glass tube 10 to 100 cm long, 2 to 8 mm in diameter, and filled with helium and neon gas in a 5:1 to 20:1 ratio to a pressure prescription of (12).

$$p \cdot d \sim 0.36 \text{ torr-cm} \qquad \text{d = diameter of bore, cm}$$

Typical currents through the discharge tube range from 5 to 100 mA for CW operation.

Such a prescription satisfies the scaling laws of a positive column discharge, a subject to be discussed in greater detail in Chapter 12. For now, we need only the experimental facts of life about low-pressure discharges.

1. The electron temperature† is directly related to the ratio of the electric field to number density of gas atoms (i.e., $T_e \propto E/N$ or E/p).

*The spectroscopic notation for neon is particularly confusing but widely used. Paschen notation, as used in Fig. 10.11, was an attempt to fit the neon spectra to a hydrogen-like theory. It did not work! Nevertheless, the notation is still with us. As far as we are concerned, the numbers and letters are names of the states, nothing more.

†The word "temperature" implies a Maxwellian distribution of electron velocities. In fact, it is not! But it is a reasonable approximation to use for the initial understanding.

TABLE 10.5 DATA ASSOCIATED WITH THE VARIOUS STATES OF NEON

Transition	J_{upper}	J_{lower}	λ(Å)	$A(10^6\ \text{sec}^{-1})$	Relative Intensity	
$3s_2 \rightarrow 2p_1$	1	0	7304.9	0.48	30	
$3s_2 \rightarrow 2p_2$	1	1	6401.1	0.6 (est.)	100	
$3s_2 \rightarrow 2p_3$	1	0	6351.9	0.7	100	
$3s_2 \rightarrow 2p_4$	1	2	6328.2	6.56	300	(common "red" laser)
$3s_2 \rightarrow 2p_5$	1	1	6293.8	1.35	100	
$3s_2 \rightarrow 2p_6$	1	2	6118.0	1.28	100	
$3s_2 \rightarrow 2p_7$	1	1	6046.1	0.68	50	
$3s_2 \rightarrow 2p_8$	1	2	5939.3	0.56	50	
$3s_2 \rightarrow 2p_9$	1	3	5882.5	Forbid $\Delta J = 2$	Not observed	
$3s_2 \rightarrow 2p_{10}$	1	1	5433.6	0.59	250	
$3s_2 \rightarrow \Sigma 2p$	1	—	Red-orange	12.8	—	
$3s_2 \rightarrow 3p_4$	1	2	33913	2.87	—	
$3s_2 \rightarrow \Sigma 3p$	1	—	IR	5.24	—	
$2p_4 \rightarrow 1s_2$	2	1	6678.3	23.8	500	
$2p_4 \rightarrow 1s_3$	2	0	6234.5	Forbid $\Delta J = 2$	Not observed	
$2p_4 \rightarrow 1s_4$	2	1	6096.2	16.9	300	
$2p_4 \rightarrow 1s_5$	2	2	5944.8	10.5	500	
$2p_4 \rightarrow \Sigma 1s$			Red-orange	51.2		
Other transitions	ΣA			λ	$A(\times 10^6)$	
$2p_1 \rightarrow \Sigma 1s$	87.9		$2s_2 - 2p_1$	1.5231 μm	0.802	
$2p_2 \rightarrow \Sigma 1s$	116.6		$2p_2$	1.1767 μm	4.089	
$2p_3 \rightarrow \Sigma 1s$	61.7		$2p_3$	1.1602 μm	0.801	
$2p_4 \rightarrow \Sigma 1s$	51.7		$2p_4$	1.1523 μm	6.537	(first gas laser)
$2p_5 \rightarrow \Sigma 1s$	53.3		$2p_5$	1.1409 μm	2.301	
$2p_6 \rightarrow \Sigma 1s$	53.6		$2p_6$	1.0844 μm	7.543	
$2p_7 \rightarrow \Sigma 1s$	49.3		$2p_7$	1.0621 μm	0.816	
$2p_8 \rightarrow \Sigma 1s$	41.2		$2p_8$	1.0295 μm	0.726	
$2p_9 \rightarrow \Sigma 1s$	43.3		$2p_9$	Forbidden	—	
$2p_{10} \rightarrow \Sigma 1s$	33.6		$2p_{10}$	0.8895 μm	1.708	

2. To a reasonable approximation, E/N is a function only of the pressure times diameter product.
3. The electron temperature (or E/N) is either constant or decreases slightly with increasing current.

Thus keeping the pd product constant implies a discharge with more or less the same voltage drop per unit length and same electron temperature. Typical values for T_e are ~80,000°K and $E/p = 28$ V/cm/torr at $pd = 0.36$ torr-cm.

The pumping sequence of the red laser is as follows: helium, being the majority gas present, is excited by the energetic electrons in the high-energy tail of the Maxwellian distribution. This is represented by the following chemical equation:

$$e(\text{K.E.}) + \text{He}(1^1S) \longrightarrow \text{He}(2^1S) + e(\text{K.E.} - 20.6\ \text{eV}) \qquad (10.5.2)$$

where the potential e
20.6 eV.

Now this partic
ground state by emi
$0 \rightarrow J = 0$ step. Co
seconds in fact—unl
That something else
the helium ladder, c
excited helium state
warm up the univers
they are deleterious t

But a neutral ne
excited helium atom.
neon according to

He(2^1S) + Ne(grou

where the excess en
colliding atoms.

Thus we have
Furthermore, since th
the $3s_2$ level, it cont
version.

Unfortunately,
dently of the $3s_2 \rightarrow$
system to low power
greater rate than is th
energy to the $2s$ man
this is the excitation n
first gas laser. If the
is an unavoidable
$2^1S \rightarrow 3s_2 - 2p_4$ is l
laser transition tends

A classic exam
6328-Å and 3.39-μr
thus having a smalle
cross section than do
are taken to reduce th
and deplete the popu

There is anoth
citation from the neo
neon sign depends or
does indeed work! Th

TATES OF NEON

sec^{-1})	Relative Intensity	
8	30	
(est.)	100	
	100	
6	300	(common "red" laser)
5	100	
8	100	
8	50	
6	50	
$\Delta J = 2$	Not observed	
9	250	
8	—	
37	—	
24	—	
8	500	
$\Delta J = 2$	Not observed	
9	300	
5	500	
2		
	$A(\times 10^6)$	
m	0.802	
m	4.089	
m	0.801	(first gas laser)
m	6.537	
m	2.301	
m	7.543	
m	0.816	
m	0.726	
n	—	
m	1.708	

unction only of the pressure

constant or decreases slightly

scharge with more or less the
n temperature. Typical values
at $pd = 0.36$ torr-cm.
is follows: helium, being the
ectrons in the high-energy tail
ed by the following chemical

K.E. − 20.6 eV) (10.5.2)

where the potential energy of the He(2^1S) state relative to the ground state is 20.6 eV.

Now this particular state is metastable; that is, it cannot decay back to the ground state by emitting a photon, as such a transition would require $J = 0 \rightarrow J = 0$ step. Consequently, such a state will live for a long time—many seconds in fact—unless something else collides with the excited helium atom. That something else may be another electron, which could excite it further up the helium ladder, or the electron could reverse the arrow of (10.5.2). The excited helium state could also diffuse to the wall to be deactivated there (and warm up the universe). None of these possibilities help the laser a bit; in fact, they are deleterious to its operation.

But a neutral neon atom can be that something else that collides with that excited helium atom. The potential energy of the He state is transferred to the neon according to

$$\text{He}(2^1S) + \text{Ne(ground)} + 387\ \text{cm}^{-1} \longrightarrow \text{He}(1^1S) + \text{Ne}(3s_2) \qquad (10.5.3)$$

where the excess energy, 387 cm^{-1}, is provided by the kinetic energy of the colliding atoms.

Thus we have a *selective* mechanism for pumping the upper laser level. Furthermore, since the lower $2p_4$ state has a much shorter radiative lifetime than the $3s_2$ level, it contributes significantly to the creation of the population inversion.

Unfortunately, the $2p_4$ level can also be excited by the discharge independently of the $3s_2 \rightarrow 2p_4$ route, and this fact ultimately dooms the He:Ne laser system to low power. For instance, the helium 2^3S state is excited at an even greater rate than is the 2^1S state. This lower helium metastable state transfers its energy to the $2s$ manifold in neon, which, in turn, radiates to $2p$ level. Indeed, this is the excitation route for the laser transition at 1.1523 μm ($2s_2 - 2p_4$)—the first gas laser. If the 6328-Å transition is desired, the $2^3S \rightarrow 2s_2 \rightarrow 2p_4$ route is an unavoidable pumping of the lower laser level. Alternatively, the $2^1S \rightarrow 3s_2 - 2p_4$ is bad for the 1.1523-μm laser. This is an example where one laser transition tends to fill the lower state of another.

A classic example of the competition for the upper state is provided by the 6328-Å and 3.39-μm transitions. The latter, being of longer wavelength and thus having a smaller Doppler width, has a much higher stimulated emission cross section than does the visible transition. Thus, unless special precautions are taken to reduce the feedback at 3.39 μm, the $3s_2 \rightarrow 3p_4$ transition will lase and deplete the population inversion of the $3s_2 \rightarrow 2p_4$.

There is another route for pumping the $2p$ levels: electron impact excitation from the neon ground state or from the neon $1s$ manifold. After all, the neon sign depends on the $2p \rightarrow 1s$ transitions for its characteristic color, and it does indeed work! Therefore the $2p$ states will be excited by a discharge. As we

MIT Wavelength Table

(not all of the lines are listed)

TABLE III

SENSITIVE LINES OF THE ELEMENTS*

Wave-length	Excitation Potential†	Intensities Arc	Intensities Spk., [Dis.]	Sensi-tivity‡
A 18 Argon				
8115.311	13.0	–	[5000]	U2
7503.867	13.4	–	[700]	U4
7067.217	13.2	–	[400]	U3
6965.430	13.3	–	[400]	U3
Ag 47 Silver				
5465.487	6.0	1000 R	500 R	U4
5209.067	6.0	1500 R	1000 R	U3
3382.891	3.6	1000 R	700 R	U2
3280.683	3.8	2000 R	1000 R	U1
2437.791	17.4	60	500 wh	V2
2246.412	17.8	25	300 hs	V3
Al 13 Aluminum				
6243.36	21.0	–	100	V3
6231.76	21.0	–	30	–
3961.527	3.1	3000	2000	U1
3944.032	3.1	2000	1000	U2
3092.713	4.0	1000	1000	U3
3082.155	4.0	800	800	U4
2816.179	17.7	10	100	V2
2669.166	10.6	3	100	V1
2631.553	21.2	–	40	–
As 33 Arsenic				
2898.71	6.7	25 r	40	–
2860.452	6.6	50 r	50	–
2780.197	6.7	75 R	75	U5
2456.53	6.5	100 r	8	U4
2370.77	6.7	50 r	3	–
2369.67	6.7	40 r	–	–
2349.84	6.6	250 R	18	U3
2288.12	6.7	250 R	5	U3
Au 79 Gold				
2802.19	>13.6	–	200	–
2675.95	4.6	250 R	100	U2
2427.95	5.1	400 R	100	U1
B 5 Boron				
3451.41	20.9	5	30	V2
2497.733	4.9	500	400	U1
2496.778	4.9	300	300	U2
Ba 56 Barium				
5777.665	3.8	500 R	100 R	U2
5535.551	2.2	1000 R	200 R	U1
5519.115	3.8	200 R	60 R	U3
5424.616	3.8	100 R	30 R	U4
4934.086	7.7	400 h	400 h	V2
4554.042	7.9	1000 R	200	V1
4130.664	10.9	50 r	60 wh	V3
3891.785	10.9	18	25	V4
3071.591	4.0	100 R	50 R	U5
2335.269	11.2	60 R	100 R	–
2304.235	11.2	60 R	80 R	–
Be 4 Beryllium				
3321.343	6.4	1000 r	30	U2
3321.086	6.4	100	–	U3
3321.013	6.4	50	–	U4
3131.072	13.2	200	150	V2
3130.416	13.2	200	200	V1
2650.781	7.4	25	–	U5
2348.610	5.4	2000 R	50	U1
Bi 83 Bismuth				
4722.552	4.0	1000	100	–
3067.716	4.0	3000 hR	2000 wh	U1
2989.029	5.5	250 wh	100 wh	–
2938.298	6.1	300 w	300 w	–
2897.975	5.6	500 WR	500 WR	U2
2809.625	6.3	200 w	100	–
2780.521	5.8	200 w	100	–
2276.578	5.4	100 R	40	–
2061.70	6.0	300 R	100	–
Br 35 Bromine				
4816.71	14.4	–	[300]	V3
4785.50	14.4	–	[400]	V2
4704.86	14.4	–	[250]	V1
C 6 Carbon				
4267.27	32.1	–	500	V2
4267.02	32.1	–	350	V3
2837.602	27.5	–	40	V5
2836.710	27.5	–	200	V4
2478.573	7.7	400	[400]	U2
2296.89	53.5	–	200	–
Ca 20 Calcium				
4454.781	4.7	200	–	U2
4434.960	4.7	150	–	U3
4425.441	4.7	100	–	U4
4226.728	2.9	500 R	50 W	U1
3968.468	9.2	500 R	500 R	V2
3933.666	9.2	600 R	600 R	V1
3179.332	13.1	100	400 w	V3
3158.869	13.1	100	300 w	V4
Cb 41 Columbium				
4137.095	3.0	100	60	U5
4123.810	3.0	200	125	U4
4100.923	3.1	300 w	200 w	U3
4079.729	3.1	500 w	200 w	U2
4058.938	3.2	1000 w	400 w	U1
3225.479	>7.6	150 w	800 wr	–
3194.977	>7.7	30	300	–
3163.402	>7.8	15	8	–
3130.786	>7.9	100	100	–
3094.183	>8.0	100	1000	V1
Cd 48 Cadmium				
6438.4696	7.3	2000	1000	–
3610.510	7.3	1000	500	–
3466.201	7.3	1000	500	–
3403.653	7.3	800	500 h	–
3261.057	3.8	300	300	–
2748.58	19.2	5	200	–
2573.09	19.2	3	150	–
2312.84	20.1	1	200	–
2288.018	5.4	1500 R	300 R	U1
2265.017	14.4	25 d	300	V2
2144.382	14.7	50	200 R	V1
Ce 58 Cerium				
4186.599	>8.6	80	25	–
4165.606	>8.6	40	6	–
4040.762	>8.7	70	5	–
4012.388	>8.7	50	20	–
Cl 17 Chlorine				
4819.46	28.3	–	[200]	V4
4810.06	28.3	–	[200]	V3
4794.54	28.3	–	[250]	V2
Co 27 Cobalt				
3529.813	4.0	1000 R	30	U3
3465.800	3.6	2000 R	25	U2
3453.505	4.0	3000 R	200	U1
3405.120	4.0	2000 R	150	–
2519.822	14.7	40	200	–
2388.918	14.1	10	35	–
2378.622	14.1	25	50 w	–
2363.787	14.2	25	50	–
2307.857	14.3	25	50 w	–
2286.156	14.3	40	300 l	V1
Cr 24 Chromium				
5208.436	3.3	500 R	100	U4
5206.039	3.3	500 R	200	U5
5204.518	3.3	400 R	100	U6
4289.721	2.9	3000 R	800 r	U3
4274.803	2.9	4000 R	800 r	U2
4254.346	2.9	5000 R	1000	U1
2860.934	12.5	60	100	V5
2855.676	12.5	60	200 wh	V4
2849.838	12.6	80	150 r	V3
2843.252	12.6	125	400 r	V2
2835.633	12.6	100	400 r	V1
Cs 55 Caesium				
8943.50	1.4	2000 R	–	U2
8521.10	1.4	5000 R	–	U1
4593.177	2.7	1000 R	50	U4
4555.355	2.7	2000 R	100	U3
Cu 29 Copper				
5218.202	6.2	700	–	U3
5153.235	6.2	600	–	U4
5105.541	3.8	500	–	U5
3273.962	3.8	3000 R	1500 R	U2
3247.540	3.8	5000 R	2000 R	U1
2824.37	–	1000	300	–
2246.995	15.9	30	500	V3
2192.260	16.2	25	500 h	V2
2135.976	16.2	25	500 w	V1
Dy 66 Dysprosium				
4211.719	>2.9	200	15	–
4167.966	>3.0	50	12	–
4077.974	>3.0	150 r	100	–
4045.983	>3.0	150	12	–
4000.454	>3.1	400	300	–
Er 68 Erbium				
3906.316	>3.2	25	12	–
3692.652	>3.4	20	12	–
3499.104	>3.5	18	15	–
Eu 63 Europium				
4661.87	–	300 R	120	550
4627.22	–	400 R	150	650
4594.02	–	500 R	200	750
4205.046	8.6	200 R	50	–
4129.737	8.6	150 R	50 R	–
F 9 Fluorine				
6902.46	14.5	–	[500]	U3
6856.02	14.4	–	[1000]	U2
5291.0	bh Ca F 200		–	–
Fe 26 Iron				
3748.264	3.4	500	200	U4
3745.903	3.4	150	100	U5
3745.564	3.4	500	500	U3
3737.133	3.4	1000 r	600	U2
3719.935	3.3	1000 R	700	U1
3581.20	–	1000 R	600 R	600
2413.309	13.1	60	100 h	V5
2410.517	13.1	50	70 h	V4
2404.882	13.0	50	100 wh	V3
2395.625	13.0	50	100 wh	V2
2382.039	13.0	40 r	100 R	V1
Ga 31 Gallium				
4172.056	3.1	2000 R	1000 R	U1
4032.982	3.1	1000 R	500 R	U2
2943.637	4.3	10	20 r	U3
2874.244	4.3	10	15 r	U4

* Compiled from a combination of empirical and theoretical data selected from the literature.

† For an ion, the ionization potential of the neutral atom has been included in the excitation potential to give an approximate idea of the excitation required to produce the line.

‡ For the neutral atom, the most sensitive line (raie ultime) is indicated by U1, and other lines by U2, U3, etc., in order of decreasing sensitivity. For the singly ionized atom, the corresponding designations are V1, V2, etc. In cases where U1 is not given, the most sensitive lines lie outside the spectral range 10,000–2000 A. Figures given in the Sensitivity Column are taken from the NBS Tables of Spectral-Line Intensities, where values for numerous other lines also can be found. (See Meggers, Corliss and Scribner, NBS Monograph 32, 1961, Government Printing Office; also C. H. Corliss, NBS Monograph 32 Supplement, 1967).

Wave-length	Excitation Potential†	Intensities Arc	Intensities Spk., [Dis.]	Sensitivity‡
Gd 64 Gadolinium				
3768.405	>3.3	20	20	–
3646.196	>3.4	200 w	150	–
Ge 32 Germanium				
4226.570	4.9	200	50	–
3269.494	4.7	300	300	U3
3039.064	4.9	1000	1000	U2
2709.626	4.6	30	20	–
2651.575	4.7	30	20	–
2651.178	4.8	40	20	–
H 1 Hydrogen				
6562.79	12.0	–	[3000]	U2
4861.327	12.7	–	[500]	U3
He 2 Helium				
5875.618	23.0	–	[1000]	U3
4685.75	75.3	–	[300]	–
3888.646	22.9	–	[1000]	U2
Hf 72 Hafnium				
7240.87	–	5000	600	50
7237.10	–	8000	1000	80
7131.82	–	7000	1000	70
7063.82	–	3000	400	20
6818.94	–	2000	300	15
6789.28	–	1000	100	8
4093.161	>7.8	25	20	–
3134.718	>8.7	80	125	–
3072.877	4.0	80	18	–
2940.772	4.2	60	12	–
2916.481	4.2	50	15	–
2904.408	4.8	30	6	–
2898.259	4.6	50	12	–
2820.224	>9.2	40	100	–
2773.357	>9.3	25	60	–
2641.406	>9.5	40	125	–
2516.881	>9.7	35	100	–
2513.028	>9.7	25	70	–
Hg 80 Mercury				
5460.753	7.7	2000	–	320
4358.35	7.7	3000 w	500	–
4046.561	7.7	200	300	–
3663.276	8.8	500	400	U5
3654.833	8.8	–	[200]	U4
3650.146	8.8	200	500	U3
2536.519	4.9	2000 R	1000 R	U2
Ho 67 Holmium				
3891.02	>3.2	200	40	–
3748.17	>3.3	60	40	–
2936.77	>7.4	–	1000 R	–
I 53 Iodine				
5464.61	22.7	–	[900]	–
5161.188	22.8	–	[300]	–
2062.38	>16.4	–	[900]	–
In 49 Indium				
4511.323	3.0	5000 R	4000 R	U1
4101.773	3.0	2000 R	1000 R	U2
3258.564	4.1	500 R	300 R	U5
3256.090	4.1	1500 R	600 R	U3
3039.356	4.1	1000 R	500 R	U4
Ir 77 Iridium				
3513.645	3.5	100 h	100	U2
3437.015	4.4	20	15	–
3220.780	4.2	100	30	U1
2924.792	4.2	25 wh	15	–
2849.725	4.3	40 h	20 h	–
2661.983	–	600 R	60	480
K 19 Potassium				
7698.979	1.6	5000 R	–	U2
7664.907	1.6	9000 R	–	U1
4047.201	3.0	400	200	U4
4044.140	3.1	800	400	U3
Kr 36 Krypton				
5870.9158	12.1	–	[3000]	U2
5570.2896	12.1	–	[2000]	U3
La 57 Lanthanum				
6249.929	2.5	300	–	U1
5930.648	2.2	250	–	U2
5455.146	2.4	200	1	U3
4123.228	8.9	500	500	V4
4077.340	8.9	600	400	V3
3949.106	9.1	1000	800	V2
Li 3 Lithium				
6707.844	1.8	3000 R	200	U1
6103.642	3.9	2000 R	300	U3
4603.00	4.5	800	–	U4
3232.61	3.8	1000 R	500	U2
Lu 71 Lutecium				
4518.57	>2.7	300	40	–
3554.43	>6.2	50	150	–
3472.48	>6.3	50	150	–
3397.07	>6.3	50	20 r	–
2911.39	>6.9	100	300	–
2894.84	>7.0	60	200	–
Mg 12 Magnesium				
5183.618	5.1	500 wh	300	–
5172.699	5.1	200 wh	100 wh	–
5167.343	5.1	100 wh	50	–
3838.258	5.9	300	200	U2
3832.306	5.9	250	200	U3
3829.350	5.9	100 w	150	U4
2852.129	4.3	300 R	100 R	U1
2802.695	12.0	150	300	V2
2795.53	12.0	150	300	V1
Mn 25 Manganese				
4034.490	3.1	250 r	20	U3
4033.073	3.1	400 r	20	U2
4030.755	3.1	500 r	20	U1
2801.064	–	600 R	60	480
2798.271	–	800 R	80	650
2605.688	12.2	100 R	500 R	V3
2593.729	12.2	200 R	1000 R	V2
2576.104	12.2	300 R	2000 R	V1
Mo 42 Molybdenum				
3902.963	3.2	1000 R	500 R	U3
3864.110	3.2	1000 R	500 R	U2
3798.252	3.3	1000 R	1000 R	U1
2909.116	11.6	25	40 h	V5
2890.994	11.7	30	50 h	V4
2871.508	11.7	100	100 h	V3
2848.232	11.8	125	200 h	V2
2816.154	11.9	200	300 h	V1
N 7 Nitrogen				
5679.56	35.1	–	[500]	V2
5676.02	35.0	–	[100]	V4
5666.64	35.0	–	[300]	V3
4109.98	13.7	–	[1000]	U2
4103.37	74.3	–	[60]	–
4099.94	13.7	–	[150]	U3
4097.31	74.3	–	[100]	–
Na 11 Sodium				
5895.923	2.1	5000 R	500 R	U2
5889.953	2.1	9000 R	1000 R	U1
5688.224	4.3	300	–	–
5682.657	4.3	80	–	–
3302.988	3.7	300 R	150 R	U4
3302.323	3.7	600 R	300 R	U3
Nd 60 Neodymium				
4303.573	>2.9	100	40	–
4177.321	>3.0	15	25	–
3951.154	>3.1	40	30	–
Ne 10 Neon				
6402.246	18.5	–	[2000]	–
5852.488	18.9	–	[2000]	–
5400.562	18.9	–	[2000]	–
Ni 28 Nickel				
3524.541	3.5	1000 R	100 wh	–
3515.054	3.6	1000 R	50 h	–
3492.956	3.6	1000 R	100 h	U2
3414.765	3.6	1000 R	50 wh	U1
3050.819	–	1000 R	–	280
2287.084	14.8	100	500	V1
2270.213	14.2	100	400	V2
2264.457	14.3	150	400	V3
2253.86	14.4	100	300	V4
O 8 Oxygen				
7775.433	10.7	–	[100]	U4
7774.138	10.7	–	[300]	U3
7771.928	10.7	–	[1000]	U2
Os 76 Osmium				
4420.468	2.8	400 R	100	–
3267.945	3.8	400 R	30	–
3262.290	4.3	500 R	50	–
3058.66	4.0	500 R	500	–
2909.061	4.2	500 R	400	U1
P 15 Phosphorus				
2554.93	7.1	60	[20]	–
2553.28	7.1	80	[20]	U3
2535.65	7.2	100	[30]	U2
2534.01	7.2	50	[20]	–
Pb 82 Lead				
5608.8	16.9	–	[40]	V2
4057.820	4.4	2000 R	300 R	U1
3683.471	4.3	300	50	U2
3639.580	4.4	300	50 h	–
2833.069	4.4	500 R	80 R	–
2614.178	>4.7	200 r	80	–
2203.505	14.7	50 W	5000 R	V1
2169.994	5.7	1000 R	1000 R	–
Pd 46 Palladium				
3634.695	4.2	2000 R	1000 R	U3
3609.548	4.4	1000 R	700 R	–
3516.943	4.5	1000 R	500 R	–
3421.24	4.6	2000 R	1000 R	U2
3404.580	4.4	2000 R	1000 R	U1
2854.581	16.6	4	500 h	–
2658.722	16.9	20	300	–
2505.739	17.5	3	30	–
2498.784	17.2	4	150 h	–
2488.921	16.3	10	30	–
Pr 59 Praseodymium				
4225.327	>2.9	50	40	–
4189.518	>2.9	100	50	–
4179.422	>3.0	200	40	–
4062.817	>3.0	150	50	–
Pt 78 Platinum				
3064.712	4.0	2000 R	300 R	U1
2997.967	4.2	1000 R	200 r	–
2929.794	4.2	800 R	200 w	–
2830.295	4.4	1000 R	600 r	–
2659.454	4.6	2000 R	500 R	U2
Ra 88 Radium				
4825.91	2.6	–	[800]	U1
4682.28	7.8	–	[800]	V2
3814.42	8.4	–	[2000]	V1
Rb 37 Rubidium				
7947.60	1.6	5000 R	–	U2
7800.227	1.6	9000 R	–	U1
4215.556	2.9	1000 R	300	U4
4201.851	2.9	2000 R	500	U3

† For an ion, the ionization potential of the neutral atom has been included in the excitation potential to give an approximate idea of the excitation required to produce the line.

‡ For the neutral atom, the most sensitive line (raie ultime) is indicated by U1, and other lines by U2, U3, etc., in order of decreasing sensitivity. For the singly ionized atom, the corresponding designations are V1, V2, etc. In cases where U1 is not given, the most sensitive lines lie outside the spectral range 10,000–2000 A. Figures given in the Sensitivity Column are taken from the NBS Tables of Spectral-Line Intensities, where values for numerous other lines also can be found. (See Meggers, Corliss and Scribner, NBS Monograph 32, 1961; also C. H. Corliss, NBS Monograph 32 Supplement, 1967).

Wavelength	Excitation Potential†	Intensities Arc	Intensities Spk., [Dia.]	Sensitivity‡
Re 75 Rhenium				
4889.17	2.5	2000 w	–	U2
3460.47	3.6	1000 W	–	U1
Rh 45 Rhodium				
3692.357	3.3	500 hd	150 wd	–
3657.987	3.6	500 W	200 W	–
3434.893	3.6	1000 r	200 r	U1
3396.85	3.6	1000 w	500	–
3323.092	3.9	1000	200	–
Rn 86 Radon				
7450.00	8.5	–	[600]	U2
7055.42	8.4	–	[400]	U3
Ru 44 Ruthenium				
3596.179	3.7	30	100	U3
3498.942	3.5	500 R	200	U1
3436.737	3.7	300 R	150	U2
2976.586	>10.5	60	200	–
2965.546	>10.6	60	200	–
2945.668	>10.6	60	300	–
2712.410	>11.0	80	300	–
2692.065	>11.0	8	200	–
2678.758	>11.0	100	300	–
S 16 Sulphur				
9237.49	7.8	–	[200]	U6
9228.11	7.8	–	[200]	U5
9212.91	7.8	–	[200]	U4
4696.25	9.1	–	[15]	U9
4695.45	9.1	–	[30]	U8
4694.13	9.1	–	[500]	U7
Sb 51 Antimony				
3267.502	5.8	150	150 Wh	–
3232.499	6.1	150	250 wh	–
2877.915	5.3	250 W	150	–
2598.062	5.8	200	100	–
2528.535	6.1	300 R	200	–
2311.469	5.3	150 R	50	–
2175.890	5.7	300	40	U2
2068.38	6.0	300 R	3	U1
Sc 21 Scandium				
4023.688	3.1	100	25	U3
4020.399	3.1	50	20	U4
3911.810	3.2	150	30	U1
3907.476	3.2	125	25	U2
3642.785	10.0	60	50	V3
3630.740	10.1	50	70	V2
3613.836	10.1	40	70	V1
Se 34 Selenium				
4742.25	>2.6	–	[500]	U6
4739.03	>2.6	–	[800]	U5
4730.78	>2.6	–	[1000]	U4
2062.788	6.3	–	[800]	U3
2039.851	6.3	–	[1000]	U2
Si 14 Silicon				
3905.528	5.1	20	15 W	–
2881.578	5.1	500	400	U1
2528.516	4.9	400	500	U2
2516.123	4.9	500	500	U3
2506.899	4.9	300	200	U4
Sm 62 Samarium				
4434.321	8.8	200	200	V2
4424.342	8.9	300	300	V1
4390.865	8.6	150	150	–
Sn 50 Tin				
4524.741	4.8	500 wh	50	–
3262.328	4.8	400 h	300 h	U3
3175.019	4.3	500 h	400 hr	–
3034.121	4.3	200 wh	150 wh	–
3009.147	4.3	300 h	200 h	–
2863.327	4.3	300 R	300 R	U2
2839.989	4.8	300 R	300 R	U1
Sr 38 Strontium				
4962.263	4.3	40	–	U4
4872.493	4.3	25	–	U3
4832.075	4.3	200	8	U2
4607.331	2.7	1000 R	50 R	U1
4305.447	11.6	40	–	–
4215.524	8.6	300 r	400 W	V2
4077.714	8.7	400 r	500 W	V1
3474.887	12.2	80	50	–
3464.57	12.2	200	200	–
3380.711	12.2	150	200	–
Ta 73 Tantalum				
3406.664	>3.6	70 w	18 s	–
3318.840	>3.7	125	35	–
3311.162	>3.7	300 w	70 w	U1
Tb 65 Terbium				
3874.18	>3.2	200	200	–
3848.75	>3.2	100	200	–
3561.74	>3.5	200	200	–
3509.17	>3.5	200	200	–
Te 52 Tellurium				
2769.67	5.8	–	[30]	–
2530.70	5.5	–	[30]	–
2385.76	5.8	600	[300]	U2
2383.25	5.8	500	[300]	U3
2142.75	5.8	600	–	55
Th 90 Thorium				
4019.137	>3.1	8	8	–
3601.040	>3.4	8	10	–
3538.75	>3.5	–	50	–
3290.59	>7.3	–	40 h	–
Ti 22 Titanium				
5007.213	3.3	200	40	–
4999.510	3.3	200	80	–
4991.066	3.3	200	100	–
4981.733	3.3	300	125	U1
3653.496	3.4	500	200	U2
3642.675	3.4	300	125	–
3635.463	3.4	200	100	–
3383.761	10.4	70	300 R	–
3372.800	10.5	80	400 R	V3
3361.213	10.5	100	600 R	V2
3349.035	11.1	125	800 R	V1
Tl 81 Thallium				
5350.46	3.3	5000 R	2000 R	U1
3775.72	3.3	3000 R	1000 R	U2
3519.24	4.5	2000 R	1000 R	U3
3229.75	4.8	2000	800	–
2918.32	5.2	400 R	200 R	–
2767.87	4.5	400 R	300 R	–
Tm 69 Thulium				
3761.917	>3.3	200	120	–
3761.333	>3.3	250	150	–
3462.21	>3.6	200	100	–
U 92 Uranium				
4241.669	>2.9	40	50	–
3672.579	>3.4	8	15	–
3552.172	>3.5	8	12	–
V 23 Vanadium				
4389.974	3.1	80 R	60 R	–
4384.722	3.1	125 R	125 R	–
4379.238	3.1	200 R	200 R	U1
3185.396	3.9	500 R	400 R	U2
3183.982	3.9	500 R	400 R	–
3183.406	3.9	200 R	100 R	–
3125.284	11.0	80	200 R	–
3118.383	11.1	70	200 R	V4
3110.706	11.1	70	300 R	V3
3102.299	11.1	70	300 R	V2
3093.108	11.2	100 R	400 R	V1
W 74 Tungsten				
4302.108	3.2	60	60	U1
4294.614	3.2	50	50	U2
4008.753	3.4	45	45	U3
3613.790	>9.2	10	30	–
3215.560	5.3	10	9	–
2589.167	>10.6	15 d	25	–
2397.091	>10.9	18	30	–
Xe 54 Xenon				
4671.226	10.9	–	[2000]	U2
4624.276	10.9	–	[1000]	U3
4500.977	11.0	–	[500]	U4
Yb 70 Ytterbium				
3987.994	>3.1	1000 R	500 R	1900
3694.203	>3.3	500 R	1000 R	3200
3289.37	>3.8	500 R	1000 R	2600
Yt 39 Yttrium				
4674.848	2.7	80	100	U1
4643.695	2.7	50	100	U2
3788.697	9.9	30	30	–
3774.332	9.9	12	100	–
3710.290	10.0	80	150	V1
3633.123	9.9	50	100	–
3600.734	10.1	100	300	–
3242.280	10.5	60	100	–
Zn 30 Zinc				
6362.347	7.7	1000 Wh	500	–
4810.534	6.6	400 w	300 h	–
4722.159	6.6	400 w	300 h	–
4680.138	6.6	300 w	200 h	–
3345.020	7.8	800	300	U2
3302.588	7.8	800	300	U3
3282.333	7.8	500 R	300	U4
2557.958	15.3	10	300	V3
2502.001	15.3	20	400 w	V4
2138.56	5.8	800 R	500	U1
2061.91	15.4	100	100	V2
2025.51	15.5	200	200	V1
Zr 40 Zirconium				
4772.312	3.2	100	–	–
4739.478	3.2	100	–	–
4710.075	3.3	60	–	–
4687.803	3.4	125	–	U4
3601.193	3.6	400	15	U1
3572.473	10.4	60	80	V4
3547.682	3.5	200	12	U2
3519.605	3.5	100	10	U3
3496.210	10.5	100	100	V3
3438.230	10.6	250	200	V2
3391.975	10.7	300	400	V1

† For an ion, the ionization potential of the neutral atom has been included in the excitation potential to give an approximate idea of the excitation required to produce the line.

‡ For the neutral atom, the most sensitive line (raie ultime) is indicated by U1, and other lines by U2, U3, etc., in order of decreasing sensitivity. For the singly ionized atom, the corresponding designations are V1, V2, etc. In cases where U1 is not given, the most sensitive lines lie outside the spectral range 10,000–2000 A. Figures given in the Sensitivity Column are taken from the NBS Tables of Spectral-Line Intensities, where values for numerous other lines also can be found. (See Meggers, Corliss and Scribner, NBS Monograph 32, 1961; also C. H. Corliss, NBS Monograph 32 Supplement, 1967).

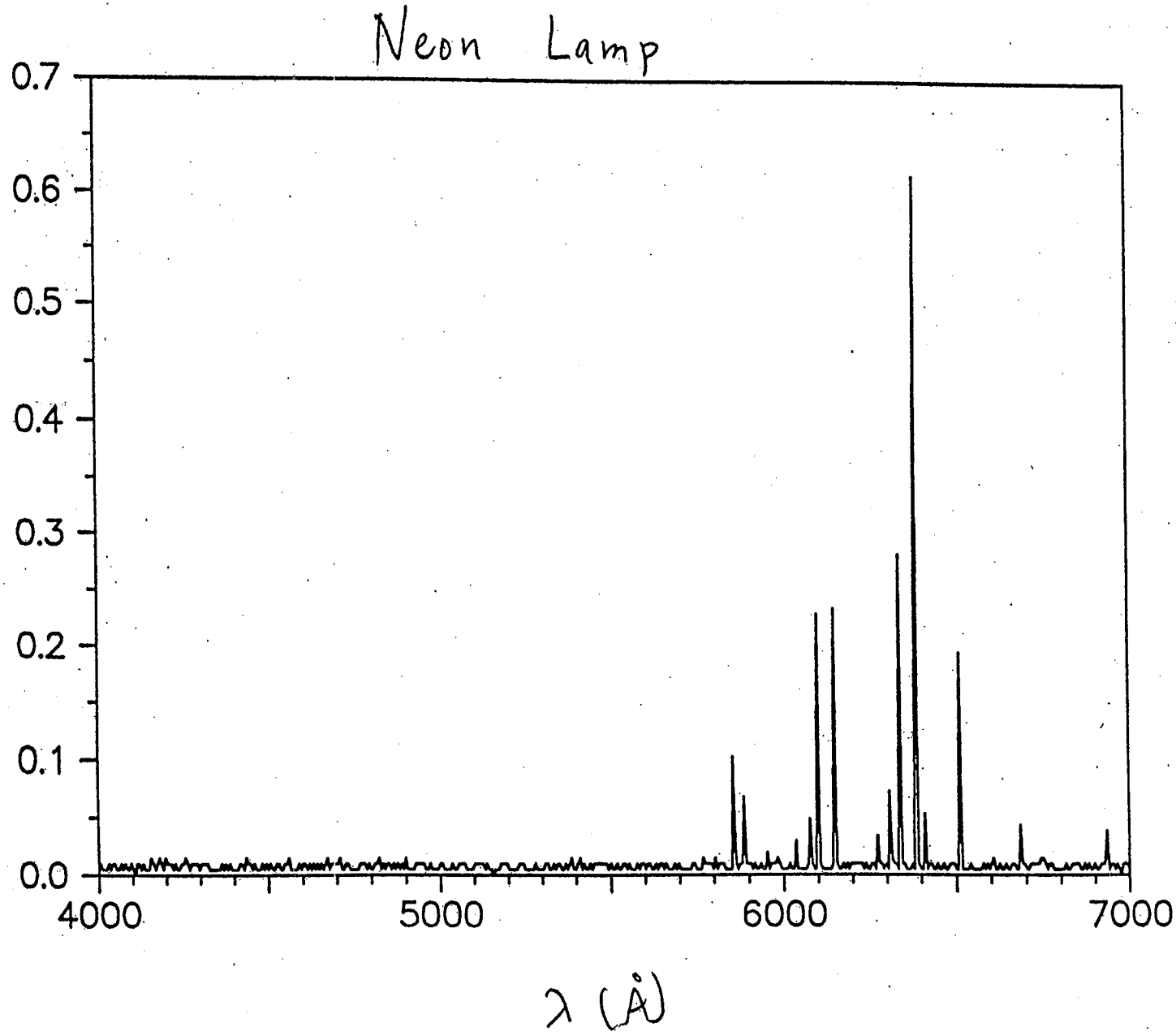
Neon Lamp
0.7
0.6
0.5
0.4
0.3
0.2
0.1
0.0
4000
5000
6000
7000
λ (Å)

Note in the following tables
the designations I & II

I → atomic line

II → singly ionized ion

⇒ look at atomic lines only

ARGON (Ar)
Z = 18

Ar I and II
Ref. 190, 203, 204, 219, — E.F.W.

Intensity		Wavelength	
		Vacuum	
30		487.227	II
50		490.650	II
30		490.701	II
30		519.327	II
30		542.912	II
200		543.203	II
70		547.461	II
70		556.817	II
70		573.362	II
30		576.736	II
70		580.263	II
30		583.437	II
70		597.700	II
30		602.858	II
30		612.372	II
500		661.867	II
30		664.562	II
200		666.011	II
1000		670.946	II
3000		671.851	II
70		676.242	II
30		677.952	II
30		679.218	II
200		679.401	II
200		718.090	II
3000		723.361	II
500		725.548	II
70		730.930	II
200		740.269	II
200		744.925	II
70		745.322	II
20		802.859	I
100		806.471	I
60		806.869	I
30		807.218	I
40		807.653	I
50		809.927	I
120		816.232	I
70		816.464	I
80		820.124	I
120		825.346	I
120		826.365	I
150		834.392	I
100		835.002	I
100		842.805	I
180		866.800	I
150		869.754	I
180	r	876.058	I
180	r	879.947	I
150		894.310	I
1000		919.781	II
1000		932.054	II
1000	r	1048.220	I
500	r	1066.660	I
		Air	
5		2420.456	II
10		2516.789	II
10		2534.709	II
15		2562.087	II
25		2891.612	II
200		2942.893	II
100		2979.050	II
50		3033.508	II
50		3093.402	II
8		3200.37	I
20		3243.689	II
25		3293.640	II
20		3307.228	II
7		3319.34	I
25		3350.924	II
7		3373.47	I
25		3376.436	II
25		3388.531	II
7		3393.73	I
7		3461.07	I
70		3476.747	II
20		3478.232	II
50		3491.244	II
100		3491.536	II
70		3509.778	II
70		3514.388	II
70		3545.596	II
70		3545.845	II
7		3554.306	I
100		3559.508	II
100		3561.030	II
70		3576.616	II
25		3581.608	II
50		3582.355	II
70		3588.441	II
7		3606.522	I
25		3622.138	II
20		3639.833	II
35		3718.206	II
70		3729.309	II
50		3737.889	II
150		3765.270	II
50		3766.119	II
20		3770.369	I
20		3770.520	II
25		3780.840	II
25		3803.172	II
50		3809.456	II
7		3834.679	I
70		3850.581	II
35		3868.528	II
35		3925.719	II
50		3928.623	II
25		3932.547	II
70		3946.097	II
7		3947.505	I
35		3948.979	I
20		3979.356	II
35		3994.792	II
50		4013.857	II
50		4033.809	II
20		4035.460	II
150		4042.894	II
50		4044.418	I
100		4052.921	II
200		4072.005	II
70		4072.385	II
25		4076.628	II
35		4079.574	II
25		4082.387	II
150		4103.912	II
300		4131.724	II
35		4156.086	II
400		4158.590	I
50		4164.180	I
35		4179.297	II
50		4181.884	I
100		4190.713	I
50		4191.029	I
200		4198.317	I
400		4200.674	I
25		4218.665	II
25		4222.637	II
25		4226.988	II
100		4228.158	II
100		4237.220	II
25		4251.185	I
200		4259.362	I
100		4266.286	I
70		4266.527	II
150		4272.169	I
550		4277.528	II
20		4282.898	II
100		4300.101	I
25		4300.650	II
70		4309.239	II
200		4331.200	II
50		4332.030	II
100		4333.561	I
50		4335.338	I
25		4345.168	I
800		4348.064	II
50		4352.205	II
25		4362.066	II
50		4367.832	II
200		4370.753	II
70		4371.329	II
50		4375.954	II
150		4379.667	II
50		4385.057	II
70		4400.097	II
200		4400.986	II
400		4426.001	II
150		4430.189	II
50		4430.996	II
50		4433.838	II
20		4439.461	II
35		4448.879	II
100		4474.759	II
200		4481.811	II
100		4510.733	I
20		4522.323	I
20		4530.552	II
400		4545.052	II
20		4564.405	II
400		4579.350	II
400		4589.898	II
15		4596.097	I
550		4609.567	II
7		4628.441	I
35		4637.233	II
400		4657.901	II
15		4702.316	I
20		4721.591	II
550		4726.868	II
50		4732.053	II
300		4735.906	II
800		4764.865	II
550		4806.020	II
150		4847.810	II
50		4865.910	II
800		4879.864	II
70		4889.042	II
20		4904.752	II
35		4933.209	II
200		4965.080	II
50		5009.334	II
70		5017.163	II
70		5062.037	II
20		5090.495	II
100		5141.783	II
70		5145.308	II
5		5151.391	I
15		5162.285	I
25		5165.773	II
20		5187.746	I
20		5216.814	II
7		5221.271	I
5		5421.352	I
10		5451.652	I
25		5495.874	I
5		5506.113	I
25		5558.702	I
10		5572.541	I
35		5606.733	I
20		5650.704	I
10		5739.520	I
5		5834.263	I
10		5860.310	I
15		5882.624	I
25		5888.584	I
50		5912.085	I
15		5928.813	I
5		5942.669	I
7		5987.302	I
5		5998.999	I
5		6025.150	I
70		6032.127	I
35		6043.223	I
10		6052.723	I
20		6059.372	I
7		6098.803	I
10		6105.635	I
100		6114.923	II
10		6145.441	I
7		6170.174	I
150		6172.278	II
10		6173.096	I
10		6212.503	I
5		6215.938	I
25		6243.120	II
7		6296.872	I
15		6307.657	I
7		6369.575	I
20		6384.717	I
70		6416.307	I
25		6483.082	II
15		6538.112	I
15		6604.853	I
25		6638.221	II
20		6639.740	II
50		6643.698	II
5		6660.676	I
5		6664.051	I
25		6666.359	II
100		6677.282	I
35		6684.293	II
150		6752.834	I
5		6756.163	I
15		6766.612	I
20		6861.269	II
150		6871.289	I
5		6879.582	I
10		6888.174	I
50		6937.664	I
7		6951.478	I
7		6960.250	I
10000		6965.431	I
150		7030.251	I
10000		7067.218	I
100		7068.736	I
25		7107.478	I
25		7125.820	I
1000		7147.042	I
15		7158.839	I
70		7206.980	I
15		7265.172	I
7		7270.664	I
2000		7272.936	I
35		7311.716	I
25		7316.005	I
5		7350.814	I
70		7353.293	I
200		7372.118	I
20		7380.426	II
10000		7383.980	I
20		7392.980	I
15		7412.337	I
10		7425.294	I
25		7435.368	I
10		7436.297	I
20000		7503.869	I
15000		7514.652	I
25000		7635.106	I
15000		7723.761	I
10000		7724.207	I
10		7891.075	I
20000		7948.176	I
20000		8006.157	I
25000		8014.786	I
7		8053.308	I
20000		8103.693	I
35000		8115.311	I
10000		8264.522	I
20		8392.27	I
15000		8408.210	I
20000		8424.648	I
15000		8521.442	I
7		8605.776	I
4500		8667.944	I
20		8771.860	II
180		8849.91	I
20		9075.394	I
35000		9122.967	I
550		9194.638	I
15000		9224.499	I
400		9291.531	I
1600		9354.220	I
25000		9657.786	I
4500		9784.503	I
180		10052.06	I
30		10332.72	I
100		10467.177	II
1600		10470.054	I
13		10478.034	I
180		10506.50	I
200		10673.565	I
11		10681.773	I
7		10683.034	II
30		10733.87	I
30		10759.16	I
7		10812.896	II
11		11078.869	I
30		11106.46	I
12		11441.832	I
400		11488.109	I
200		11668.710	I
12		11719.488	I
200		12112.326	I
50		12139.738	I
50		12343.393	I
200		12402.827	I
200		12439.321	I
100		12456.12	I
200		12487.663	I
150		12702.281	I
30		12733.418	I
12		12746.232	I
200		12802.739	I
50		12933.195	I
500		12956.659	I
200		13008.264	I
200		13213.99	I
200		13228.107	I
100		13230.90	I
500		13272.64	I
1000		13313.210	I
1000		13367.111	I
30		13499.41	I
1000		13504.191	I
11		13573.617	I
30		13599.333	I
400		13622.659	I
200		13678.550	I
1000		13718.577	I
10		13825.715	I
10		13907.478	I
200		14093.640	I
100		15046.50	I
25		15172.69	I
10		15329.34	I
30		15989.49	I
30		16519.86	I
500		16940.58	I
12		18427.76	I
50		20616.23	I
30		20986.11	I
20		23133.20	I
20		23966.52	I

Ar III
Ref. 367, 372, 373, 375 — E.F.W.

Intensity		Wavelength	
		Vacuum	
12		769.15	II

Hafnium (Cont.)

15	1305.24	IV
12	1357.40	IV
40	1390.39	IV
50	1491.67	IV
35	1528.82	IV
15	1560.18	IV
25	1572.03	IV
100	1717.21	IV
20	1718.57	IV

Air

100	2054.46	IV
7	2014.06	IV
20	7751.29	IV
10	7267.58	IV

Hf-V
Ref. 410 — R.L.K.

Intensity	Wavelength	
	Vacuum	
220	545.41	V
180	600.00	V
100	816.81	V
100	830.69	V
100	836.74	V
100	846.87	V
100	856.32	V
100	861.80	V
135	865.16	V
270	867.25	V
180	875.88	V
135	877.87	V
135	880.37	V
100	880.85	V
180	885.58	V
135	885.80	V
135	894.24	V
100	894.41	V
180	896.14	V
100	896.47	V
135	899.70	V
180	901.54	V
135	901.92	V
135	904.95	V
135	909.70	V
135	913.68	V
135	918.48	V
180	919.10	V
270	921.67	V
135	928.01	V
135	931.50	V
135	947.12	V
245	951.62	V
180	960.12	V
180	964.74	V
160	971.51	V
135	974.62	V
120	984.64	V
135	991.50	V
100	1078.42	V
100	1079.92	V
160	1092.76	V
135	1097.28	V
135	1137.49	V
160	1201.76	V
135	1208.88	V
135	1224.62	V
135	1227.98	V
135	1230.21	V
270	1232.03	V
200	1233.59	V
160	1237.42	V
100	1238.85	V
160	1239.53	V
160	1244.46	V
100	1259.25	V
440	1396.66	V
270	1400.09	V
160	1401.70	V
135	1405.77	V
370	1407.17	V
370	1408.38	V
270	1412.28	V
270	1413.51	V
160	1421.96	V
220	1422.53	V
370	1433.43	V
370	1437.27	V
500	1437.73	V
370	1445.40	V
270	1457.91	V
270	1719.32	V
550	1729.08	V
750	1731.83	V
750	1733.96	V
440	1741.74	V
1000	1749.11	V
1000	1750.19	V
500	1760.89	V
370	1765.62	V
270	1774.02	V
135	1792.39	V

HELIUM (He)
Z = 2

He I and II
Ref. 16, 94, 173, 183, 317
W.C.M.

Intensity	Wavelength	
	Vacuum	
15	231.454	II
20	232.584	II
30	234.347	II
50	237.331	II
100	243.027	II
300	256.317	II
1000	303.780	II
500	303.786	II
10	320.293	I
2	505.500	I
3	505.684	I
4	505.912	I
5	506.200	I
7	506.570	I
10	507.058	I
15	507.718	I
20	508.643	I
25	509.998	I
35	512.098	I
50	515.616	I
100	522.213	I
400	537.030	I
1000	584.334	I
50	591.412	I
5	958.70	II
6	972.11	II
8	992.36	II
15	1025.27	II
30	1084.94	II
35	1215.09	II
50	1215.17	II
120	1640.34	II
180	1640.47	II
	Air	
7	2385.40	II
9	2511.20	II
50	2577.6	I
1	2723.19	I
12	2733.30	II
2	2763.80	I
10	2818.2	I
4	2829.08	I
10	2945.11	I
40	3013.7	I
20	3187.74	I
3	3202.96	II
15	3203.10	II
1	3354.55	I
2	3447.59	I
1	3587.27	I
3	3613.64	I
2	3634.23	I
3	3705.00	I
1	3732.86	I
10	3819.607	I
1	3819.76	I
500	3888.65	I
20	3964.729	I
1	4009.27	I
50	4026.191	I
5	4026.36	I
12	4120.82	I
2	4120.99	I
3	4143.76	I
10	4387.929	I
3	4437.55	I
200	4471.479	I
25	4471.68	I
6	4685.4	II
30	4685.7	II
30	4713.146	I
4	4713.38	I
20	4921.931	I
100	5015.678	I
10	5047.74	I
5	5411.52	II
500	5875.62	I
100	5875.97	I
8	6560.10	II
100	6678.15	I
3	6867.48	I
200	7065.19	I
30	7065.71	I
50	7281.35	I
1	7816.15	I
2	8361.69	I
2	9063.27	I
2	9210.34	I
10	9463.61	I
4	9516.60	I
3	9526.17	I
1	9529.27	I
1	9603.42	I
3	9702.60	I
6	10027.73	I
2	10031.16	I
15	10123.6	II
1	10138.50	I
10	10311.23	I
2	10311.54	I
3	10667.65	I
300	10829.09	I
1000	10830.25	I
2000	10830.34	I
9	10913.05	I
3	10917.10	I
4	11626.4	II
30	11969.12	I
20	12527.52	I
50	12784.99	I
20	12790.57	I
7	12845.96	I
10	12968.45	I
2	12984.89	I
12	15083.64	I
200	17002.47	I
1	18555.55	I
6	18636.8	II
500	18685.34	I
200	18697.23	I
100	19089.38	I
20	19543.08	I
1000	20581.30	I
80	21120.07	I
10	21121.43	I
20	21132.03	I
3	30908.5	II
4	40478.90	I

HOLMIUM (Ho)
Z = 67

Ho I and II
Ref. 1 — C.H.C.

Intensity		Wavelength	
		Air	
170		2502.91	II
80		2508.53	II
110		2513.55	II
95		2518.73	II
170		2533.80	I
130		2536.86	II
80		2556.84	I
80		2567.73	II
80		2586.52	I
60		2591.05	II
95		2592.99	I
190		2605.86	II
110		2610.51	II
95		2613.99	II
60		2625.20	II
80		2640.09	I
80		2640.30	II
60		2649.68	II
80		2666.24	II
70		2689.03	II
210		2713.65	II
230		2733.95	II
270		2750.35	II
110	c	2759.35	II
110		2766.85	II
270		2769.89	II
110		2772.83	II
140		2777.10	II
140		2794.41	II
100		2799.99	II
100		2806.72	II
160	c	2809.99	II
220		2811.36	II
180		2812.00	II
190		2814.74	II
300		2824.20	II
140		2826.64	II
270	c	2831.69	II
210		2834.99	II
110		2835.85	II
110		2844.18	II
100		2844.68	II
270		2849.10	II
100		2861.23	II
230		2861.49	II
150		2862.72	II
210		2871.99	II
230		2874.06	II
160		2874.43	II
360		2880.26	II
460		2880.98	II
340		2894.99	II
160		2895.62	II
170		2900.84	II
570	c	2909.41	II
170		2915.82	II
300		2919.62	II
110		2925.35	II
160		2926.09	II
300	c	2928.30	II
220		2942.05	II
300		2944.49	II
250	c	2953.11	II
390		2973.00	II
410	c	2979.63	II
180		2981.46	II
140		2985.48	II
410		2987.64	II
250		2990.27	II
110		2995.86	II
320	c	3008.10	II
220		3014.60	II
270		3038.69	II
480	c	3049.38	II
410	c	3054.00	II
500	c	3057.45	II
230		3074.30	II
500	c	3082.34	II
910		3084.36	II
430	c	3086.54	II
200		3108.31	II
200	c	3109.91	II
760		3118.50	II
300	c	3130.99	II
200	c	3134.39	II
300	c	3144.36	II
200		3156.18	II
270		3156.97	II
200	c	3159.67	II
580	c	3166.62	II
390	D1	3171.72	II
810		3173.78	II
390		3174.84	II
270	c	3176.97	II
810	c	3181.50	II
390		3183.84	II
270	Cw	3184.48	II
200		3186.37	I
390	c	3197.83	II
390		3201.76	II
200		3206.86	II
270	c	3210.41	II
200	c	3221.42	II
320		3233.34	II
200		3236.90	II
200		3237.40	II
200	c	3257.45	II
390	c	3278.15	II
270		3279.25	II
980	c	3281.97	II
390		3288.46	II
270	c	3290.96	II
200	c	3305.16	II
200		3319.87	II
230		3320.25	II
200		3331.93	II
630	c	3337.23	II
390	c	3338.86	II
980	c	3343.58	II
200		3344.47	II
360		3350.49	II
320		3352.10	II
320	Cw	3353.55	II
320		3354.58	II
320		3357.91	II
320		3364.27	II
290		3370.87	II
230		3374.16	II
290	c	3390.75	II
320	c	3394.60	II
8100	c	3398.98	II
810	c	3410.26	II
1200		3421.63	II
3200		3453.14	II
390	c	3410.65	II
1400	c	3414.90	II
5400		3416.46	II
2000	c	3425.34	II
2000	c	3428.13	II
630	c	3429.18	II
320	c	3432.10	II
390		3449.35	I
810	c	3455.70	II
16000	c	3456.00	II
1600		3461.97	II
360	c	3467.07	II
810	c	3473.91	II
5400	c	3474.26	II
6300		3484.84	II
490		3489.58	II
580	c	3493.09	II

Holmium (Cont.)

12		7602.31	II
16		7605.35	I
12		7617.05	I
14		7627.98	I
40	c	7628.42	I
9	c	7641.14	I
4		7648.16	I
14	c	7653.80	I
12	c	7667.30	I
20		7690.43	I
50	c	7693.15	I
40	Cw	7715.06	I
16		7719.05	I
16	h	7738.98	I
8	c	7752.01	I
60	Cw	7815.48	I
40	Cw	7823.63	I
8	h	7879.22	I
60		7894.64	I
10	h	8464.66	I
10	h	8482.67	I
50		8512.94	I
20		8545.61	II
18		8601.84	II
40		8670.19	I
8	h	8697.32	
16	h	8805.48	II
20	c	8834.49	I
90		8915.98	II

HYDROGEN (H)
Z = I

H I
Ref. 214 — W.C.M.

Intensity		Wavelength	
		Vacuum	
15		926.226	I
20		930.748	I
30		937.803	I
50		949.743	I
100		972.537	I
300		1025.722	I
1000		1215.668	I
500		1215.674	I
		Air	
5		3835.384	I
6		3889.049	I
8		3970.072	I
15		4101.74	I
30		4340.47	I
80		4861.33	I
120		6562.72	I
180		6562.852	I
5		9545.97	I
7		10049.4	I
12		10938.1	I
20		12818.1	I
40		18751.0	I
5		21655.3	I
8		26251.5	I
15		40511.6	I
4		46525.1	I
6		74578	I
3		123685	I

INDIUM (In)
Z = 49

In I and II
Ref. 1, 132, 348—350 — C.H.C.

Intensity		Wavelength	
		Vacuum	
2		1648.00	I
1	h	1676.16	I
5	h	1711.54	I
2	h	1741.23	I
1	h	1758.49	I
		Air	
10		2103.89	II
10		2166.88	II
2		2179.90	I
2		2182.40	I
2		2187.40	I
2		2190.84	I
15		2195.67	II
2		2197.41	I
2		2202.24	I
50		2205.28	II
3		2211.14	I
5		2230.70	I
3		2241.66	I
30		2255.79	II
10		2259.99	I
5		2278.20	I
40		2281.64	II
2		2283.75	I
2		2298.33	I
2		2298.70	I
2		2302.49	I
100	c	2306.05	II
25		2306.86	I
3		2309.32	I
2		2309.75	I
90	d	2313.21	II
2		2315.09	I
30		2323.40	II
5		2324.41	I
3		2324.92	I
70	d	2327.95	II
3		2332.76	I
80	h	2334.57	II
10		2340.19	I
8		2345.90	I
5		2346.56	I
50	d	2350.75	II
5		2358.70	I
15		2378.14	I
10		2379.00	I
110	d	2382.63	II
40		2389.54	I
40		2393.18	II
10		2399.18	I
50	h	2406.47	II
50		2408.76	II
50		2419.06	II
50		2419.20	II
70	h	2427.20	II
20		2429.86	I
10		2430.99	I
50		2432.73	II
60		2442.63	II
100		2447.90	II
60		2453.23	II
60		2460.08	I
30	h	2468.02	I
70		2486.15	II
110	d	2488.62	II
90		2488.95	II
80		2498.59	II
100		2499.60	II
90	d	2500.99	II
60		2508.16	II
110	d	2512.31	II
100		2521.37	I
10		2522.98	I
70		2553.56	II
160	d	2554.44	II
1100		2560.15	I
70		2565.13	II
70	d	2598.75	II
200		2601.76	I
50		2604.04	II
90	d	2654.70	II
100	d	2662.63	II
140	d	2668.65	II
140	d	2674.56	II
80		2683.12	II
1600		2710.26	I
300		2713.94	I
130	d	2749.75	II
700		2753.88	I
40		2775.37	I
60		2798.76	II
90	d	2818.97	II
180	c	2836.92	I
30	c	2858.14	I
80		2865.68	II
120	d	2890.18	II
1100		2932.63	I
100		2941.05	II
20	c	2957.01	I
60	d	2966.17	II
110	c	2999.40	II
8000		3039.36	I
8	d	3051.15	I
110	d	3099.80	II
180	c	3101.8	II
130	c	3138.60	II
80	c	3142.75	II
130	d	3146.70	II
150		3155.77	II
100	c	3158.40	II
90	c	3176.30	II
90	d	3198.11	II
13000		3256.09	I
3000		3258.56	I
90	c	3338.50	II
75	c	3376.59	II
100	c	3404.28	II
110	d	3438.40	II
180	c	3693.91	II
95	c	3708.13	II
380	w	3716.14	II
120	c	3718.30	II
160	c	3718.72	II
160	c	3723.40	II
170	w	3795.21	II
230	c	3799.21	II
250	c	3834.65	II
200	c	3842.18	II
100		3889.78	II
100	c	3902.07	II
60	d	3922.12	II
65	c	3934.40	II
250	w	3962.35	II
120	c	4004.66	II
140	d	4013.92	II
410	w	4056.94	II
17000		4101.76	I
140	c	4205.14	II
100	d	4213.04	II
110	d	4219.66	II
150	d	4372.87	II
150	c	4500.78	II
18000		4511.31	I
110	c	4549.01	II
140	c	4570.85	II
180	w	4578.02	II
180	w	4578.40	II
140	c	4616.08	II
170	c	4617.17	II
250	c	4620.14	II
150	w	4620.70	II
170	c	4627.30	II
140	c	4637.04	II
380	c	4638.16	II
220	c	4644.58	II
360	c	4655.62	II
320	w	4656.74	II
190	c	4681.11	II
450	w	4684.8	II
3		4878.37	I
90	d	4907.06	II
70	h	4924.93	II
150	c	4973.77	II
80	h	5109.36	II
100	w	5115.14	II
140	c	5117.40	II
270	c	5120.80	II
200	w	5121.75	II
80	d	5129.85	II
240	c	5175.42	II
140	c	5184.44	II
30		5254.32	I
12		5262.74	I
150	c	5309.45	II
80		5411.41	II
140	c	5418.45	II
220	w	5436.70	II
130	c	5497.50	II
140	c	5507.08	II
320	c	5513.00	II
250	w	5523.28	II
130	c	5536.50	II
190	w	5555.45	II
240	c	5576.90	II
200	w	5636.70	II
160	c	5708.50	II
50		5709.91	I
100	c	5721.80	II
50		5727.68	I
210	c	5853.15	II
490	w	5903.4	II
260	w	5915.4	II
120	c	5918.78	II
130	c	6062.9	II
250	c	6095.95	II
210	c	6108.66	II
100	c	6115.9	II
230	w	6128.7	II
240	w	6129.4	II
320	w	6132.1	II
150	c	6140.0	II
90		6143.23	II
140	c	6148.10	II
190	w	6149.5	II
80		6161.15	II
180	w	6162.45	II
100	c	6224.28	II
280	w	6228.3	II
140	w	6231.1	II
270	w	6304.8	II
290	w	6362.3	II
300	w	6469.0	II
210	c	6541.20	II
190	c	6751.88	II
180	c	6765.9	II
100	c	6783.72	II
8	h	6847.44	I
320	w	6891.5	II
4	h	6900.13	I
380	w	7182.9	II
180	c	7255.0	II
210	c	7276.5	II
180	c	7303.4	II
320	c	7350.6	II
100	c	7632.7	II
100	c	7682.9	II
210	c	7740.7	II
100	c	7776.96	II
160	c	7789.0	II
70	c	7806.8	II
70	c	7814.5	II
90	c	7840.9	II
20	h	8050.78	I
240	c	8227.0	II
30	h	8238.66	I
15	h	8314.92	I
50	c	8434.55	II
30		8678.95	I
20		8682.63	I
50		8700.25	I
100	w	8813.5	II
80	c	8832.6	II
40		8894.47	I
10		9170.08	I
120	c	9197.7	II
120	c	9202.0	II
220	w	9213.0	II
160	d	9241.1	II
40	h	9349.83	I
60	h	9370.27	I
20		9427.99	I
100		9977.86	I
200		10257.03	I
60	h	10717.42	I
100	h	10744.31	I
20		11334.72	I
20		11731.48	I
10		12912.59	I
9		13429.96	I
5		13824.48	I
6		14316.25	I
3		14419.20	I
6		14668.66	I
7		14719.08	I
2		16504.31	I
6		22291.06	I
2		23879.13	I

In III
Ref. 351 — C.H.C.

Intensity		Wavelength	
		Vacuum	
7		685.31	III
5		691.62	III
1		782.17	III
10		882.24	III
10		890.84	III
10		915.87	III
2		917.45	III
5		926.83	III
30		1403.08	III
30		1434.85	III
20		1487.70	III
20		1494.14	III
10		1524.78	III
20		1530.21	III
30		1532.95	III
100		1625.42	III
20		1642.28	III
20		1702.53	III
100		1748.83	III
2		1767.88	III
1		1810.71	III
30		1842.41	III
40		1850.30	III
15		1862.98	III
		Air	
30		2154.08	III
2		2154.42	III
10		2199.52	III
5		2232.18	III
20		2261.26	III
5		2266.26	III
5		2272.41	III
5		2272.84	III
10		2300.90	III
100		2527.41	III
50		2725.52	III
80		2726.15	III
100		2982.80	III
100		3008.08	III
30		3008.82	III
30		3293.55	III
8		3350.91	III
5		3562.32	III
100		3852.82	III
100		4023.77	III
150		4032.32	III
50		4062.30	III
100		4071.57	III
100		4072.93	III
100		4252.68	III
40		4509.58	III
200		5248.77	III

Manganese (Cont.)

75	1787.04	IV
75	1787.38	IV
75	1788.64	IV
75	1790.44	IV
80	1795.65	IV
80	1795.79	IV
60	1907.03	IV
75	1910.25	IV
65	1997.54	IV

Mn V
Ref. 405 — C.H.C.

Intensity	Wavelength	
	Vacuum	
300	404.36	V
380	406.02	V
300	406.40	V
600	410.30	V
600	410.60	V
480	410.98	V
400	411.32	V
460	412.74	V
460	413.75	V
600	415.62	V
650	415.98	V
350	419.80	V
600	428.59	V
500	429.05	V
400	433.54	V
600	435.67	V
350	436.16	V
500	436.18	V
450	438.74	V
350	439.35	V
1000	441.72	V
850	442.49	V
400	467.32	V
300	474.82	V

MERCURY (198) (Hg)
Z = 80

Hg I and II (198)
Ref. 43, 50, 69, 145, 229, 242 — R.W.S.

Intensity	Wavelength	
	Vacuum	
80	1250.564	I
8	1259.242	I
100	1268.825	I
5	1307.751	I
20	1402.619	I
10	1435.503	I
1000	1849.492	I
	Air	
60	2262.210	II
20	2302.065	I
20	2345.440	I
100	2378.325	I
20	2380.004	I
40	2399.349	I
20	2399.729	I
20	2446.900	I
15	2464.064	I
40	2481.999	I
30	2482.713	I
40	2483.821	I
90	2534.769	I
15000	2536.506	I
25	2563.861	I
25	2576.290	I
250	2652.043	I
400	2653.683	I
100	2655.130	I
50	2698.831	I
80	2752.783	I
20	2759.710	I
40	2803.471	I
30	2804.438	I
750	2847.675	II
50	2856.939	I
150	2893.598	I
150	2916.227	II
60	2925.413	I
1200	2967.283	I
300	3021.500	I
120	3023.476	I
30	3025.608	I
50	3027.490	I
400	3125.670	I
320	3131.551	I
320	3131.842	I
80	3341.481	I
2800	3650.157	I
300	3654.839	I
80	3662.883	I
240	3663.281	I
30	3701.432	I
35	3704.170	I
30	3801.660	I
20	3901.867	I
60	3906.372	I
200	3983.839	II
1800	4046.572	I
150	4077.838	I
40	4108.057	I
250	4339.224	I
400	4347.496	I
4000	4358.337	I
80	4916.068	I
1100	5460.753	I
160	5675.922	I
240	5769.598	I
280	5790.663	I
20	6072.713	I
30	6234.402	I
160	6716.429	I
250	6907.461	I
240	11287.407	I

MERCURY (NATURAL) (Hg)
Z = 80

Hg I and II (nat.)
Ref. 34, 45, 90, 117, 133, 189, 235, 304, 327, 328 — R.W.S.

Intensity	Wavelength	
	Vacuum	
400	893.08	II
300	915.83	II
150	923.39	II
200	940.80	II
100	962.74	II
50	969.13	II
800	1099.26	II
80	1250.58	I
8	1259.24	I
100	1268.82	I
5	1307.75	I
300	1307.93	II
400	1321.71	II
400	1331.74	II
80	1350.07	II
200	1361.27	II
20	1402.62	I
200	1414.43	II
10	1435.51	I
15	1619.46	II
120	1623.95	II
20	1628.25	II
150	1649.94	II
50	1653.64	II
200	1672.41	II
100	1702.73	II
100	1707.40	II
120	1727.18	II
250	1732.14	II
20	1775.68	I
40	1783.70	II
30	1796.22	II
200	1796.90	II
60	1798.74	II
30	1803.89	II
40	1808.29	II
400	1820.34	II
5	1832.74	I
1000	1849.50	I
160	1869.23	II
300	1870.55	II
200	1875.54	II
20	1900.28	II
30	1927.60	II
300	1942.27	II
100	1972.94	II
200	1973.89	II
150	1987.98	II
	Air	
90	2026.97	II
90	2052.93	II
70	2148.00	II
5	2247.55	I
60	2262.23	II
20	2302.06	I
15	2323.20	I
5	2340.57	I
20	2345.43	I
20	2352.48	I
100	2378.32	I
20	2380.00	I
40	2399.38	I
20	2399.73	I
10	2400.49	I
60	2407.35	II
50	2414.13	II
5	2441.06	I
20	2446.90	I
15	2464.06	I
40	2482.00	I
30	2482.72	I
40	2483.82	I
90	2534.77	I
15000	2536.52	I
25	2563.86	I
25	2576.29	I
5	2578.91	I
15	2625.19	I
5	2639.78	I
250	2652.04	I
400	2653.69	I
100	2655.13	I
5	2674.91	I
50	2698.83	I
50	2699.38	I
80	2705.36	II
80	2752.78	I
20	2759.71	I
40	2803.46	I
30	2804.43	I
2	2805.34	I
2	2806.77	I
150	2814.93	II
750	2847.68	II
50	2856.94	I
150	2893.60	I
150	2916.27	II
60	2925.41	I
150	2935.94	II
400	2947.08	II
1200	2967.28	I
300	3021.50	I
120	3023.47	I
30	3025.61	I
50	3027.49	I
400	3125.67	I
320	3131.55	I
320	3131.84	I
400	3208.20	II
400	3264.06	II
80	3341.48	I
100	3385.25	II
400	3451.69	II
200	3549.42	II
2800	3650.15	I
300	3654.84	I
80	3662.88	I
240	3663.28	I
30	3701.44	I
35	3704.17	I
30	3801.66	I
100	3806.38	II
20	3901.87	I
60	3906.37	I
100	3918.92	II
200	3983.96	II
1800	4046.56	I
150	4077.83	I
40	4108.05	I
250	4339.22	I
400	4347.49	I
4000	4358.33	I
100	4398.62	II
90	4660.28	II
80	4855.72	II
5	4883.00	I
5	4889.91	I
80	4916.07	I
5	4970.37	I
5	4980.64	I
20	5102.70	I
40	5120.64	I
100	5128.45	II
20	5137.94	I
20	5290.74	I
5	5316.78	I
60	5354.05	I
30	5384.63	I
1100	5460.74	I
30	5549.63	I
160	5675.86	I
240	5769.60	I
100	5789.66	I
280	5790.66	I
140	5803.78	I
60	5859.25	I
60	5871.73	II
20	5871.98	I
20	6072.72	I
1000	6149.50	II
30	6234.40	I
80	6521.13	II
160	6716.43	I
250	6907.52	I
250	7081.90	I
200	7091.86	I
40	7346.37	II
100	7485.87	II
20	7728.82	I
100	7944.66	II
2000	10139.75	I
240	11287.40	I
120	13209.95	I
140	13426.57	I
60	13468.38	I
80	13505.58	I
500	13570.21	I
450	13673.51	I
200	13950.55	I
500	15295.82	I
100	16881.48	I
400	16920.16	I
300	16942.00	I
500	17072.79	I
400	17109.93	I
20	17116.75	I
20	17198.67	I
20	17213.20	I
70	17329.41	I
30	17436.18	I
50	18130.38	I
40	19700.17	I
	22493.28	I
250	23253.07	I
	32148.06	I
	36303.03	I

Hg III
Ref. 343 — C.H.C.

Intensity	Wavelength	
	Vacuum	
3	621.44	III
2	679.68	III
2	878.59	III
1	886.48	III
1	988.89	III
2	1009.29	III
5	1068.03	III
2	1161.95	III
9	1681.40	III
15	1759.75	III
1	1894.77	III
	Air	
7	2314.15	III
4	2380.55	III
8	2431.65	III
5	2480.56	III
7	2484.50	III
2	2612.92	III
4	2617.97	III
3	2670.49	III
70	2724.43	III
6	2769.22	III
3	2844.76	III
15	3090.05	III
5	3283.02	III
12	3312.28	III
8	3389.01	III
5	3450.77	III
3	3500.35	III
4	3538.88	III
5	3557.24	III
15	3803.51	III
70	4122.07	III
10	4140.34	III
100	4216.74	III
15	4470.58	III
12	4552.84	III
50	4797.01	III
10	4869.85	III
80	4973.57	III
30	5210.82	III
6	5695.71	III
25	6220.35	III
35	6418.98	III
40	6501.38	III
10	6584.26	III
6	6610.12	III
30	6709.29	III
12	7517.46	III
7	7808.10	III
25	7946.75	III
50	7984.51	III
5	8151.64	III

12	1602.08	IV
13	1603.18	IV
13	1603.73	IV
13	1604.88	IV
13	1605.68	IV
15	1605.97	IV
13	1606.98	IV
17	1609.10	IV
14	1609.83	IV
13	1610.47	IV
13	1611.20	IV
13	1613.64	IV
15	1614.02	IV
13	1614.64	IV
13	1615.00	IV
12	1615.61	IV
16	1616.68	IV
14	1617.68	IV
14	1619.02	IV
12	1620.91	IV
13	1621.16	IV
14	1621.57	IV
13	1623.38	IV
13	1623.53	IV
15	1626.47	IV
14	1626.90	IV
13	1628.54	IV
13	1630.18	IV
17	1631.08	IV
12	1632.08	IV
14	1632.40	IV
13	1634.01	IV
12	1638.07	IV
12	1638.30	IV
14	1639.40	IV
16	1640.04	IV
14	1640.16	IV
15	1641.87	IV
12	1642.88	IV
15	1647.09	IV
15	1651.58	IV
15	1652.90	IV
13	1653.41	IV
13	1656.11	IV
15	1656.65	IV
12	1657.82	IV
12	1658.43	IV
14	1660.10	IV
12	1661.57	IV
13	1662.32	IV
13	1662.52	IV
13	1663.54	IV
13	1668.09	IV
12	1669.61	IV
14	1671.04	IV
12	1672.86	IV
13	1673.68	IV
14	1675.66	IV
12	1676.78	IV
12	1677.12	IV
13	1681.36	IV
12	1681.95	IV
15	1687.69	IV
15	1698.88	IV
12	1700.40	IV
12	1704.93	IV
13	1709.81	IV
15	1711.41	IV
14	1712.76	IV
12	1717.11	IV
14	1717.90	IV
14	1718.16	IV
12	1718.42	IV
14	1719.46	IV
14	1722.71	IV
14	1724.06	IV
12	1724.26	IV
16	1725.63	IV
13	1761.08	IV
12	1764.92	IV
12	1767.36	IV
13	1792.10	IV
13	1796.93	IV
12	1805.32	IV
12	1820.42	IV
13	1827.98	IV
12	1840.24	IV
12	1860.42	IV
12	1869.64	IV
12	1874.23	IV

Fe V

Ref. 381 — J.R.

Intensity	Wavelength	
	Vacuum	
300	361.28	V
300	365.43	V
300	365.86	V
300	374.24	V
300	374.87	V
300	375.98	V
300	379.59	V
300	380.31	V
300	381.27	V
300	384.96	V
300	384.97	V
300	385.03	V
300	385.11	V
300	385.25	V
300	385.26	V
300	385.30	V
300	385.75	V
300	385.88	V
350	386.16	V
300	386.74	V
300	386.78	V
300	386.85	V
300	386.88	V
350	386.88	V
400	387.20	V
400	387.50	V
300	387.62	V
400	387.76	V
400	387.78	V
300	387.98	V
300	388.61	V
300	388.82	V
300	390.11	V
300	390.19	V
300	390.78	V
300	391.94	V
300	392.06	V
300	392.38	V
300	392.50	V
300	392.51	V
300	392.70	V
300	392.91	V
300	393.27	V
300	393.72	V
300	393.73	V
300	393.91	V
300	393.97	V
300	394.04	V
300	394.64	V
300	395.15	V
300	395.79	V
400	395.90	V
300	399.84	V
300	400.11	V
300	400.51	V
300	400.52	V
300	400.63	V
300	401.04	V
300	401.64	V
300	401.86	V
300	402.87	V
300	403.06	V
400	404.62	V
400	405.50	V
800	407.42	V
600	407.44	V
400	407.49	V
500	407.75	V
400	409.71	V
400	410.20	V
600	411.55	V
300	415.01	V
300	416.66	V
300	416.84	V
700	417.39	V
700	418.04	V
500	418.47	V
300	420.56	V
700	421.06	V
500	421.78	V
300	422.28	V
500	422.31	V
300	423.23	V
500	426.06	V
500	426.11	V
300	426.83	V
350	426.97	V
300	434.42	V
300	439.22	V
300	444.70	V
300	445.44	V
300	446.04	V
300	458.16	V
300	486.17	V
400	1317.86	V
300	1318.35	V
300	1320.41	V
300	1321.34	V
300	1321.49	V
400	1323.27	V
400	1330.40	V
300	1345.61	V
400	1359.01	V
300	1361.28	V
300	1361.45	V
600	1361.82	V
300	1363.08	V
300	1363.64	V
300	1365.57	V
700	1373.59	V
600	1373.67	V
300	1374.12	V
500	1376.34	V
300	1376.46	V
500	1378.56	V
300	1385.68	V
800	1387.94	V
400	1397.97	V
600	1400.24	V
800	1402.39	V
400	1406.67	V
500	1406.82	V
400	1407.25	V
300	1409.03	V
300	1409.22	V
600	1409.45	V
400	1415.20	V
300	1418.12	V
600	1420.46	V
800	1430.57	V
800	1440.53	V
300	1440.79	V
400	1442.22	V
800	1446.62	V
700	1448.85	V
400	1449.93	V
300	1455.56	V
700	1456.16	V
500	1459.83	V
400	1460.73	V
500	1462.63	V
700	1464.68	V
500	1465.38	V
400	1466.65	V
500	1469.00	V
300	1475.60	V
500	1479.47	V
300	1584.32	V

KRYTPON (Kr)
Z = 36

Kr I and II

Ref. 61, 121, 123, 147, 208, 232 — E.F.W.

Intensity		Wavelength	
		Vacuum	
60		729.40	II
200		761.18	II
100		763.98	II
60		766.20	II
200		771.03	II
60	p	773.69	II
200		782.10	II
100		783.72	II
60		818.15	II
60		830.38	II
100		844.06	II
60		864.82	II
60		868.87	II
200		884.14	II
1000		886.30	II
400		891.01	II
200		911.39	II
2000		917.43	II
50		945.44	I
50		946.54	I
20		951.06	I
50		953.40	I
50		963.37	I
2000		964.97	II
100		1001.06	I
100		1003.55	I
100		1030.02	I
200		1164.87	I
650		1235.84	I
		Air	
100	h	2464.77	II
60		2492.48	II
80	h	2712.40	II
100		2833.00	II
100	h	3607.88	II
200		3631.889	II
250		3653.928	II
80		3665.324	I
150		3669.01	II
100		3679.559	I
80		3686.182	II
300	h	3718.02	II
200		3718.595	II
150		3721.350	II
200		3741.638	II
150		3744.80	II
80		3754.245	II
500		3778.089	II
500		3783.095	II
150	h	3875.44	II
150		3906.177	II
200		3920.081	II
100		3994.840	II
100	h	3997.793	II
300		4057.037	II
300		4065.128	II
500		4088.337	II
250		4098.729	II
100		4109.248	II
250		4145.122	II
150		4250.580	II
1000		4273.969	I
100		4282.967	I
600		4292.923	II
200		4300.49	II
500	h	4317.81	II
400		4318.551	I
1000		4319.579	I
150	h	4322.98	II
100		4351.359	I
3000		4355.477	II
500		4362.641	I
200		4369.69	II
800		4376.121	I
300	h	4386.54	II
200		4399.965	I
100		4425.189	I
500		4431.685	II
600		4436.812	II
600		4453.917	I
800		4463.689	I
800		4475.014	II
400	h	4489.88	II
600		4502.353	I
400	h	4523.14	II
200	h	4556.61	II
800		4577.209	II
300		4582.978	II
150	h	4592.80	II
500		4615.292	II
1000		4619.166	II
800		4633.885	II
2000		4658.876	II
500		4680.406	II
100		4691.301	II
200		4694.360	II
3000		4739.092	II
300		4762.435	II
1000		4765.744	II
300		4811.76	II
300		4825.18	II
800		4832.077	II
700		4846.612	II
150		4857.20	II
300		4945.59	II
200		5022.40	II
250		5086.52	II
400	h	5125.73	II
500		5208.32	II
200		5308.66	II
500		5333.41	II
200		5468.17	II
500		5562.224	I
2000		5570.288	I
80		5580.386	I
100		5649.561	I
400		5681.89	II
200	h	5690.35	II
100		5832.855	I
3000		5870.914	I
200		5992.22	II
60		5993.849	I
60		6056.125	I
300		6420.18	II
100		6421.026	I
200		6456.288	I
150		6570.07	II
60		6699.228	I
100		6904.678	I
250		7213.13	II
100		7224.104	I
80		7287.258	I
400		7289.78	II
400		7407.02	II
60		7425.541	I
200		7435.78	II
100		7486.862	I
300		7524.46	II
1000		7587.411	I
2000		7601.544	I
150		7641.16	II
1000		7685.244	I
1200		7694.538	I
250		7735.69	II
150		7746.827	I
800		7854.821	I
200		7913.423	I
180		7928.597	I
200		7933.22	II
120		7973.62	II
100		7982.401	I
1500		8059.503	I
4000		8104.364	I

Krypton (Cont.)

6000		8112.899	I
60		8132.967	I
3000		8190.054	I
200		8202.72	II
80		8218.365	I
3000		8263.240	I
100		8272.353	I
5000		8298.107	I
1500		8281.050	I
100		8412.430	I
3000		8508.870	I
150		8764.110	I
6000		8776.748	I
2000		8928.692	I
500		9238.48	II
500	hL	9293.82	II
200	h	9320.99	II
300		9361.95	II
100		9362.082	I
200	h	9402.82	II
200	h	9470.93	II
500		9577.52	II
500	h	9605.80	II
400	h	9619.61	II
200		9663.34	II
200	h	9711.60	II
2000		9751.758	I
500		9803.14	II
500		9856.314	I
1000		10221.46	II
100		11187.108	I
200		11257.711	I
150		11259.126	I
500		11457.481	I
150		11792.425	I
1500		11819.377	I
600		11997.105	I
160		12077.224	I
100		12861.892	I
1100		13177.412	I
1000		13622.415	I
2400		13634.220	I
800		13658.394	I
200		13711.036	I
600		13738.851	I
150		13974.027	I
550		14045.657	I
140		14104.298	I
180		14402.22	I
2000		14426.793	I
100		14517.84	I
1600		14734.436	I
550		14762.672	I
450		14765.472	I
400		14961.894	I
120		15005.307	I
140		15209.526	I
1700		15239.615	I
130		15326.480	I
1500		15334.958	I
700		15372.037	I
200		15474.026	I
180		15681.02	I
120		15820.09	I
200		16726.513	I
2000		16785.128	I
1000		16853.488	I
2400		16890.441	I
1600		16896.753	I
1800		16935.806	I
600		17098.771	I
700		17367.606	I
120		17404.443	I
150		17616.854	I
650		17842.737	I
700		18002.229	I
2600		18167.315	I
100		18399.786	I
150		18580.896	I
300		18696.294	I
170		18785.460	I
200		18797.703	I
140		20209.878	I
300		20423.964	I
140		20446.971	I
600		21165.471	I
1800		21902.513	I
120		22485.775	I
180		23340.416	I
120		24260.506	I
180		24292.221	I
600		25233.820	I
180		28610.55	I
1000		28655.72	I
150		28769.71	I
140		28822.49	I
300		29236.69	I
300		30663.54	I
300		30979.16	I
500		39300.6	I
1100		39486.52	I
220		39557.25	I
100		39572.60	I
1400		39588.4	I
1100		39589.6	I
500		39954.8	I
300		39966.6	I
1300		40306.1	I
250		40685.16	I

Kr III
Ref. 208, 366, 390, 421 — E.F.W.

Intensity		Wavelength	
		Vacuum	
30		467.35	III
30		540.86	III
30		565.64	III
30		569.16	III
30		571.98	III
30		579.83	III
30		585.14	III
30		585.96	III
30		593.70	III
30		594.10	III
30		596.41	III
40		600.17	III
30		603.67	III
50		605.86	III
35		606.47	III
50		611.12	III
35		616.72	III
40		621.45	III
45		622.80	III
50		625.02	III
30		625.76	III
45		628.59	III
50		630.04	III
35		633.09	III
50		639.98	III
60		646.41	III
30		651.20	III
50		659.72	III
30		664.86	III
40		672.34	III
35		672.85	III
35		676.57	III
35		680.13	III
35		683.68	III
45		686.25	III
45		687.98	III
45		691.93	III
50		695.61	III
30		698.05	III
50		708.36	III
50		714.00	III
100	p	722.04	III
30		746.70	III
60		785.97	III
50		837.66	III
50		854.73	III
60		862.58	III
40		870.84	III
50		876.08	III
75		897.81	III
50		987.29	III
30		1158.74	III
6		1638.82	III
6		1914.09	III
		Air	
40		2393.94	III
40		2494.01	III
30		2563.25	III
60		2639.76	III
30		2680.32	III
40		2681.19	III
30		2841.00	III
30		2851.16	III
50		2870.61	III
100		2892.18	III
30		2909.17	III
50		2952.56	III
60		2992.22	III
50		3022.30	III
80		3024.45	III
50		3046.93	III
30		3056.72	III
60		3063.13	III
40		3097.16	III
60		3112.25	III
30		3120.61	III
100		3124.39	III
60		3141.35	III
100		3189.11	III
80		3191.21	III
40		3239.52	III
40		3240.44	III
300		3245.69	III
150		3264.81	III
100		3268.48	III
30		3271.65	III
30		3285.89	III
30		3304.75	III
50		3311.47	III
200		3325.75	III
60		3330.76	III
50		3342.48	III
100		3351.93	III
40		3374.96	III
100		3439.46	III
70		3474.65	III
100		3488.59	III
200		3507.42	III
100		3564.23	III
30		3641.34	III
30		3690.65	III
40	h	3868.70	III
50		4067.37	III
40		4131.33	III
40		4154.46	III
20	h	5016.45	III
10		5501.43	III
10	h	6037.17	III
10	h	6078.38	III
10		6310.22	III

Kr IV
Ref. 366, 409, 417 — E.F.W.

Intensity		Wavelength	
		Vacuum	
		793.44	IV
		794.11	IV
7		805.76	IV
18		816.82	IV
22		842.04	IV
		Air	
3		2237.34	IV
6		2291.26	IV
3		2329.3	IV
4		2336.75	IV
4		2348.27	IV
3		2358.5	IV
3		2388.05	IV
4		2416.9	IV
3		2428.04	IV
5		2442.68	IV
4		2451.7	IV
6		2459.74	IV
5		2474.06	IV
4		2517.0	IV
5		2518.02	IV
6		2519.38	IV
5		2524.5	IV
5		2546.0	IV
6		2547.0	IV
4		2558.08	IV
3		2586.9	IV
5		2606.17	IV
10		2609.5	IV
8		2615.3	IV
7		2621.11	IV
3		2730.55	IV
8		2748.18	IV
6		2774.70	IV
3		2829.60	IV
3		2836.08	IV
5		2853.0	IV
3		2859.3	IV
3		3142.01	IV
6		3224.99	IV
3		3261.70	IV
3		3809.30	IV
5		3860.58	IV
5		3934.29	IV

Kr V
Ref. 409, 421 — E.F.W.

Intensity		Wavelength	
		Vacuum	
150		472.16	V
100		484.39	V
250		496.25	V
120		500.77	V
200		507.20	V
60		548.04	V
120		637.87	V
		690.86	V
		691.75	V
600		708.85	V
		810.70	V

LANTHANUM (La)
Z = 57

La I and II

Ref. 1 — C.H.C.

Intensity		Wavelength	
		Air	
240		2187.87	II
770		2256.76	II
200		2319.44	II
400		2610.34	II
420		2808.39	II
130		2885.14	II
160		2893.07	II
110		2950.50	II
180		3104.59	II
130		3142.76	II
510		3245.13	II
260		3249.35	II
550		3265.67	II
800		3303.11	II
1500		3337.49	II
870		3344.56	II
200		3376.33	II
1500		3380.91	II
130		3452.18	II
180		3453.17	II
200		3574.43	I
320		3628.83	II
120		3637.15	II
170	d	3641.53	I
		3641.66	II
1000		3645.42	II
390		3650.18	II
170		3662.08	II
120		3704.54	I
320		3705.82	II
550		3713.54	II
140		3714.87	II
270		3715.53	II
2400		3759.08	II
120		3780.67	II
3700		3790.83	II
3900		3794.78	II
190		3835.08	II
600		3840.72	II
120		3846.00	II
1600		3849.02	II
130		3854.91	II
3400		3871.64	II
1700		3886.37	II
1300		3916.05	II
1100		3921.54	II
160		3927.56	I
2200		3929.22	II
180		3936.22	II
9000		3949.10	II
4400		3988.52	II
3600		3995.75	II
180		4015.39	I
250		4025.88	II
2800		4031.69	II
140		4037.21	I
3000		4042.91	II
320		4050.08	II
220		4060.33	I
160		4064.79	I
850		4067.39	II
110		4076.71	II
2800		4077.35	II
120		4079.18	I
5500		4086.72	II
180		4089.61	I
280		4099.54	II
110		4104.87	I
4400		4125.23	II
110		4137.04	I
550		4141.74	II
1100		4151.97	II
220		4152.78	II
100		4160.26	I
280		4187.32	I
280		4192.36	II
1500		4196.55	II
240		4204.04	II
300		4217.56	II
200		4230.95	II
1600		4238.38	II
140		4249.99	II
320		4263.59	II
480		4269.50	II
240		4275.64	II
300		4280.27	I
600		4286.97	II
600		4296.05	II
120		4300.44	II
440		4322.51	II
4600		4333.74	II
550		4354.40	II
110		4364.67	II
110	b1	4371.97	L
110	b1	4375.84	L
110		4378.10	II
280		4383.44	II
100		4385.20	II

Neodymium (Cont.)

120		4527.25	I
340		4541.27	II
340		4542.61	II
100		4556.14	II
170		4559.67	I
340		4563.22	II
200		4578.89	II
200		4579.32	II
100		4586.62	I
200		4597.02	II
100		4603.82	I
100		4609.87	I
300		4621.94	I
100		4627.98	I
510		4634.24	I
340		4641.10	I
250		4645.77	II
200		4646.40	I
300		4649.67	I
200		4654.73	I
130		4670.56	II
170		4680.74	II
310		4683.45	I
110		4684.04	I
110		4690.35	I
190		4696.44	I
130		4703.57	II
470		4706.54	II
140		4706.96	I
190		4709.71	II
190		4715.59	II
240		4719.02	I
190		4724.35	II
140		4731.77	I
120		4779.46	I
170		4789.41	II
120		4797.15	II
240		4811.34	II
140		4820.34	II
350		4825.48	II
130		4832.28	II
110		4849.06	II
280		4859.02	II
190		4866.74	I
350		4883.81	I
140		4889.10	II
220		4890.70	II
240		4891.07	I
280		4896.93	I
120		4901.53	I
210		4901.84	I
110		4902.03	II
190		4913.41	I
170		4914.37	II
330		4920.68	II
470		4924.53	I
260		4944.83	I
290		4954.78	I
290		4959.13	II
150		4961.39	II
250		4989.94	II
150		5033.52	II
110		5063.73	II
360		5076.59	II
150	h	5089.84	II
360		5092.80	II
180		5102.39	II
150	d	5105.21	II
		5105.35	I
360		5107.59	II
340		5123.79	II
680		5130.60	II
170		5132.33	II
170		5165.14	II
130		5181.17	II
120		5182.60	II
500		5191.45	II
630		5192.62	II
330		5200.12	II
310		5212.37	II
150		5213.23	I
130		5225.05	II
130		5228.43	II
450		5234.20	II
250		5239.79	II
720		5249.59	II
200		5250.82	II
360		5255.51	II
120		5269.48	II
590		5273.43	II
150		5276.88	II
110		5291.67	I
680		5293.17	II
160		5302.28	II
110		5306.47	II
220		5311.46	II
500		5319.82	II
180		5356.98	II
290		5361.47	II
150		5371.94	II
110		5385.90	II
160		5431.53	II
110		5451.12	II
170		5485.70	II
35		5501.47	I
45		5525.72	I
90		5533.82	I
55		5535.27	II
55		5543.24	I
55		5548.47	II
55		5561.17	I
27		5575.50	I
27		5576.70	I
27		5577.70	I
27		5587.61	I
240		5594.43	II
55		5601.43	I
45		5601.92	I
220		5620.54	I
65		5635.76	I
45		5639.54	I
35		5653.57	I
70		5668.87	II
65		5669.77	I
140	d	5675.97	I
55		5676.33	I
220		5688.53	II
23		5689.51	I
30		5701.57	I
130		5702.24	II
80		5706.21	II
160		5708.28	II
80		5718.12	II
65		5726.83	II
100		5729.29	I
23		5734.55	
70		5740.86	II
55		5749.19	I
27		5749.66	I
23		5767.33	I
45		5776.12	I
45		5784.96	I
45		5788.22	I
45		5800.09	I
160		5804.02	II
80		5811.57	II
45		5813.89	I
27		5820.37	I
70		5825.87	II
30		5826.74	I
80		5842.39	II
30		5844.66	I
23		5845.95	I
55		5858.91	I
35		5867.08	I
30		5868.90	I
27		5871.04	I
30		5883.29	I
23		5886.24	I
30		5887.91	I
27		5921.22	I
27		5955.87	I
30		5994.76	I
27		5996.47	I
45		6007.67	I
35		6031.27	II
27		6033.29	I
45		6034.24	II
55		6066.03	I
27		6071.70	I
30		6073.97	I
23	d	6133.47	II
27		6149.28	I
27		6155.06	I
35		6157.83	II
23		6166.67	II
35		6170.49	II
45		6178.59	I
27		6183.91	II
27		6208.24	I
45		6223.39	I
27		6226.50	I
23		6238.50	II
35		6244.08	I
23		6257.49	I
27		6258.73	II
23		6277.29	II
27		6285.79	I
23		6292.84	II
23		6297.07	I
55		6310.49	I
27		6341.51	II
23		6382.07	II
65		6385.20	II
35		6485.69	I
45		6630.14	I
35		6637.96	II
45		6650.57	II
30		6655.67	I
25		6737.79	II
40		6740.11	II
25		6742.54	I
30		6790.37	II
30		6804.00	II
25		6846.72	II
40		6900.43	II
24		6941.39	II
17	h	7010.80	II
8		7018.85	II
17		7020.92	II
17		7024.58	II
10		7033.21	
35		7037.30	II
7		7052.14	II
7		7054.74	II
7		7061.47	II
40		7066.89	II
8		7082.93	II
12	h	7089.71	II
12	h	7092.09	
12	h	7092.74	II
12	h	7092.94	
17	h	7093.98	I
20	h	7095.42	I
29		7129.35	II
12	h	7142.04	II
10		7143.72	
8		7151.03	II
6		7153.09	I
6	h	7185.01	
10		7189.09	II
24		7189.42	II
20		7192.01	II
10		7199.00	II
8	h	7227.01	I
15		7236.54	II
7	h	7261.64	II
9		7285.29	II
9		7288.56	II
6		7291.38	II
7		7298.72	II
12		7316.81	II
7	h	7321.43	I
7		7323.12	II
6		7334.54	I
6		7357.10	I
6		7374.04	II
7		7381.79	II
9		7401.31	I
10		7406.62	II
6		7411.20	II
10		7418.18	II
9		7427.41	II
9		7448.71	II
5		7481.28	II
12		7511.16	II
17		7513.73	II
7	h	7514.44	II
7		7516.02	II
9		7526.45	II
12		7528.99	II
10		7538.26	II
5		7540.97	II
7		7547.00	II
5		7577.54	II
7		7587.65	II
6		7590.75	II
6		7603.73	II
5		7605.92	II
5		7614.72	I
9		7639.79	II
8		7646.00	II
6		7663.52	II
12		7696.56	II
6		7718.20	II
4		7743.90	II
4		7748.92	II
10		7750.95	II
6		7773.06	II
7		7792.22	II
6		7796.40	II
8		7797.32	II
5		7798.32	II
10		7808.47	II
7		7818.83	II
5		7825.20	II
12		7863.04	II
5	h	7872.03	I
7		7886.60	II
4	h	7896.50	II
9		7900.40	II
5	h	7906.03	I
12		7917.01	II
10		7925.03	II
5		7947.93	II
10		7949.68	II
5	h	7955.38	II
12		7958.95	I
12		7965.73	II
15		7982.09	II
12		7982.68	II
12		8000.76	II
9		8007.70	I
4	h	8020.07	
8		8026.35	
10		8043.24	I
8		8051.33	II
5		8064.00	II
10		8099.17	I
10		8120.93	II
12		8122.07	II
12		8141.75	II
12		8143.27	II
7	h	8164.97	I
8		8172.56	II
9		8179.83	II
9		8182.41	II
4		8185.58	II
7	h	8205.38	II
10		8231.52	II
4		8248.76	II
5	h	8249.68	II
4	h	8262.80	II
7	h	8266.72	II
4		8272.79	II
4	h	8302.74	II
10		8307.72	II
6		8324.50	II
4		8332.01	II
12		8346.36	II
4		8375.16	II
4		8375.33	II
4		8394.71	II
7		8400.85	II
5	h	8456.87	II
4		8530.53	II
5		8582.03	II
5		8591.53	II
7		8594.87	II
8	c	8643.43	II
5		8667.07	II
5		8677.48	
6		8691.29	II
6		8695.07	II
6		8712.82	II
6		8715.03	I
17		8839.10	II

NEON (Ne)
Z = 10

Ne I and II
Ref. 56, 58, 118, 150, 230 — S.P.D.

Intensity		Wavelength	
		Vacuum	
90		352.956	II
60		354.962	II
90		361.433	II
60		362.455	II
150		405.854	II
120		407.138	II
200		445.040	II
300		446.256	II
250		446.590	II
180		447.815	II
150		454.654	II
200		455.274	II
10		456.275	II
120		456.348	II
90		456.896	II
1000		460.728	II
500		462.391	II
35		587.213	I
35		589.179	I
35		589.911	I
70		591.830	I
100		595.920	I
75		598.706	I
35		598.891	I
70		600.036	I
170		602.726	I
170		615.628	I
170		618.672	I
120		619.102	I
200		626.823	I
200		629.739	I
1000		735.896	I
400		743.720	I
60		993.88	II
70		1068.65	II
90		1131.72	II
100		1131.85	II
90		1229.83	II
90		1418.38	II
90		1428.58	II
90		1436.09	II
120		1681.68	II
180		1688.36	II
100		1888.11	II
100		1889.71	II
200		1907.49	II
500		1916.08	II
300		1930.03	II
200		1938.83	II
100	c	1945.46	II
		AIR	

Week 3 Notes

Optics Hecht / Addison-Wesley (1987, 2nd Ed.)

maximum has a broad flat top; in other words, at the origin, which is the center of the peak, the second derivative of the irradiance function is zero; there is no change in slope (Fig. 10.40).

Unlike the Rayleigh rule, which rather tacitly assumes incoherence, the Sparrow condition can readily be generalized to coherent sources. In addition, astronomical studies of equal-brightness stars have shown that Sparrow's criterion is by far the more realistic.

10.2.7 The Diffraction Grating

A repetitive array of diffracting elements, either apertures or obstacles, that has the effect of producing periodic alterations in the phase, amplitude, or both of an emergent wave is said to be a **diffraction grating**. One of the simplest such arrangements is the multiple-slit configuration of Section 10.2.3. It seems to have been invented by the American astronomer David Rittenhouse in about 1785. Some years later Joseph von Fraunhofer independently rediscovered the principle and went on to make a number of important contributions to both the theory and technology of gratings. The earliest devices were indeed multiple-slit assemblies, usually consisting of a grid of fine wire or thread wound about and extending between two parallel screws, which served as spacers. A wavefront, in passing through such a system, is confronted by alternate opaque and transparent regions, so that it undergoes a modulation in *amplitude*. Accordingly, a multiple-slit configuration is said to be a *transmission amplitude grating*. Another, more common form of transmission grating is made by ruling or scratching parallel notches into the surface of a flat, clear glass plate [Fig. 10.34(a)]. Each of the scratches serves as a source of scattered light, and together they form a regular array of parallel line sources. When the grating is totally transparent, so that there is negligible amplitude modulation, the regular variations in the optical thickness across the grating yield a modulation in *phase*, and we have what is known as a *transmission phase grating* (Fig. 10.35). In the Huygens–Fresnel representation you can envision the wavelets as radiated with different phases over the grating surface. An emerging wavefront therefore contains

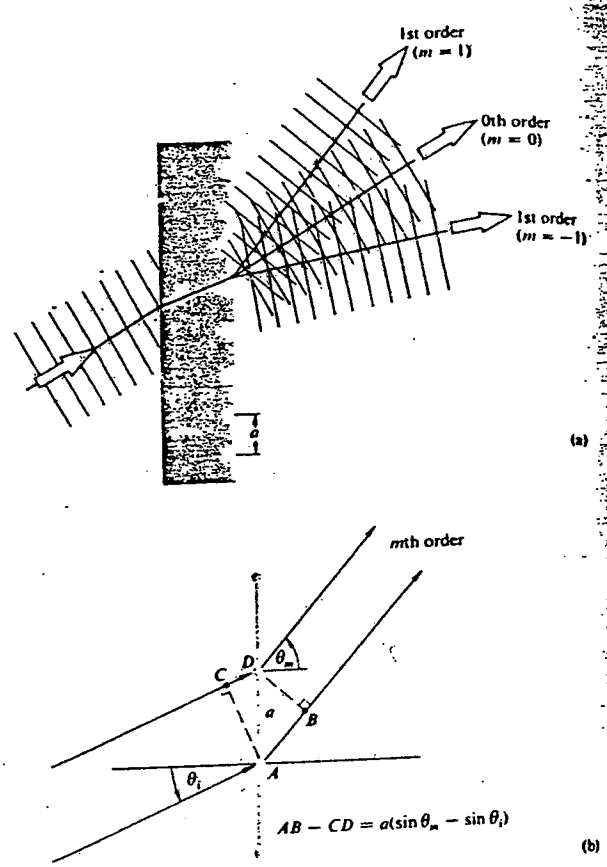

Figure 10.34 A transmission grating.

periodic variations in its shape rather than its amplitude. This in turn is equivalent to an angular distribution of constituent plane waves.

On reflection from this kind of grating, light scattered by the various periodic surface features will arrive at some point P with a definite phase relationship. The consequent interference pattern generated after reflection is quite similar to that arising from transmission. Gratings designed specifically to function in this fashion are known as *reflection phase gratings* (Fig. 10.36). Contemporary gratings of this sort are generally ruled in thin films of aluminum that have been evaporated onto optically flat glass blanks. The aluminum, being fairly

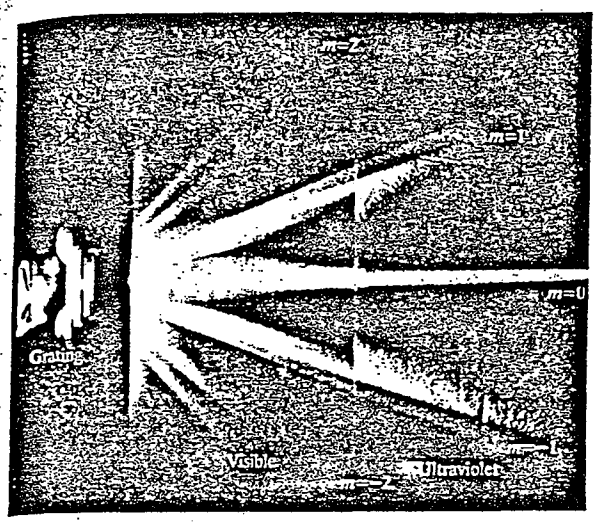

Figure 10.35 Light passing through a grating. The region on the left is the visible spectrum, that on the right, the ultraviolet. (Photo courtesy Klinger Scientific Apparatus Corp.)

soft, results in less wear on the diamond ruling tool and is also a better reflector in the ultraviolet region.

The manufacture of ruled gratings is extremely difficult, and relatively few are made. In actuality most gratings are exceedingly good plastic castings or *replicas* of fine, master ruled gratings.

If you were to look perpendicularly through a transmission grating at a distant parallel line source, your eye would serve as a focusing lens for the diffraction pattern. Recall the analysis of Section 10.2.3 and the expression

$$a \sin \theta_m = m\lambda, \qquad [10.32]$$

which is known as the **grating equation** for normal incidence. The values of m specify the *order* of the various principal maxima. For a source having a broad continuous spectrum, such as a tungsten filament, the $m = 0$, or zeroth-order, image corresponds to the undeflected, $\theta_0 = 0$, white-light view of the source. The grating equation is dependent on λ, and so for any value of $m \neq 0$ the various colored images of the source corresponding to slightly different angles (θ_m) spread out into a continuous spectrum. The regions occupied by the faint subsidiary maxima will show up as bands seemingly devoid of any light. The first-order spectrum $m = \pm 1$ appears on either side of $\theta = 0$ and is followed, along with alternate intervals of darkness, by the higher-order spectra, $m = \pm 2, \pm 3, \ldots$. Notice that the smaller a becomes in Eq. (10.32), the fewer will be the number of visible orders.

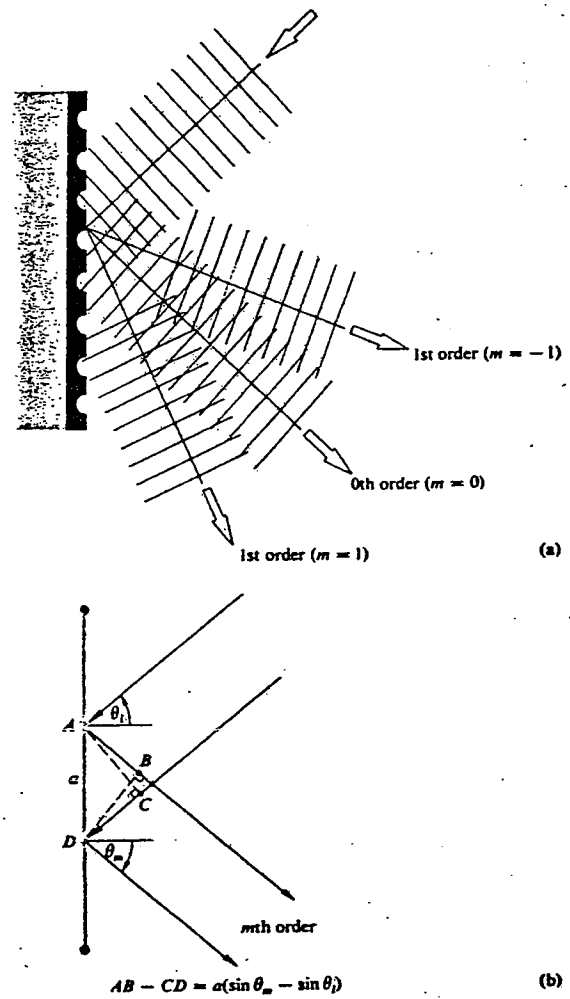

Figure 10.36 A reflection grating.

It should be no surprise that the grating equation is in fact Eq. (9.29), which describes the location of the maxima in Young's double-slit setup. The interference maxima, all located at the same angles, are now simply sharper (just as the multiple beam operation of the Fabry–Perot etalon made its fringes sharper). In the double-slit case when the point of observation is somewhat off the exact center of an irradiance maximum the two waves, one from each slit, will still be more or less in phase, and the irradiance, though reduced, will still be appreciable. Thus the bright regions are fairly broad. By contrast, with multiple-beam systems though all the waves interfere constructively at the centers of the maxima, even a small displacement will cause certain ones to arrive out of phase by $\frac{1}{2}\lambda$ with respect to others. For example, suppose P is slightly off from θ_1 so that $a \sin \theta = 1.010\lambda$ instead of 1.000λ. Each of the waves from successive slits will arrive at P shifted by 0.01λ with respect to the previous one. Then 50 slits down from the first, the path length will have shifted by $\frac{1}{2}\lambda$, and the light from slit 1 and slit 51 will essentially cancel. The same would be true for slit-pairs 2 and 52, 3 and 53, and so forth. The result is a rapid fall off in irradiance beyond the centers of the maxima.

Consider next the somewhat more general situation of oblique incidence, as depicted in Figs. 10.34 and 10.36. The grating equation, for both transmission and reflection, becomes

$$a(\sin \theta_m - \sin \theta_i) = m\lambda. \qquad (10.61)$$

This expression applies equally well, regardless of the refractive index of the transmission grating itself (Problem 10.37). One of the main disadvantages of the devices examined thus far, and in fact the reason for their obsolescence, is that they spread the available light energy out over a number of low-irradiance spectral orders. For a grating like that shown in Fig. 10.36, most of the incident light undergoes *specular reflection*, as if from a plane mirror. It follows from the grating equation that $\theta_m = \theta_i$ corresponds to the zeroth order, $m = 0$. All of this light is essentially wasted, at least for spectroscopic purposes, since the constituent wavelengths overlap.

In an article in the *Encyclopaedia Britannica* of 1888 Lord Rayleigh suggested that it was at least theoretically possible to shift energy out of the useless zeroth order into one of the higher-order spectra. So motivated, Robert Williams Wood (1868–1955) succeeded in 1910 in ruling grooves with a controlled shape, as shown in Fig. 10.37. Most modern gratings are of this shaped or blazed variety. The angular positions of the nonzero orders, θ_m-values, are determined by a, λ, and, of more immediate interest, θ_i. But θ_i and θ_m are measured from the normal to the grating plane and not with respect to the individual groove surfaces. On the other hand, the location of the peak in the single-facet diffraction pattern corresponds to *specular reflection* off that face, for each groove. It is governed by the *blaze angle* γ and can be varied independently of θ_m. This is some-

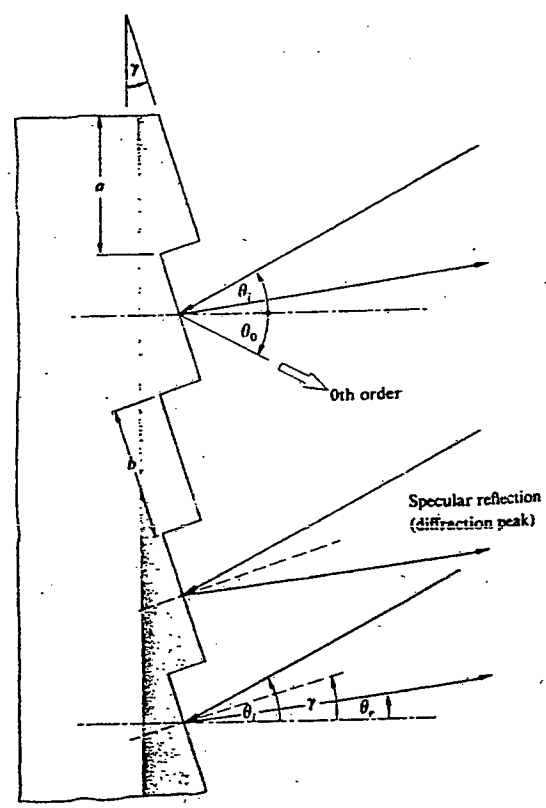

Figure 10.37 Section of a blazed reflection phase grating.

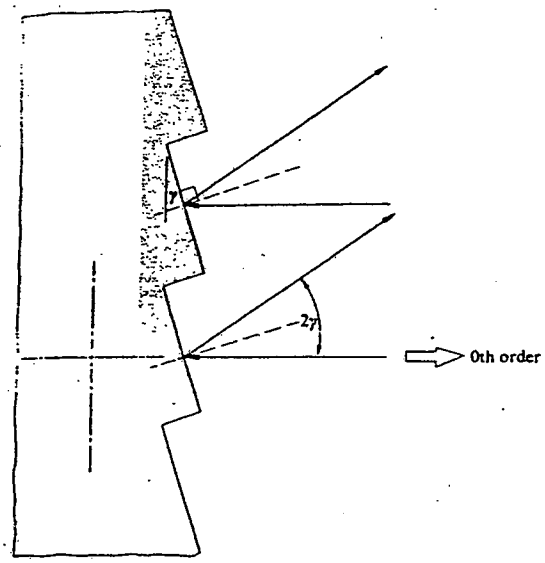

Figure 10.38 Blazed grating.

what analogous to the antenna array of Section 10.1.3, where we were able to control the spatial position of the interference pattern (10.6) by adjusting the relative phase shift between sources without actually changing their orientations.

Consider the situation depicted in Fig. 10.38 when the incident wave is normal to the plane of a blazed reflection grating; that is, $\theta_i = 0$, so for $m = 0$, $\theta_0 = 0$. For *specular reflection* $\theta_i - \theta_r = 2\gamma$ (Fig. 10.37), most of the diffracted radiation is concentrated about $\theta_r = -2\gamma$. (θ_r is negative because the incident and reflected rays are on the same side of the grating normal.) This will correspond to a particular nonzero order, on one side of the central image, when $\theta_m = -2\gamma$; in other words, $a \sin(-2\gamma) = m\lambda$ for the desired λ and m.

Grating Spectroscopy

Quantum mechanics, which evolved in the early 1920s, had its initial thrust in the area of atomic physics. Predictions were made concerning the detailed structure of the hydrogen atom as manifested by its emitted radiation, and spectroscopy provided the vital proving ground. The need for larger and better gratings became apparent. Grating spectrometers, used over the range from soft x-rays to the far infrared, have enjoyed continued interest. In the hands of the astrophysicist or rocket-borne, they yield information concerning the very origins of the universe, information as varied as the temperature of a star, the rotation of a galaxy, and the red shift in the spectrum of a quasar. In the mid-1900s George R. Harrison and George W. Stroke remarkably improved the quality of high-resolution gratings. They used a ruling engine* whose operation was controlled by an interferometrically guided servomechanism.

Let us now examine in some detail a few of the major features of the grating spectrum. Assume an infinitesimally narrow incoherent source. The effective width of an emergent spectral line may be defined as the angular distance between the zeros on either side of a principal maximum; in other words, $\Delta\alpha = 2\pi/N$, which follows from Eq. (10.33). At oblique incidence we can redefine α as $(ka/2)(\sin\theta - \sin\theta_i)$, and so a small change in α is given by

$$\Delta\alpha = (ka/2)\cos\theta(\Delta\theta) = 2\pi/N, \qquad (10.62)$$

where the angle of incidence is constant, that is, $\Delta\theta_i = 0$. Thus even when the incident light is monochromatic

$$\Delta\theta = 2\lambda/(Na\cos\theta_m) \qquad (10.63)$$

is the *angular width of a line*, due to *instrumental broadening*. Interestingly enough, the angular linewidth varies inversely with the width of the grating itself, Na. Another important quantity is the difference in angular position corresponding to a difference in wavelength. The **angular dispersion**, as in the case of a prism, is defined as

$$\mathcal{D} = d\theta/d\lambda. \qquad (10.64)$$

Differentiating the grating equation yields

$$\mathcal{D} = m/a\cos\theta_m. \qquad (10.65)$$

This means that the angular separation between two

* For more details about these marvelous machines see A. R. Ingalls, *Sci. Amer.* 186, 45 (1952), or the article by E. W. Palmer and J. F. Verrill, *Contemp. Phys.* 9, 257 (1968).

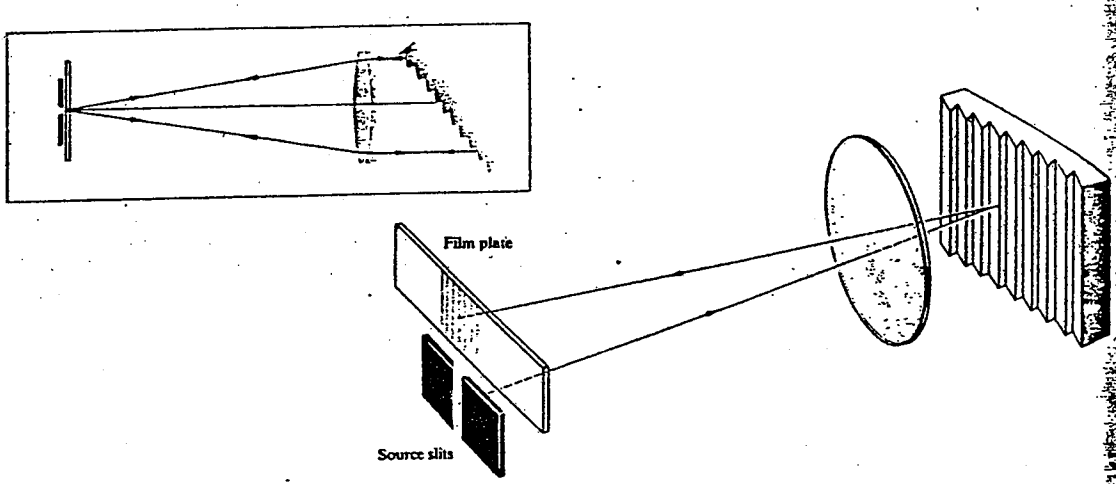

Figure 10.39 The Littrow autocollimation mounting.

different frequency lines will increase as the order increases.

Blazed plane gratings with nearly rectangular grooves are most often mounted so that the incident propagation vector is almost normal to either one of the groove faces. This is the condition of *autocollimation*, in which θ_i and θ_m are on the same side of the normal and $\gamma = \theta_i = -\theta_m$ (see Fig. 10.39), whereupon

$$\mathcal{D}_{\text{auto}} = 2 \tan \theta_i / \lambda, \tag{10.66}$$

which is independent of a.

When the wavelength difference between two lines is small enough so that they overlap, the resultant peak becomes somewhat ambiguous. The chromatic resolving power $\mathcal{R}$ of a spectrometer is defined as

$$\mathcal{R} = \lambda / (\Delta\lambda)_{\min}, \tag{10.76}$$

where $(\Delta\lambda)_{\min}$ is the least resolvable wavelength difference, or limit of resolution, and λ is the mean wavelength. Lord Rayleigh's criterion for the resolution of two fringes with equal flux density requires that the principal maximum of one coincide with the first minimum of the other. (Compare this with the equivalent statement used in Section 9.6.1.) As shown in Fig. 10.40, at the limit of resolution the angular separation is half the linewidth, or from Eq. (10.63)

$$(\Delta\theta)_{\min} = \lambda / Na \cos \theta_m.$$

Applying the expression for the dispersion, we get

$$(\Delta\theta)_{\min} = (\Delta\lambda)_{\min} m / a \cos \theta_m.$$

The combination of these two equations provides us with $\mathcal{R}$, that is,

$$\lambda / (\Delta\lambda)_{\min} = mN \tag{10.67}$$

or

$$\mathcal{R} = \frac{Na(\sin \theta_m - \sin \theta_i)}{\lambda}. \tag{10.68}$$

The resolving power is a function of the grating width Na, the angle of incidence, and λ. A grating 6 inches wide and containing 15,000 lines per inch will have a total of 9×10^4 lines and a resolving power, in the second order, of 1.8×10^5. In the vicinity of 540 nm the grating could resolve a wavelength difference of 0.003 nm. Notice that the resolving power cannot exceed $2Na/\lambda$, which occurs when $\theta_i = -\theta_m = 90°$. The largest values of $\mathcal{R}$ are obtained when the grating is used in autocollimation, whereupon

$$\mathcal{R}_{\text{auto}} = \frac{2Na \sin \theta_i}{\lambda}, \tag{10.69}$$

and again θ_i and θ_m are on the same side of the normal. For one of Harrison's 260-mm–wide blazed gratings at about 75° in a Littrow mount, with $\lambda = 500$ nm, the resolving power just exceeds 10^6.

We now need to consider the problem of overlapping orders. The grating equation makes it quite clear that a line of 600 nm in the first order will have precisely the same position, θ_m, as a 300-nm line in the second order or a 200-nm line when $m = 3$. If two lines of wavelength λ and $(\lambda + \Delta\lambda)$ in successive orders $(m + 1)$ and m just coincide, then

$$a(\sin\theta_m - \sin\theta_i) = (m + 1)\lambda = m(\lambda + \Delta\lambda).$$

That precise wavelength difference is known as the **free spectral range**,

$$(\Delta\lambda)_{fsr} = \lambda/m, \qquad (10.70)$$

as it was for the Fabry–Perot interferometer. In comparison with that device, whose resolving power was

$$\mathcal{R} = \mathcal{F}m, \qquad [9.76]$$

we might take N to be the finesse of a diffraction grating (Problem 10.38).

A high-resolution grating blazed for the first order, so as to have the greatest free spectral range, will require a high groove density (up to about 1200 lines per millimeter) in order to maintain $\mathcal{R}$. Equation (10.68) shows that $\mathcal{R}$ can be kept constant by ruling fewer lines with increasing spacing, such that the grating width Na is constant. But this requires an increase in m and a subsequent decrease in free spectral range, characterized by overlapping orders. If this time N is held constant while a alone is made larger, $\mathcal{R}$ increases as does m, so that $(\Delta\lambda)_{fsr}$ again decreases. The angular width of a line is reduced (i.e., the spectral lines become sharper), the coarser the grating is, but the dispersion in a given order diminishes, with the effect that the lines in that spectrum approach each other.

Thus far we have considered a particular type of periodic array, namely, the *line grating*. A good deal more information is available in the literature* concern-

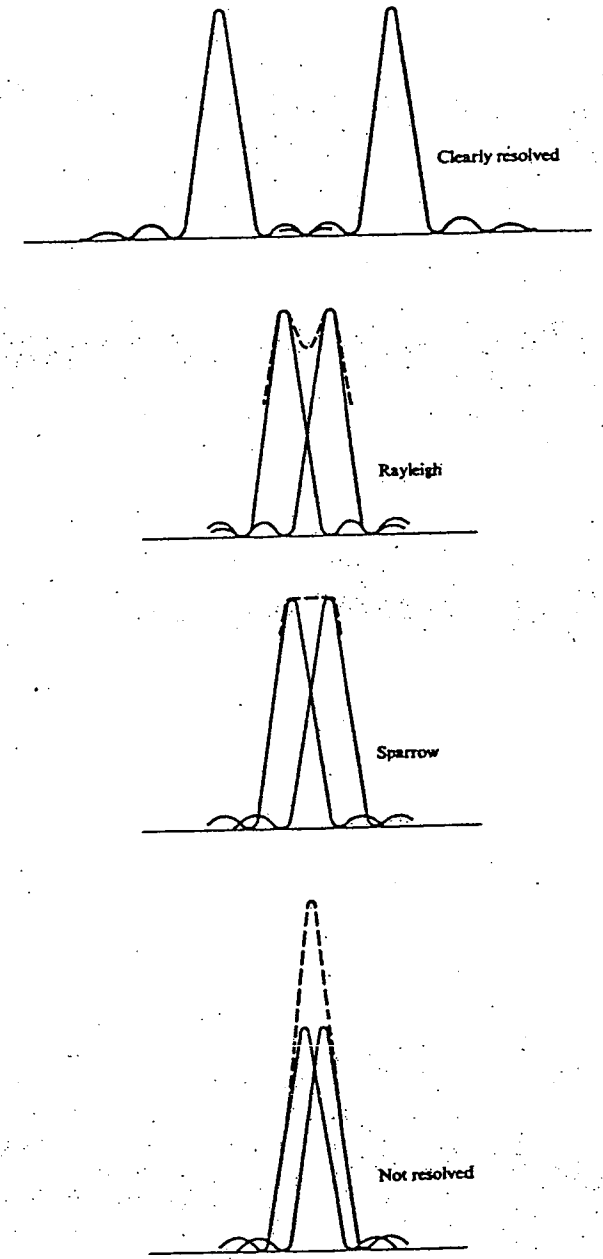

Figure 10.40 Overlapping point images.

* See F. Kneubühl, "Diffraction Grating Spectroscopy", *Appl. Opt.* 8, 505 (1969); R. S. Longhurst, *Geometrical and Physical Optics*; and the extensive article by G. W. Stroke in the *Encyclopedia of Physics*, Vol. 29, edited by S. Flügge, p. 426.

ing their shapes, mountings, uses, and so forth.

There are a few unlikely household items that can be used as crude gratings, along with a small light source. The grooved surface of a phonograph record works nicely near grazing incidence. And surprisingly enough, under the same conditions an ordinary fine-toothed comb will separate out the constituent wavelengths of white light. This occurs in exactly the same fashion as it would with a more orthodox reflection grating. In a letter to a friend dated May 12, 1673, James Gregory pointed out that sunlight passing through a feather would produce a colored pattern, and he asked that his observations be conveyed to Mr. Newton. If you've got one, a feather makes a nice transmission grating.

Two- and Three-Dimensional Gratings

Suppose that the diffracting screen Σ contains a large number, N, of identical diffracting objects (apertures or obstacles). These are to be envisioned as distributed over the surface of Σ in a completely random manner. We also require that each and every one be similarly oriented. Imagine the diffracting screen to be illuminated by plane waves that are focused by a perfect lens L_2, after emerging from Σ (see Fig. 10.15). The individual apertures generate identical Fraunhofer diffraction patterns, all of which overlap on the image plane σ. If there is no regular periodicity in the location of the apertures, we cannot anticipate anything but a random distribution in the relative phases of the waves arriving at an arbitrary point P on σ. We have to be rather careful, however, because there is one exception, which occurs when P is on the central axis, that is, $P = P_0$. All rays, from all apertures, parallel to the central axis will traverse equal optical path lengths before reaching P_0. They will therefore arrive in phase and interfere constructively.

Now consider a group of arbitrarily directed parallel rays (not in the direction of the central axis), each one emitted from a different aperture. These will be focused at some point on σ, such that each corresponding wave will have an equal probability of arriving with any phase between 0 and 2π. What must be determined is the resultant field arising from the superposition of N equal-amplitude phasors all having random relative phases. The solution to this problem requires an elaborate analysis in terms of probability theory, which is a little too far afield to do here.* The important point is that the sum of a number of phasors taken at random angles is not simply zero, as might be thought. The general analysis begins, for statistical reasons, by assuming that there are a large number of individual aperture screens, each containing N random diffracting apertures and each illuminated, in turn, by a monochromatic wave. We shouldn't be surprised if there is some difference, however small, between the diffraction patterns of two different random distributions of, say, $N = 100$ holes—after all, they are different, and the smaller N is, the more obvious that becomes. Indeed, we can expect their similarities to show up statistically on considering a large number of such masks—ergo the general approach.

If the many individual resulting irradiance distributions are all averaged for a particular *off-axis* point on σ, it will be found that the average irradiance (I_{av}) there equals N times the irradiance (I_0) due to a single aperture: $I_{av} = NI_0$. Still, the irradiance at any point arising from any one aperture screen can differ from this average value by a fairly large amount, regardless of how great N is. These point-to-point fluctuations about the average manifest themselves in each particular pattern as a granularity that tends to show a radial fiberlike structure. If this fine-grained mottling is averaged over a small region of the pattern, which nonetheless contains many fluctuations, it will average out to NI_0.

Of course, in any real experiment the situation will not quite match the ideal—there is no such thing as monochromatic light or a truly random array of (non-overlapping) diffracting objects. Nonetheless, with a screen containing N "random" apertures illuminated by quasimonochromatic, nearly plane-wave illumination, we can anticipate seeing a mottled flux-density distribution closely resembling that of an individual aperture but N times as strong. Moreover, a bright spot

* For a statistical treatment, consult J. M. Stone, *Radiation and Optics*, p. 146, and Sommerfeld, *Optics*, p. 194. Also take a look at "Diffraction Plates for Classroom Demonstrations," by R. B. Hoover, *Am. J. Phys.* 37, 871 (1969), and T. A. Wiggins, "Hole Gratings for Optics Experiments," *Am. J. Phys.* 53, 227 (1985).

More on the grating measurements.

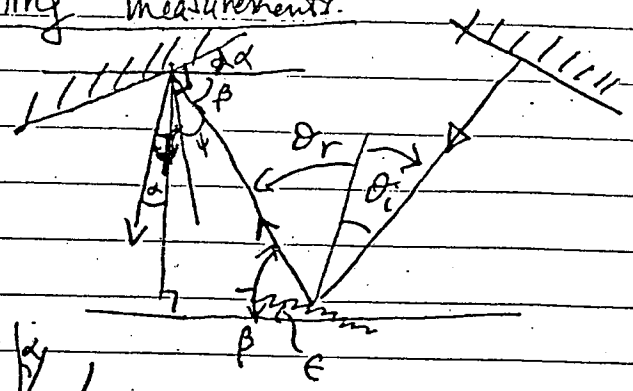

Angles

$\psi = 90 - \alpha - \beta$

$\alpha = 2\psi + \beta - 90$

$= 180 - 2\alpha - 2\beta + \beta - 90$

$= 90 - 2\alpha - \beta$

Focusing by a Lens

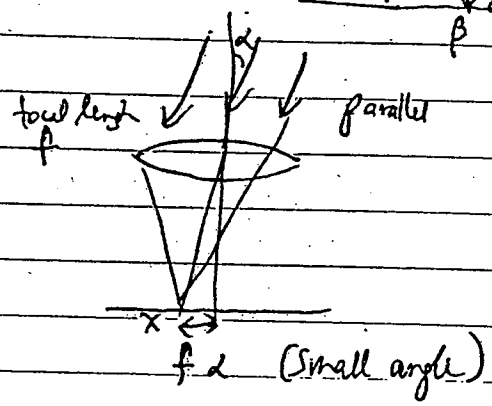

A) ⇒ Spectral width of light going through the exit slit (width w) [spectral resolution]

$(\Delta x) = f(\alpha) = w \qquad \Delta\alpha = ?$

Grating fixed so θ_i fixed $\qquad m\lambda = d(\sin\theta_i - \sin\theta_r)$

so θ_r changes for a change in λ $\qquad m\delta\lambda = -d\cos\theta_r\,\delta\theta_r$

but $\delta\theta_r \Rightarrow \delta\beta \Rightarrow \delta\alpha$ $\qquad$ so $|\delta\alpha| = \left|\frac{m\,\delta\lambda}{d\cos\theta_r^{ref}}\right|$ $\qquad |\delta\alpha| f \Rightarrow$ spectral dispersion

$$w = \frac{mf}{d}\frac{\delta\lambda}{\cos\theta_r^{ref}} \qquad \boxed{\delta\lambda = \frac{wd}{mf}\cos\theta_r^{ref}}$$

→ Calculate this resolution for your spectrometer

B) ⇒ Angular tuning of gratings needed to tune across visible spectrum

You tune ϵ (which you can determine) and see λ change

During tuning α always $= 0$ ⇒ β doesn't change

so $\theta_i + \theta_r$ doesn't change

So always $\quad m\lambda = d(\sin(\theta_i + \delta\epsilon) - \sin(\theta_r - \delta\epsilon))$

so as $\delta\epsilon$ is changed λ is changed

→ Do your calculations agree with your measurements?